UNIVERSITAT POLITÈCNICA DE VALÈNCIA

DEPARTAMENTO DE INGENIERÍA HIDRÁULICA Y MEDIO AMBIENTE

UNIVERSITAT POLITÈCNICA DE VALÈNCIA

Monitorización de cambios en la lámina libre de agua en humedales mediante teledetección

TESIS DOCTORAL

Presentada por:

D. Jesús Pena Regueiro

Dirigida por:

Dra. Dª. María Teresa Sebastiá Frasquet

Dr. D. Javier Estornell Cremades

Valencia, julio de 2023

A mi hijo Bruno, a mi esposa Sandra y mi familia.

AGRADECIMIENTOS

Me gustaría mostrar mi más sincero agradecimiento a los tutores de mi tesis, a la Dra. Dª María Teresa Sebastiá Frasquet y al Dr. D. Javier Estornell Cremades por su incondicional apoyo y dedicación en todos estos años de mi trayectoria investigadora. Gracias por darme esta oportunidad tan increíble de poder desarrollar mi carrera profesional, de brindarme con esa incansable actitud de motivación, dedicación y de orientación profesional en todo momento.

Muchas gracias.

RESUMEN

Los humedales son uno de los ecosistemas que reciben mayor atención por parte de la comunidad científica. Su importancia se puede explicar teniendo en cuenta que ayudan a mitigar los efectos de inundaciones, pueden actuar como filtros de agua y constituyen hábitats de valiosas especies de fauna y flora. En los últimos años este tipo de ambientes están cada vez más amenazados como consecuencia de la contaminación, alteraciones de los niveles de agua asociadas a los efectos del cambio climático y usos antrópicos, introducción de especies invasoras y los efectos negativos de algunos cambios de usos del suelo y determinadas prácticas asociados a ellos (agrícolas, pastoreo y urbanización). Para analizar estos ecosistemas, la teledetección se presenta como una herramienta con alto potencial que permite identificar, evaluar y monitorizar estos espacios. En esta tesis se utilizaron imágenes Sentinel-2A/B, Landsat-5 TM y Landsat-8 OLI para extraer láminas de agua libre en dos entornos: humedales mediterráneos costeros (Prat Cabanes-Torreblanca, Marjal de Sagunto, Marjal de La Safor y Marjal Pego-Oliva) y el humedal de llanura aluvial situado en el centro de España las Tablas de Daimiel. Para ello, se realizó un análisis de siete índices de agua (NDWI, mNDWI, Cedex, Re-NDWI, Awei(sh), AWEI (nsh) y B_Blue) y de umbrales para obtener la cartografía de las masas de agua libre en estos espacios. El objetivo principal es definir el índice y el umbral que permitan un uso más amplio de la metodología para su aplicación en otras zonas húmedas. También se utilizó información LiDAR (Laser Imaging Detection and Ranging) en el humedal de La Safor para analizar los efectos de la superficie inundada en diferentes usos del suelo. La evaluación de los resultados se realizó a partir de la validación con un conjunto de muestras obtenidas a partir de imágenes de elevada resolución espacial. Se calcularon la fiabilidad global y el índice kappa en los humedales analizados para distintas fechas y sensores. En el caso de los humedales costeros, el índice de agua NDWI con un umbral de −0,30 proporcionó los resultados con mayor precisión obteniendo un valor promedio de 0,89 en fiabilidad global. En el caso del humedal de las Tablas de Daimiel, se seleccionaron el índice MNDWI y umbral −0,15 para imágenes Landsat-5 (fiabilidad global 0,88), el índice MNDWI y umbral −0,25 para imágenes Landsat-8 (fiabilidad global 0,99) y el índice NDWI y umbral −0,20 (fiabilidad global 0,99) en el caso de

imágenes Sentinel-2A/B. En el humedal de las Tablas de Daimiel se realizó un análisis temporal desde el año 2000 al 2021 que permitió calcular las anomalías de la superficie de agua, de la precipitación, del nivel piezométrico y del caudal hidrológico. Esta reconstrucción temporal también permitió comparar los resultados derivados a partir de las imágenes Sentinel-2A/B y de las imágenes Landsat 8. Se realizó un análisis de correlación entre los índices de anomalías calculados, que revela una correlación no significativa entre las anomalías precipitación y de superficie de agua. Mientras que el índice de anomalías de superficie de agua si presentó una correlación estadísticamente significativa con los índices de anomalía de caudal y de niveles piezométricos. En cuanto al análisis comparativo entre las imágenes Landsat-8 y Sentinel-2 se obtuvo una relación lineal entre la superficie de agua estimada por ambos sensores con un valor de $R^2 = 0,87$. No obstante, la mayor resolución espacial de Sentinel-2 permite detectar masas de agua más pequeñas contribuyendo a un mejor análisis de los patrones de variabilidad en el área de estudio. La información derivada de esta tesis presenta una aplicabilidad de interés medioambiental para el seguimiento del estado de los humedales ayudando a adaptar planes de gestión que conduzcan a un estado de conservación adecuado.

RESUM

Els aiguamolls són un dels ecosistemes que reben major atenció per part de la comunitat científica. La seua importància es pot explicar tenint en compte que ajuden a mitigar els efectes d'inundacions, poden actuar com a filtres d'aigua i constitueixen hàbitats de valuoses espècies de fauna i flora. En els últims anys aquest tipus d'ambients estan cada vegada més amenaçats a conseqüència de la contaminació, alteracions dels nivells d'aigua associades a l'efecte del canvi climàtic i usos antròpics, introducció d'espècies invasores i els efectes negatius d'alguns canvis d'usos del sòl i determinades pràctiques associades a ells (agrícoles, pasturatge i urbanització). Per a analitzar aquests ecosistemes, la teledetecció es presenta com una eina amb alt potencial que permet identificar, avaluar i monitorar aquests espais. En aquesta tesi es van utilitzar imatges Sentinel-2A/B, Landsat-5 TM i Landsat-8 OLI per a extraure làmines d'aigua lliure en dos entorns: aiguamolls mediterranis costaners (Prat Cabanes-Torreblanca, Marjal de Sagunt, Marjal de La Safor i Marjal Pego-Oliva) i l'aiguamoll de plana al·luvial situat en el centre d'Espanya les Taules de Daimiel. Per a això, es va realitzar una anàlisi de set índexs d'aigua (NDWI, mNDWI, Cedex, Re-NDWI, Awei (sh), AWEI (nsh) i B_Blue) i de llindars per a obtindre la cartografia de les masses d'aigua lliure en aquests espais. L'objectiu principal és definir l'índex i el llindar que permeten un ús més ampli de la metodologia per a la seua aplicació en altres zones humides. També es va utilitzar informació LiDAR (Laser Imaging Detection and Ranging) en l'aiguamoll de La Safor per a analitzar els efectes de la superfície inundada en diferents usos del sòl. L'avaluació dels resultats es va realitzar a partir de la validació amb un conjunt de mostres obtingudes a partir d'imatges d'elevada resolució espacial. Es van calcular la fiabilitat global i l'índex kappa en els aiguamolls analitzats per a diferents dates i sensors. En el cas dels aiguamolls costaners, l'índex d'aigua NDWI amb un llindar de −0,30 va proporcionar els resultats amb major precisió obtenint un valor mitjà de 0,89 en fiabilitat global. En el cas de l'aiguamoll de les Taules de Daimiel, es van seleccionar l'índex MNDWI i llindar −0,15 per a imatges Landsat-5 (fiabilitat global 0,88), l'índex MNDWI i llindar −0,25 per a imatges Landsat-8 (fiabilitat global 0,99) i l'índex NDWI i llindar −0,20 (fiabilitat global 0,99) en el cas d'imatges Sentinel-2A/B. En l'aiguamoll de les Taules de Daimiel es va realitzar una anàlisi temporal des de l'any 2000 al 2021 que va permetre calcular les

anomalies de la superfície d'aigua, de la precipitació, del nivell piezomètric i del cabal hidrològic. Aquesta reconstrucció temporal també va permetre comparar els resultats derivats a partir de les imatges Sentinel-2A/B i de les imatges Landsat 8. Es va realitzar una anàlisi de correlació entre els índexs d'anomalies calculats, que revela una correlació no significativa entre les anomalies precipitació i de superfície d'aigua. Mentre que l'índex d'anomalies de superfície d'aigua si va presentar una correlació estadísticament significativa amb els índexs d'anomalia de cabal i de nivells piezomètrics. Quant a l'anàlisi comparativa entre les imatges Landsat-8 i Sentinel-2 es va obtindre una relació lineal entre la superfície d'aigua estimada per tots dos sensors amb un valor de R^2 = 0,87. No obstant això, la major resolució espacial de Sentinel-2 permet detectar masses d'aigua de menor grandària contribuint a una millor anàlisi dels patrons de variabilitat en l'àrea d'estudi. La informació derivada d'aquesta tesi presenta una aplicabilitat d'interés mediambiental per al seguiment de l'estat dels aiguamolls ajudant a adaptar plans de gestió que condueixen a un estat de conservació adequat.

ABSTRACT

Wetlands are one of the ecosystems that receive the most attention from the scientific community. Their importance can be explained by the fact that they help mitigate the effects of flooding, can act as water filters, and provide habitats for valuable species of fauna and flora. In recent years, these types of environments are increasingly threatened as a result of pollution, alterations in water levels associated with the effects of climate change and anthropic uses, the introduction of invasive species and the negative effects of some changes in land use and certain practices associated with them (agriculture, grazing and urbanization). To analyze these ecosystems, remote sensing is presented as a tool with high potential to identify, evaluate and monitor these areas. In this thesis, Sentinel-2A/B, Landsat-5 TM and Landsat-8 OLI images were used to extract free water bodies in two environments: coastal Mediterranean wetlands (Prat Cabanes-Torreblanca, Marjal de Sagunto, Marjal de La Safor and Marjal Pego-Oliva) and the alluvial plain wetland located in the center of Spain, the Tablas de Daimiel. For this purpose, an analysis of seven water indices (NDWI, mNDWI, Cedex, Re-NDWI, Awei (sh), AWEI (nsh) and B_Blue) and thresholds were carried out to obtain the mapping of free water bodies in these areas. The main objective is to define the index and threshold that allow a wider use of the methodology for its application in other wetlands. LiDAR (Laser Imaging Detection and Ranging) information was also used in La Safor wetland to analyze the effects of the flooded surface on different land uses. The evaluation of the results was carried out based on the validation with a set of samples obtained from high spatial resolution images. The overall accuracy and the kappa index were calculated for the wetlands analyzed for different dates and sensors. In the case of the coastal wetlands, the NDWI water index with a threshold of −0.30 provided the most accurate results with an average value of 0.89 in global accuracy. In the case of Las Tablas de Daimiel wetland, the MNDWI index and threshold −0.15 were selected for Landsat-5 images (overall accuracy 0.88), the MNDWI index and threshold −0.25 for Landsat-8 images (overall accuracy 0.99) and the NDWI index and threshold −0.20 (overall accuracy 0.99) in the case of Sentinel-2A/B images. In Las Tablas de Daimiel wetland, a temporal analysis was carried out from 2000 to 2021 to calculate the anomalies of the water surface, precipitation, piezometric level and hydrological flow. This temporal reconstruction also

made it possible to compare the results derived from Sentinel-2A/B images and Landsat 8 images. A correlation analysis was performed between the calculated anomaly indices, which revealed a non-significant correlation between the precipitation and water surface anomalies. However, the water surface anomaly index did show a statistically significant correlation with the flow anomaly and piezometric level indexes. As for the comparative analysis between Landsat-8 and Sentinel-2 images, a linear relationship was obtained between the water surface estimated by both sensors with a value of $R^2 = 0.87$. However, the higher spatial resolution of Sentinel-2 allows the detection of smaller water masses contributing to a better analysis of the variability patterns in the study area. The information derived from this thesis presents an application of environmental interest for monitoring the state of wetlands helping to adapt management plans that lead to an adequate conservation status.

INDICE

1 CAPÍTULO 1: INTRODUCCIÓN 15

1.1 LOS HUMEDALES Y LOS SERVICIOS ECOSISTÉMICOS 15
1.2 TELEDETECCIÓN PARA EL SEGUIMIENTO DE HUMEDALES CON MASAS DE AGUA DE REDUCIDO TAMAÑO 22
1.3 OBJETIVOS Y ALCANCE DE LA TESIS 23
1.4 ESTRUCTURA DE LA TESIS 24
1.5 REFERENCIAS 27

2 CAPÍTULO 2: SENTINEL-2 APPLICATION TO THE SURFACE CHARACTERIZATION OF SMALL WATER BODIES IN WETLANDS 30

2.1 INTRODUCTION 31
2.2 MATERIALS AND METHODS 32
2.2.1 STUDY AREA 32
2.2.2 IMAGE PROCESSING 36
2.3 RESULTS 39
2.4 DISCUSSION 45
2.5 CONCLUSIONS 48
2.6 REFERENCES 49

3 CAPÍTULO 3: SENTINEL-2 ANALYSIS OF FLOODED AREAS: APPLIED CASE STUDY – LA SAFOR WETLAND, SPAIN 55

3.1 INTRODUCTION 56
3.2 MATERIALS AND METHODS 57
3.2.1 STUDY AREA 57
3.2.2 IMAGE PROCESSING 59
3.3 RESULTS AND DISCUSSION 59
3.4 CONCLUSION 63
3.5 REFERENCES 64

4 CAPÍTULO 4: REMOTE SENSING TEMPORAL RECONSTRUCTION OF THE FLOODED AREA IN "TABLAS DE DAIMIEL" INLAND WETLAND 2000–2021 66

4.1 INTRODUCTION 67
4.2 MATERIALS AND METHODS 69
4.2.1 STUDY AREA 69
4.2.2 IMAGE PROCESSING 70
4.3 RESULTS 75
4.4 DISCUSSIONS 82
4.5 CONCLUSIONS 85
4.6 APPENDIX A 86
4.7 REFERENCES 89

5 CAPÍTULO 5: DISCUSIÓN 93

5.1 REFERENCIAS 97

6 CAPÍTULO 6: CONCLUSIONES Y FUTURA INVESTIGACIÓN 99

6.1 CONCLUSIONES 99
6.2 FUTURA INVESTIGACIÓN 100

INDICE DE FIGURAS

Figure 2.1. Wetlands location in the Valencian Region (East Spain). 33

Figure 2.2. Wetlands area according to the official delimitation of the protected area (Valencian Wetland Inventory). Spatial Reference System: European Terrestrial Reference System1989, UTM coordinates Zone 30S. 39

Figure 2.3. Overall accuracy of tested indexes at different thresholds. 41

Figure 2.4. Kappa index of tested indexes at different thresholds. 41

Figure 2.5. Delimited water bodies in two wetlands are represented: (1) Safor wetland 2017 and (2) Prat Cabanes-Torreblanca wetland 2018. A: orthophoto, B: NDWI index (threshold −0.30), C: mNDWI index (threshold −0.35), D: CEDEX index (threshold +0.4), E: Re-NDWI (threshold −0.15), F: Awei sh index (threshold −1500), G: Awei nsh index (threshold −3000) and H: NDWI/BLUE-NIR index (threshold −0.45). 42

Figure 2.6. Overall accuracy of NDWI index tested at four studies areas and 3 years for the threshold range (−0.50 to 0.50). 43

Figure 2.7. Kappa index of NDWI index tested at four studies areas and 3 years for the threshold range (−0.50 to 0.50). 43

Figure 2.8. Delimited wetland bodies of water in blue color outline (A, C, E, G) versus the result of the NDWI index for the threshold −0.30 in light blue (B, D, F, H). Water sampling points in yellow and non-water in red. False negatives and false positives are marked. Figure A–B: Prat Cabanes-Torreblanca wetland (2018), Figure C–D: Sagunto wetland (2017), Figure E–F: La Safor wetland (2017) and figure G–H: Pego-Oliva wetland (2018). 44

Figure 2.9. Delimited water bodies with the NDWI index in Safor wetland. 46

Figure 3.1. Study area location. The red triangle is the Xeraco town meteorological station. 57

Figure 3.2. Land uses and municipality limits in the La Safor wetland. 58

Figure 3.3. Aerial image, 1956. Marked in yellow is the channel “Escorredor de Xeresa”. 59

Figure 3.4. LIDAR-derived digital elevation model 60

Figure 3.5. La Safor wetland: (a) Natural colour image and NDWI mask, January 16, 2017. 61
Figure 3.6. In yellow: fire area burned on November 9, 2016 the in La Safor wetland. 62
Figure 4.1. Study area including the perimeter of the Tablas de Daimiel National Park (blue polygon), gauging stations (red points), piezometers (black points), rivers (cyan lines) and municipalities in which the studied wetland is located (black polygons). 70
Figure 4.2. Overall accuracies for a set of thresholds applied to the Landsat-5 (a), Landsat-8 (b) and Sentinel-2 images (c). Light shaded colors show the indices and thresholds with poorest performance. Shaded in red color are used for indices and thresholds with the most accurate (closer to 1). 77
Figure 4.3. Water Surface Anomaly Index (IAW) and Precipitation Anomaly Index (IAP) in the period 2001-2010 (a) and 2011 – 2021 (b). 78
Figure 4.4. Water Surface Anomaly Index (IAW) and Flow Anomaly Index (IAF) in the period 2001-2010 (a) and 2011 – 2021 (b). 80
Figure 4.5. Water Surface Anomaly Index (IAW) and Piezometric Anomaly Index (IAPZ) in the period 2009 – 2021. 81
Figure 4.6. Comparison between water areas derived from Landsat-8 and Sentinel-2A/B images in the period 2015 - 2021. 81
Figure 4.7. Water bodies in the Tablas de Daimiel National Park delimited according to the mNDWI spectral index. Landsat-5 TM images (threshold −0.15): (A) September 2008, (B) April 2009, (C) July 2009, (D) November 2009, (E) January 2010, (F) May 2010, (G) July 2010, (H) December 2010, (I) February 2011, (J) April 2011, (K) July 2011, and (L) October 2011. 83
Figure 4.8. Water bodies in the Tablas de Daimiel National Park delimited according to the mNDWI Landsat-8 OLI images; (**A**) March 2021, (**B**) April 2021, (**C**) August 2021, and (**D**) October 2021. spectral index for Landsat-8 OLI (threshold −0.25) and NDWI for Sentinel-2 A/B (threshold −0.20). Sentinel-2 A/B images: (**E**) March 2021, (**F**) April 2021, (**G**) August 2021, and (**H**) October 2021. 85

INDICE DE TABLAS

Tabla 1.1. Relación de capítulos de la tesis y su respectivo artículo científico. 26

Table 2.1. Annual precipitation data (mm) and location of meteorological stations. Available in: http://riegos.ivia.es/datos-meteorologicos 34

Table 2.2. Natura 2000 Habitat types present in the study areas according to the European Union (EU) Habitats Directive Annex I classification (source: https://eunis.eea.europa.eu/index.jsp). Empty cell means the habitat is not present in that wetland. 35

Table 2.3. List of images used in the study by date. 36

Table 2.4. Calculated spectral indices. 37

Table 4.1. Calculated spectral indices. 72

Table 4.2. Spearman coefficient values among anomaly indices. 79

Table A.1 List of images used in the study by date. 86

1 CAPÍTULO 1: INTRODUCCIÓN

1.1 LOS HUMEDALES Y LOS SERVICIOS ECOSISTÉMICOS

Los humedales son recursos naturales valiosos que brindan muchos servicios ecosistémicos. Por lo tanto, cartografiar los humedales y obtener mapas precisos es de crucial importancia para preservar las funciones del ecosistema proporcionadas por estos elementos (Knight et al., 2013; Mahdavi et al., 2018).

Los servicios de los ecosistemas son activos naturales producidos por el medio ambiente y utilizados por los seres humanos, como aire, agua y alimentos (Maltby y Acreman, 2011). Los servicios de los ecosistemas de humedales se pueden categorizar de varias maneras. Inicialmente los valores de los humedales se clasificaron en tres niveles de jerarquía biológica: población, ecosistema y global (Mitsch y Gosselink, 2015). A nivel de población los valores incluyen aquellos relacionados con poblaciones ecológicas específicas (por ejemplo, provisión de hábitats para aves, peces, etc.). A nivel de ecosistemas se refiere a valores que requieren del ecosistema completo (por ejemplo, mejorar la calidad del agua, mitigar los daños causados por tormentas e inundaciones, recargar los acuíferos, etc.). A nivel global se incluyen los valores que influyen en el mantenimiento de la calidad del agua y el aire en una escala mucho más amplia (por ejemplo, ciclos regionales del carbono). Con la publicación de la Evaluación de los Ecosistemas del Milenio (Millenium Ecosystem Assessment, 2005) surgió una clasificación alternativa que, en términos generales, son valores de aprovisionamiento, de regulación, culturales y de apoyo (Maltby y Acreman, 2011; Mitsch et al., 2015). Los servicios ecosistémicos de aprovisionamiento incluyen productos obtenidos de los ecosistemas. Los de regulación incluyen la regulación de la calidad del aire, la regulación del clima, la purificación del agua, la regulación de enfermedades, la regulación de peligros naturales, etc. Los culturales incluyen los beneficios que las personas obtienen relacionados con la recreación, el ecoturismo, la educación formal e informal, el patrimonio cultural, etc. Los de apoyo incluyen los procesos ecosistémicos básicos del ciclo de nutrientes y la productividad primaria que, a su vez, pueden dar lugar a los otros tres servicios enumerados anteriormente (Maltby y Acreman, 2011; Mitsch et al., 2015).

Existe una ambigüedad frecuente entre la comunidad científica en cuanto a qué constituye exactamente un “humedal”. El predominio del agua, al menos periódicamente,

es la característica definitoria de los humedales (Maltby y Acreman, 2011; Mitsch et al., 2015). La Convención de Ramsar sobre Humedales de Importancia Internacional adoptó una definición inclusiva: "áreas de marismas, pantanos, turberas o aguas, sean naturales o artificiales, permanentes o temporales, estancadas o corrientes, dulces, salobres o saladas, incluidas las extensiones de agua marina, cuya profundidad en marea baja no exceda de seis metros" (Davis, 1993). Cualesquiera que sean los conflictos de opinión, existen al menos tres características de los humedales que, por separado o en conjunto, pueden considerarse diagnósticas (Maltby y Acreman, 2011):

1. La presencia predominante y la dinámica del agua ya sea en o sobre la superficie o dentro de la zona de raíces.

2. Condiciones únicas de suelo o sedimentos que difieren de las áreas adyacentes que no son humedales (terrestres o completamente acuáticas).

3. Vegetación (y generalmente animales) adaptada específicamente a condiciones húmedas permanentes o estacionales.

La variación en los regímenes hidrológicos, que determina en gran medida la estructura, procesos y funcionamiento, da como resultado una amplia gama de tipos de ecosistemas de humedales. Aunque se ha realizado un esfuerzo considerable en el desarrollo de clasificaciones de humedales nacionales y regionales, el único intento de establecer un sistema global fue bajo los auspicios de la Convención de Ramsar (Maltby y Acreman, 2011; Mitsch et al., 2015). La Convención estableció un Sistema de Clasificación de Tipos de Humedales que identifica 42 tipos agrupados en 3 categorías principales: marinos y costeros, continentales y artificiales (Ramsar, 2016). Así pues, una determinada zona húmeda se identifica con un tipo principal de humedal según su predominancia, pero puede tener presentes más de un tipo, siendo esto lo más común. A nivel mundial, esta clasificación de humedales es la más utilizada (Semeniuk y Semeniuk, 1997). La tipología de los humedales brinda información importante tanto para los administradores de los recursos hídricos como para los planificadores de la conservación. Uno de los objetivos más importantes de asignar humedales a un cierto tipo o clase es proporcionar información sobre los servicios ecosistémicos que proporciona el humedal (Sieben et al., 2018). El sistema de clasificación de arriba hacia abajo más utilizado asigna humedales en unidades hidrogeomórficas, que funcionan como una sola unidad en términos de hidrología y geomorfología (Sieben et al., 2018). Este tipo de clasificación

es más útil para la planificación de los recursos hídricos, ya que proporciona información sobre cómo está conectado el humedal a la red de drenaje y cuáles son las entradas, salidas y salidas de agua del humedal (Sieben et al., 2018). A gran escala, la mayoría de los servicios ecosistémicos pueden derivarse superficialmente del tipo de unidad hidrogeomórfica y la forma en que el agua se mueve a través de un humedal (Sieben et al., 2018).

La relación de los humedales con el ciclo del agua es muy relevante para preocupaciones sociales más amplias, como los problemas de asignación alternativa de recursos hídricos, la calidad del agua y el riesgo de inundación. Cuestiones polémicas que rigen la gestión de un recurso por el que existe una competencia intensa y una incertidumbre cada vez mayor debido al cambio climático (McCartney y Acreman, 2009).

En los países desarrollados, el desarrollo económico ha llevado a una gran pérdida de humedales. La transformación de los humedales ha dado lugar a la prestación de otros servicios, como la producción de alimentos a partir de tierras de cultivo, y no servicios, como el uso residencial o industrial. Esto ha requerido una alteración hidrológica fundamental para preservar estos usos. Así por ejemplo en algunos humedales se llega a bombear importantes caudales de la reserva de agua dulce para verterlos al mar con el fin de disminuir el nivel freático o la lámina inundada (Sebastiá-Frasquet et al., 2014; Sebastiá-Frasquet et al., 2012). Esto se hace con el fin de evitar la asfixia radicular de cultivos que no toleran condiciones de inundación (por ejemplo, cítricos) o para evitar la inundación de zonas urbanizadas o con otros usos terciarios como el camping (Sebastiá-Frasquet et al. 214). Esta práctica conlleva riesgos ya que las modificaciones pueden hacer más vulnerables estos ecosistemas a fenómenos extremos o los efectos del cambio climático (Maltby y Acreman, 2011). Además, las propiedades de los humedales que los hacen atractivos en primer lugar para usos alternativos pueden depender del mantenimiento de un determinado régimen hidrológico. La gestión a largo plazo de los humedales es esencial y requiere apoyo institucional, por ejemplo, a través de instrumentos legales que faciliten la convivencia sostenible de usos (Maltby y Acreman, 2011; Sebastiá-Frasquet et al., 2014).

Para que esta gestión a largo plazo sea exitosa es fundamental satisfacer las necesidades reales de información de los organismos y los usuarios que inciden en la conservación y el uso racional de los humedales. Esta información requiere de tecnologías

y procedimientos que permitan monitorear el cambio ecológico en los humedales seleccionados y debe de permitir la actualización periódica dada la alta variabilidad intrínseca de estos ecosistemas (Rapinel et al., 2019). En los últimos años una gran cantidad de estudios científicos han abordado la cartografía y monitoreo de hábitats naturales a través del usos de datos de sensores remotos y la obtención de indicadores sobre su estado de conservación (Mahdavi et al., 2018; Mahdianpari et al., 2020; Rapinel et al., 2019). Una de las variables cuyo seguimiento es clave es la superficie libre de lámina de agua o superficie inundada dada la importancia como sostén de servicios ecosistémicos. Sin embargo, cabe destacar que, de las 3 categorías principales de humedales establecidas por Ramsar, se identifican una serie de subtipos que se caracteriza por su tamaño, morfología, vegetación y período de permanencia de la lámina de agua. Concretamente:

Para humedales continentales:

- Ríos/ arroyos permanentes
- Pantanos/ charcas permanentes de agua dulce
- Lagos permanentes de agua dulce
- Pantanos/ esteros/ charcas estacionales/ intermitentes de agua dulce en suelos inorgánicos
- Turberas permanentes no arboladas
- Humedales boscosos de agua dulce
- Ríos/ arroyos estacionales/ intermitentes/ irregulares
- Pantanos con vegetación arbustiva
- Turberas arboladas permanentes
- Lagos estacionales/ intermitentes de agua dulce
- Manantiales permanentes de agua dulce, oasis
- Pantanos/ esteros/ charcas estacionales/ intermitentes salinos/ salobres/ alcalinos
- Pantanos/ esteros/ charcas permanentes salinas/ salobres/ alcalinos
- Lagos permanentes salinos/ salobres/ alcalinos

- Lagos y zonas inundadas estacionales/ intermitentes salinos/ salobres/ alcalinos
- Deltas interiores permanentes
- Sistemas kársticos y otros sistemas hídricos subterráneos
- Pantanos/ esteros/ charcas permanentes de agua dulce
- Humedales de montaña

Humedales marinos o costeros

- Playas de arena o de guijarros
- Aguas marinas someras permanentes
- Pantanos y esteros intermareales
- Bajos intermareales de lodo, arena o con suelos salinos
- Lagunas costeras salobres/ saladas
- Estuarios
- Humedales intermareales arbolados
- Lechos marinos submareales (vegetación subacuática)
- Costas marinas rocosas
- Lagunas costeras de agua dulce
- Arrecifes de coral
- Sistemas kársticos y otros sistemas hídricos subterráneos
- Arrecifes de bivalvos (mariscos)

Humedales artificiales

- Canales de transportación y de drenaje
- Tierras agrícolas inundadas estacionalmente
- Áreas de almacenamiento de agua
- Tierras de regadío
- Estanques artificiales

- Estanques de acuicultura
- Zonas de explotación de sal
- Excavaciones
- Áreas de tratamiento de áreas residuales
- Sistemas hídricos subterráneos artificiales

Tal y como se ha explicado anteriormente, una zona húmeda suele identificarse con un tipo principal, pero suele tener representación de varios subtipos que por sus características de tamaño principalmente presente una dificultad añadida para el seguimiento del estado de estos ecosistemas (Gallant, 2015). Esto es especialmente relevante en regiones áridas y semiáridas (Kolarik et al., 2023), las cuales se ven frecuentemente afectadas por sequías, y esto provoca un uso más intensivo de las aguas subterráneas que agrava los problemas ocasionados por la ausencia de precipitaciones. En consecuencia, los cuerpos de agua se desconectan y se caracterizan por tamaños más pequeños que en otros climas, siendo la resolución espacial un parámetro clave para la aplicación de los datos de sensores remotos (Perin et al., 2022). Según Huang et al. (2014) en ambientes áridos, semiáridos y mediterráneos, alrededor del 30% de los humedales estacionales incluidos en la lista de Ramsar son pequeños, con un tamaño mínimo de 10 ha, y con una distribución irregular de los cuerpos de agua en forma de pequeños parches.

Un ejemplo representativo del pequeño tamaño de los parches de agua se puede observar debido al alto grado de antropización de estos ecosistemas y su modificación para hacer posibles determinados usos agrícolas no compatibles con la inundación. Es este el caso de los humedales costeros mediterráneos en lo que actualmente convive el cultivo citrícola, para evitar el encharcamiento de sus raíces y la consiguiente pérdida de productividad, una práctica habitual era elevar el terreno por franjas excavando para ello las franjas adyacentes para extraer el material edáfico (Sebastiá-Frasquet et al., 2014). Como resultado se observan franjas de agua libre al aflorar las aguas subterráneas en estas zonas excavadas, junto a franjas donde el terreno está más elevado (Sebastiá-Frasquet et al., 2014). Aunque esta práctica hoy en día no se realiza, se observan en el paisaje sus consecuencias, tal y como se ilustra en las siguientes fotografías.

Fotografía 1 Parcela de cítricos elevada junto a masa de agua libre en parcela excavada, Marjal de La Safor (Valencia, España). Fuente: elaboración propia.

Fotografía 2 Parcela de cítricos elevada junto a acequia en la Marjal de La Safor Safor (Valencia, España). Fuente: elaboración propia.

1.2 TELEDETECCIÓN PARA EL SEGUIMIENTO DE HUMEDALES CON MASAS DE AGUA DE REDUCIDO TAMAÑO

Tal y como se ha expuesto en el anterior apartado contar con herramientas y metodologías que puedan proporcionar información fiable y periódica a los gestores de los humedales es necesario para hacer una gestión consciente e informada de estos espacios. En este sentido las herramientas de teledetección, que incluye el uso de cualquier dato de Observación de la Tierra (EO), como fotos aéreas, imágenes satelitales o tecnología LiDAR, son la apuesta de la comunidad científica en los últimos años para poder obtener información más exhaustiva que la proporcionada por las tradicionales medidas in situ (Mahdavi et al., 2018; Mahdianpari et al., 2020; Rapinel et al., 2019). Los métodos in situ son inviables dado el costo y los requisitos de tiempo, así como las dificultades de acceso a muchos humedales, dado que gran cantidad de humedales se encuentran en áreas remotas, donde la topografía, la cubierta vegetal y la hidrología hacen que las visitas de campo sean desafiantes y costosas (Mahdavi et al., 2018).

Un método común para la delimitación de humedales es la interpretación de imágenes aéreas, que fue el primer método de teledetección empleado para cartografiar humedales (Mahdavi et al., 2018). Las imágenes aéreas suelen tener una resolución espacial más alta en comparación con las imágenes de satélite y, en consecuencia, permiten el reconocimiento de humedales pequeños o angostos (Mahdavi et al., 2018). Sin embargo, la aplicación de imágenes aéreas para el monitoreo de humedales no es una solución de bajo coste, los recursos disponibles de forma gratuita tienen una baja periodicidad y dependiendo del área de la zona húmeda puede consumir más tiempo en comparación con la aplicación de imágenes de satélite. En esta tesis las imágenes aéreas libres se utilizan para contrastar los resultados obtenidos a través del análisis de imágenes satelitales.

El modelo digital de elevaciones (DEM) obtenido de imágenes LiDAR puede generar resoluciones espaciales de hasta 15–30 cm y ha sido utilizado para distinguir clases de humedales, o para encontrar la distribución y ubicación de los humedales a partir de las características topográficas extraídas del DEM (Huang et al., 2014; Mahdavi et al., 2018). Además, los DEM también se pueden incluir en el procedimiento para obtener cartografía de humedales para corregir las áreas de clasificación errónea como resultado de la escala y el sombreado (Huang et al., 2014; Mahdavi et al., 2018).

La evolución de la resolución espacial y temporal de los sensores remotos, y en particular de los sensores con datos de acceso abierto permite afrontar el reto de cartografiar con mayor precisión y periodicidad estos ecosistemas altamente variables.

Los datos de teledetección de los satélites Landsat (Landsat 5 (TM), Landsat 7 (ETM+) y Landsat 8 (OLI)) se han utilizado ampliamente desde el lanzamiento de Landsat (TM) en 1984. Sin embargo su resolución espacial de 30 m lo hace útil para humedales que tengan más de 1 ha (Perin et al., 2022).

El satélite Sentinel-2 lanzado por la Agencia Espacial Europea (ESA) en 2015 incluye una constelación de dos satélites en órbita polar con una resolución temporal de 5 días y una resolución espacial máxima de 10 m. La resolución más alta de Sentinel-2, tanto espacial como temporal, puede mejorar significativamente el rango de monitoreo, especialmente para sitios pequeños que no pueden ser cubiertos por el satélite Landsat (Zhang et al., 2022).

Para realizar una adecuada gestión de los humedales, es esencial disponer de series temporales lo suficientemente largas que permitan observar el efecto de las medidas aplicadas sobre el ciclo hidrológico. Dado que los datos de Sentinel-2 actualmente ofrecen una serie de datos todavía corta (2015- 2023), es de gran interés estudiar la correlación entre los datos obtenidos a partir de estos Sentinel-2 y Landsat, con la finalidad de poder construir series temporales más largas.

A partir de las imágenes obtenidas de Sentinel-2 y Landsat, podemos extraer píxeles de agua a través de diferentes metodologías, una de las más utilizadas son los índices de agua porque son más reproducibles y por lo tanto más generalizables (Doña et al., 2021). Al seleccionar el umbral apropiado para estos índices, los píxeles de la imagen se pueden categorizar en agua o no agua, y se pueden cartografiar las condiciones de inundación de los humedales.

1.3 OBJETIVOS Y ALCANCE DE LA TESIS

Esta tesis tiene como objetivo principal extraer cartografía de masas de agua libre en humedales utilizando imágenes de satélite a partir del análisis de siete índices de agua (NDWI, mNDWI, Cedex, Re-NDWI, Awei(sh), AWEI (nsh) y B_Blue) y de un conjunto de umbrales que aplicados sobre ellos permiten extraer las zonas inundadas. Para ello, se utilizaron imágenes satelitales Sentinel-2, Landsat-5 TM, Landsat-8 OLI en dos zonas:

humedales mediterráneos costeros (Prat Cabanes-Torreblanca, Marjal de Sagunto, Marjal de La Safor y Marjal Pego-Oliva) y el humedal de llanura aluvial situado en el centro de España, las Tablas de Daimiel. Los resultados que se esperan obtener de esta tesis permitirán monitorizar las masas de agua libre de los diferentes humedales y dotar de herramientas basadas en información espectral para su vigilancia. Estas pueden permitir a las administraciones públicas elaborar nuevos estudios y políticas sobre las diferentes problemáticas en los humedales, teniendo en cuenta la repercusión de las medidas de gestión sobre la lámina de agua libre.

Los objetivos específicos de esta investigación son los siguientes:

- Comparar el rendimiento de índices de agua obtenidos a partir de imágenes de satélite en diferentes humedales y fechas, con diferentes sensores.
- Calcular el índice de anomalía de la superficie agua para monitorizar las masas de agua en humedales.
- Analizar los efectos de la superficie inundada sobre los usos del suelo mediante imágenes Sentinel-2.
- Comparar el uso de imágenes satelitales Sentinel-2 y Landsat-8 en la determinación de masas de agua libre en humedales.
- Evaluar la correlación entre las anomalías de la superficie de agua y las anomalías de parámetros climáticos (precipitación) e hidrológicos (nivel piezométrico del acuífero y caudal del río) a través del cálculo de índices de anomalía.

1.4 ESTRUCTURA DE LA TESIS

Esta tesis se presenta como un compendio de artículos. La memoria de la tesis se estructura en 6 capítulos:

- Capítulo 1: se hace una introducción que incluye la relevancia de los humedales y los servicios ecosistémicos que sustentan, dependientes en gran medida de la lámina de agua, y por tanto la importancia de monitorear esta. También se aborda el estado del arte del uso de la teledetección para su estudio.
- Capítulo 2 al capítulo 4: se presentan 3 estudios basados en el uso de la teledetección para detectar masas de agua libre en humedales y sus aplicaciones. Estos estudios contienen la versión de autor, que fueron enviados a diferentes

revistas de reconocido prestigio y sometidos a revisión por pares. En la tabla 1.1 se detallan estos artículos y su estado actual.

- Capítulo 5: discusión general de los resultados obtenidos durante estas investigaciones.
- Capítulo 6: las conclusiones obtenidas y las futuras líneas de investigación propuestas.

Tabla 1.1. Relación de capítulos de la tesis y su respectivo artículo científico.

Capítulo	Título del artículo	Autores	Revista	Indexación	Estado
2	Sentinel-2 Application to the Surface Characterization of Small Water Bodies in Wetlands.	Pena-Regueiro, J.; Sebastiá-Frasquet , M.T.; Estornell, J.; Aguilar-Maldonado, J.A.	Water ISSN 2073-4441	Q1 JCR Hydrology Factor de impacto: 3,103 (año 2020)	Publicado en 2020 Volumen 12, Nº 5 Página 1487
3	Sentinel-2 analysis of flooded areas: applied case study “La Safor wetland, Spain”.	Pena-Regueiro, J.; Sebastiá-Frasquet, M.T.; Aguilar-Maldonado, J.A.; Estornell Cremades, J.; Sanchís Blay, J.A.; Morell-Monzó, S.; Altur Grau, V.	WIT Transactions on Ecology and the Environment (Online) ISSN: 1743-3541	SCOPUS Factor de impacto: SJR 0.180/ SNIP 0.320 (año 2020)	Publicado en 2020 Volumen 242, Páginas 63-70
4	Remote Sensing Temporal Reconstruction of the Flooded Area in “Tablas de Daimiel” Inland Wetland 2000–2021	Pena-Regueiro, J.; Estornell Cremades, J.; Aguilar-Maldonado, J.A; Sebastiá-Frasquet, M.T	Sensors ISSN 1424-8220	Q2 JCR Factor de impacto: 3,847 (año 2021)	Publicado en 2023 Volumen 23, Nº 8 Página 4096

1.5 REFERENCIAS

1. Brinson, Mark M. 1993. A hydrogeomorphic classification for wetlands. Technical Report (Wetlands Research Program (U.S.)); no. Technical Report WRP-DE-4. 103 pages. Publisher U.S. Army Engineer Waterways Experiment Station. https://erdc-library.erdc.dren.mil/jspui/handle/11681/6483
2. Davis, T.J. 1993. Towards the wise use of wetlands, Gland: Switzerland: Ramsar Convention Bureau.
3. Doña, C., Morant, D., Picazo, A., Rochera, C., Sánchez, J. M., Camacho, A. 2021. Estimation of Water Coverage in Permanent and Temporary Shallow Lakes and Wetlands by Combining Remote Sensing Techniques and Genetic Programming: Application to the Mediterranean Basin of the Iberian Peninsula. Remote Sensing, 13(4), 652.
4. Franklin, S. E. y Ahmed, O. S. 2017. Object-Based Wetland Characterization Using Radarsat-2 Quad-Polarimetric SAR Data, Landsat-8 OLI Imagery, and Airborne Lidar-Derived Geomorphometric Variables. Photogrammetric Engineering & Remote Sensing 83: 27–36. https://doi.org/10.14358/PERS.83.1.27
5. Gallant, A. 2015. The challenges of remote monitoring of wetlands. Remote Sensing, 7(8), 10938-10950. https://doi.org/10.3390/rs70810938.
6. Huang, C., Peng, Y., Lang, M., Yeo, I.-Y., McCarty, G. 2014. Wetland inundation mapping and change monitoring using Landsat and airborne LiDAR data. Remote Sensing of Environment, 141, 231–242. http://dx.doi.org/10.1016/j.rse.2013.10.020
7. Knight, J. F., Tolcser, B. P., Corcoran, J. M., Rampi, L. P. 2013. The effects of data selection and thematic detail on the accuracy of high spatial resolution wetland classifications. Photogrammetric Engineering & Remote Sensing, 79(7), 613–623.
8. Kolarik, N. E., Roopsind, A., Pickens, A., Brandt, J.S. 2023. A satellite-based monitoring system for quantifying surface water and mesic vegetation dynamics in a semi-arid region. Ecological Indicators, 147, 109965. https://doi.org/10.1016/j.ecolind.2023.109965
9. Mahdavi, S., Salehi, B., Granger, J., Amani, M., Brisco, B., Huang, W. 2018. Remote sensing for wetland classification: A comprehensive review. GIScience

& Remote Sensing, 55(5), 623–658. https://doi.org/10.1080/15481603.2017.1419602

10. Maltby, E. and Acreman, M.C. 2011. Ecosystem services of wetlands: pathfinder for a new paradigm. Hydrological Sciences Journal, 56 (8), 1341–1359. https://doi.org/10.1080/02626667.2011.631014
11. Mahdianpari, M., Granger, J. E., Mohammadimanesh, F., Salehi, B., Brisco, B., Homayouni, S.,Gill, E., Huberty, B., Lang, M. 2020. Meta-analysis of wetland classification using remote sensing: A systematic review of a 40-year trend in North America. Remote Sensing, 12(11), 1882. https://doi.org/10.3390/rs12111882
12. McCartney, M.P. y Acreman, M.C. 2009. Water resources and wetlands. In The wetlands handbook, Edited by: Maltby, E. and Baker, T. Oxford: Wiley-Blackwell.
13. Millennium Ecosystem Assessment. 2005. Ecosystems and human well-being: synthesis. Washington, DC: Island Press.
14. Mitsch, W.J., Bernal, B., Hernandez, M.E. 2015. Ecosystem services of wetlands, International Journal of Biodiversity Science, Ecosystem Services & Management, 11:1, 1–4, https://doi.org/10.1080/21513732.2015.1006250
15. Mitsch WJ, Gosselink JG. 2015. Wetlands. 5th ed. Hoboken,NJ: JohnWiley&Sons,Inc.
16. Perin, V., Tulbure, M.G., Gaines, M.D., Reba, M.L., Yaeger, M.A. 2022. A multi-sensor satellite imagery approach to monitor on-farm reservoirs. Remote Sensing of Environment, 270, 112796. https://doi.org/10.1016/j.rse.2021.112796
17. Ramsar, 2016. Introducción a la Convención sobre los Humedales, Secretaría de la Convención de Ramsar, Gland, Suiza.
18. Rapinel, S., Fabre, E., Dufour, S., Arvor, D., Mony, C., Hubert-Moy, L. 2019. Mapping potential, existing and efficient wetlands using free remote sensing data. Journal of environmental management, 247, 829–839. https://doi.org/10.1016/j.jenvman.2019.06.098
19. Scott, D.A., Jones, T.A. 1995. Classification and inventory of wetlands: A global overview. Vegetatio 118, 3–16. https://doi.org/10.1007/BF00045186
20. Sebastiá-Frasquet, M.-T.; Altur Grau, V.J.; Sanchís Blay, J.A. 2014. Wetland Planning: Current Problems and Environmental Management Proposals at Supra-

Municipal Scale (Spanish Mediterranean Coast). Water, 3 (6), 620–641. https://doi.org/10.3390/w6030620

21. Sebastiá-Frasquet, M.T., Rodilla, M., Sanchís Blay, J.A., Altur Grau, V.J., Gadea Perez, M.I., Falco Giaccaglia, S.L. 2012. Influence of nutrient inputs from a wetland dominated by agriculture on the phytoplankton community in a shallow harbour at the Spanish Mediterranean coast. Agriculture Ecosystems & Environment, 3 (152), 10–20. https://doi.org/10.1016/j.agee.2012.02.006
22. Semeniuk, C.A., Semeniuk, V. 1995. A geomorphic approach to global classification for inland wetlands. In: Finlayson, C.M., van der Valk, A.G. (eds) Classification and Inventory of the World's Wetlands. Advances in Vegetation Science, 16. Springer, Dordrecht. https://doi.org/10.1007/978-94-011-0427-2_9
23. Semeniuk, V., Semeniuk, C. 1997. A geomorphic approach to global classification for natural inland wetlands and rationalization of the system used by the Ramsar Convention – a discussion. Wetlands Ecology and Management 5, 145–158. https://doi.org/10.1023/A:1008207726826
24. Sieben, E.J.J., Khubeka, S.P., Sithole, S. et al. 2018. The classification of wetlands: integration of top-down and bottom-up approaches and their significance for ecosystem service determination. Wetlands Ecology and Management 26, 441–458. https://doi.org/10.1007/s11273-017-9585-4
25. Zhang, L., Hu, Q., Tang, Z. 2022. Using Sentinel-2 Imagery and Machine Learning Algorithms to Assess the Inundation Status of Nebraska Conservation Easements during 2018–2021. Remote Sensing, 14(17), 4382.

2 CAPÍTULO 2:
SENTINEL-2 APPLICATION TO THE SURFACE CHARACTERIZATION OF SMALL WATER BODIES IN WETLANDS

Pena-Regueiro, J., Sebastiá-Frasquet, M.-T., Estornell, J. & Aguilar-Maldonado, J.A. 2020. Sentinel-2 application to the surface characterization of small water bodies in wetlands. *Water,* 12, 1487. https://doi.org/10.3390/w12051487

2.1 INTRODUCTION

Wetlands, and especially coastal wetlands, are listed amongst the most threatened ecosystems suffering from anthropogenic activities [1]. These ecosystems provide a wide range of ecosystem services. Among others, they are an important freshwater reserve and a source for ground water recharge, and in coastal areas they provide defence against marine intrusion. Wetland hydrologic regime (e.g., flooded area and flooding duration) has a direct effect on nutrient dynamics at a watershed scale, but it also impacts greenhouse gas emissions and carbon cycles in the wetlands themselves [2]. The crucial role of flooding extent to wetland functioning and carbon storage has been underlined by several studies [3]. The spatial and temporal variation in flooded areas can be high, and it is due to hydrological processes (e.g., precipitation, evapotranspiration), but also to human activities [3]. Impacts on hydrological processes can affect other ecosystems functions such as groundwater recharge and nutrient cycling [4] or species distributions and composition [5]. So, monitoring spatial-temporal dynamics of flooded areas is both important for water management and biodiversity conservation [6].

In recent years, monitoring programs relied on in situ detectors to collect data used by regulatory agencies and research institutions. However, gauge measurements offer little information about spatial patterns like flooding status [6,7]. On the other side, remotely sensed data can provide spatial maps with different accuracy depending on the sensor [7]. Remote sensing has already proved to be a useful tool to acquire spatial and temporal information about wetlands [8,9] and it has the potential to provide the information needed for accurate wetland inventory, assessment, and monitoring [5]. Detection and analysis of wetlands using satellite images are based mainly on supervised and unsupervised classification and the definition of water indices and their subsequent classification using thresholds [10,11]. For supervised classification, several algorithms can be found such as random forest [12], support vector machines [13], and artificial neural networks [14]. The development of Earth Observation (EO) satellites of high spatial resolution and the emergence of Unmanned Aerial Vehicle (UAV) contributed to the definition of new approaches to map wetlands at sub-meter scale such as object-oriented algorithms [15]. The high resolution of images registered by UAVs allow to monitor and to extract the flooding surface with detail and to develop ecological indicators [16].

For the approach based on water indices, a simple global threshold can be applied to classify water pixels using atmospherically corrected satellite images of different data and places [17]. Images from satellite sensor of low spatial resolution such as AVHRR (Advanced Very High Resolution Radiometer) and MODIS (Moderate Resolution Imaging Spectroradiometer) have been used to monitor flood extent by differentiating flooded/non-flooded or mixed pixels [6,7]. Studies using these sensors focused mainly on relatively large wetlands covering at least 50 km2, and to a lesser extent to smaller wetlands (<25 km2) [7]. Other sensors with higher spatial resolution, such as those on-board Landsat MSS/TM/ETM+and SPOT, have been used for smaller wetlands monitoring [3]. The coarser spatial resolution sensors have the advantage of a higher temporal resolution and more frequent observations than higher spatial resolution sensors. According to Huang et al. [7] in arid, semi-arid, and Mediterranean environments, about 30% of Ramsar-listed seasonal wetlands are small-sized, with a minimum size of 10 ha, which can show a patchy distribution of water bodies. From 2015 onward, Sentinel-2A/B images are available (ESA), with high temporal resolution and bands of 10 m that allow to explore the suitability of these images to extract small-sized water bodies that cannot be mapped using Landsat and MODIS images.

In recent years, there is a growing interest in developing indicators to monitor environmental change in wetlands through remote sensing [18]. Some of the original constraints (e.g., insufficient spatial and temporal resolution) of this technique have been overcome with the last satellites launching. However, we still have the constraint of developing indicators that can be global, and non-specific for a type of wetland or location.

The aim of this study is to test Sentinel-2A/B images suitability for detecting small water bodies in wetlands characterized by high diversity of temporal and spatial flooding patterns using previously published indices.

2.2 MATERIALS AND METHODS

2.2.1 STUDY AREA

Mediterranean wetlands are ecosystems identified for priority protection by the European Union (EU) [19]. These ecosystems have been studied as prototypes of coastal wetlands where urban and agricultural pressure compete directly with

environmental water uses [20]. The Mediterranean is one of the regions with the highest pressure on wetlands, and especially in coastal areas [21,22]. We selected 4 representative coastal wetlands in the Valencia Region (East Spain, Mediterranean Sea), from North to South: Prat Cabanes-Torreblanca, Sagunto, Safor, and Pego-Oliva (Figure 2.1). These wetlands are included in both the Valencian Wetlands Inventory, and in the Spanish Wetlands Inventory (included in 2011 by Resolution of 9 March Dirección General de Medio Natural y Política Forestal (Spanish Official Gazette (BOE), Number 71, 24 March 2011)). Pego-Oliva and Prat Cabanes-Torreblanca are also declared Natural Parks. The importance of these wetlands is also recognized at international level, all of them are Special Protection Areas (SPAs) for birds and Sites of Community Importance (SCIs) (Habitats Directive, European Council Directive 92/43/EEC). In addition, Prat Cabanes-Torreblanca and Pego-Oliva are Ramsar Sites (Ramsar Convention).

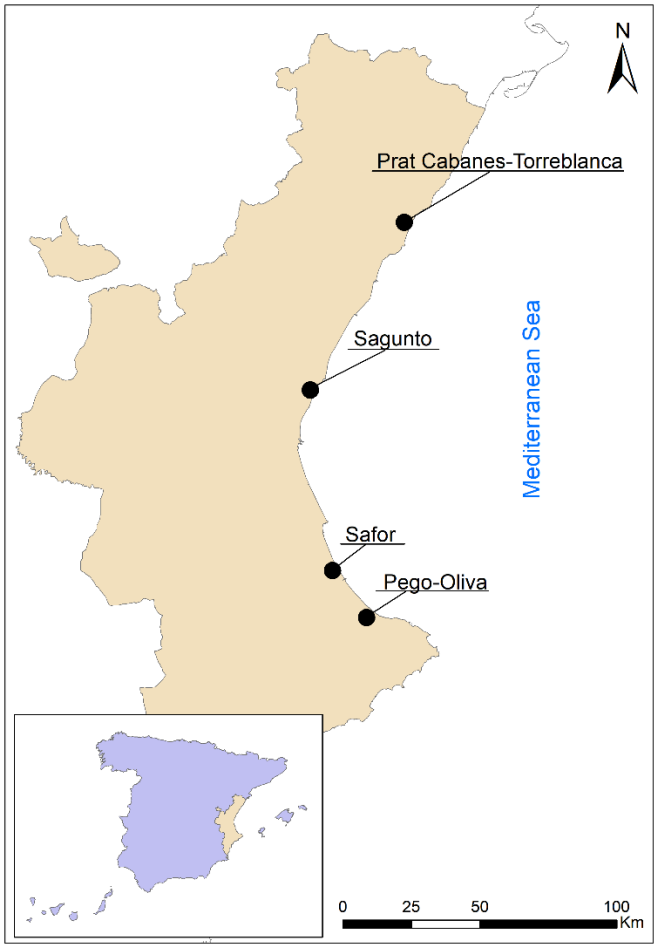

Figure 2.1. Wetlands location in the Valencian Region (East Spain).

These wetlands are set on detrital aquifers formed from the Quaternary fluvial sedimentation that filled the coastal plains and separated from the sea with beach barriers. Detrital aquifers are, in turn, fed by Mesozoic karstic aquifers in the near limestone reliefs. The wetlands are fed by groundwater discharges and depend on them to keep permanent surface of water [23]. Phreatic level is subject to seasonal variations but usually emerges very close to the surface. Groundwater upwelling creates water ponds, known as "ullals", in the wetland environment. The wetland discharge is mainly due to natural drainage to the sea through rivers and to groundwater pumping for several purposes. Specifically, the shallow phreatic level in these unconfined aquifers causes problems of root asphyxia to citrus crops and flooding of urban areas. To prevent this problem, freshwater from the aquifer is pumped into the sea through irrigation channels [24]. The cycle of the wetlands and the size of flooded areas is highly dependent on precipitation, which rapidly infiltrates in the karstic aquifers and discharges to the detrital aquifers [23,25]. However, anthropogenic management is also very important. The precipitation regime is characterized by a very marked seasonality, the highest rainfall in autumn, and secondarily in spring; during the summer there is a strong drought [26]. The average annual precipitation shows a spatial gradient, Pego-Oliva (southernmost area) annual average is 841.3 mm, while Prat Cabanes is 447 mm (northernmost area). Table 2.1 shows annual precipitation data from the closest meteorological station [27].

Table 2.1. Annual precipitation data (mm) and location of meteorological stations. Available in: http://riegos.ivia.es/datos-meteorologicos.

	Year			Coordinates	
Wetland	**2016**	**2017**	**2018**	**UTM X**	**UTM Y**
Prat Cabanes	231.09	414.74	200.54	768076.000	4447370.000
Sagunto	226.60	662.61	234.38	732200.000	4392210.000
Safor	285.29	791.36	405.74	738207.000	4316410.000
Pego-Oliva	380.57	924.31	360.97	767731.000	4298290.000

Water depth in the flooded areas of these wetland range from wet soil to 70 cm [28], only the "ullals" have higher depths. Table 2.2 shows the diversity of habitats present in

these wetlands and included in the EU Habitats Directive (Council Directive 92/43/EEC) according to the European Nature Information System [29].

Table 2.2. Natura 2000 Habitat types present in the study areas according to the European Union (EU) Habitats Directive Annex I classification (source: https://eunis.eea.europa.eu/index.jsp). Empty cell means the habitat is not present in that wetland.

Code	Annex I Habitat types	Prat Cabanes	Sagunto	Safor	Pego-Oliva
		Cover (ha)			
1150	Coastal lagoons	19.40	79.74		12.55
1410	Mediterranean salt meadows (*Juncetalia maritimi*)	97.00	46.49		150.60
1420	Mediterranean and thermo-Atlantic halophilous scrubs (*Sarcocornetea fruticosi*)	19.40	27.25		
1510	Mediterranean salt steppes (*Limonietalia*)		4.82		
3150	Natural eutrophic lakes with Magnopotamion or Hydrocharition -type vegetation			248.97	25.10
3160	Natural dystrophic lakes and ponds			186.73	12.55
3170	Mediterranean temporary ponds	19.40			
3280	Constantly flowing Mediterranean rivers with Paspalo-Agrostidion species and hanging curtains of *Salix* and *Populus alba*			62.24	25.10
5330	Thermo-Mediterranean and pre-desert scrub		0.35		125.5 0
6110	Rupicolous calcareous or basophilic grasslands of the Alysso-Sedion albi				25.10
6220	Pseudo-steppe with grasses and annuals of the Thero-Brachypodietea				62.75
6420	Mediterranean tall humid grasslands of the Molinio-Holoschoenion	194.00	0.37	62.24	150.60
6430	Hydrophilous tall herb fringe communities of plains and of the montane to alpine levels			62.24	12.55
7210	Calcareous fens with *Cladium mariscus* and species of the *Caricion davallianae*	388.00	133.60	622.43	

2.2.2 IMAGE PROCESSING

Sentinel-2A/B images processed at level 1C were obtained from Copernicus (https://scihub.copernicus.eu/dhus/#/home) and EarthExplorer (https://earthexplorer.usgs.gov). The atmospheric correction was done with Sen2Cor tool (version 02.05.05) using SNAP software (ESA, version 6.0.0). The following reference parameters were defined: aerosol and MID LAT (Auto); ozone (value 0, determined automatically by the processor); Bidirectional Reflectance Distribution Function (BRDF) correction (value 21, standard recommended value); BRDF lower (value 0.22, standard value of the lower limit of the correction factor BRDF); visibility (40 km, appropriate value for the Iberian Peninsula); altitude (2 m above sea level). Images of high spatial resolution were used for validation (Table 2.3) [11,30]. These images were obtained from the Valencian Cartography Institute (ICV) Orthophoto 2017 and 2018 CC BY 4.0 © Institut Cartogràfic Valencià, Generalitat (spatial resolution 0.25 m, http://www.icv.gva.es/va/) and Google Earth ©. The dates of these images were the closest to Sentinel-2A/B image acquisitions.

Table 2.3. List of images used in the study by date.

Wetland	Orthophoto		Sentinel-2A/B
	Data	Spatial Resolution	Data
Prat Cabanes-Torreblanca	28 July 2018	0.25 m	30 July 2018
	5 July 2017	0.25 m	5 July 2017
Sagunto	8 July 2018	0.25 m	5 July 2018
	18 June 2017	0.25 m	15 June 2017
	17 November 2016	n. i.*	17 November 2016
Safor	13 June 2018	0.25 m	20 June 2018
	18 August 2017	0.25 m	4 August 2017
	11 November 2016	n. i.*	7 November 2016
Pego-Oliva	13 June 2018	0.25 m	20 June 2018
	11 November 2016	n. i.*	7 November 2016

* n. i. no information available for Google Earth images.

The official cartography of these protected areas (Valencian Wetland Inventory) was used to delimitate each wetland (Figure 2.2). The methodology was applied to the polygons classified as natural areas in the SIOSE (Information System on Land Use in Spain) cartography. For each date and area, we delimited the water and non-water polygons. Water polygons smaller than 100 m^2 were excluded, considering the maximum spatial resolution of Sentinel-2A/B bands used in this study. The water and non-water polygons were delineated through visual examination using as a base map high-resolution image (orthophoto) and was done with the software ArcGis 10.5 (ESRI 2016. ArcGIS Desktop: Release 10.5 Redlands, CA: Environmental Systems Research Institute). In Figure 2.3 delineated polygons can be observed (blue colour). The visual delimitation was possible thanks to the high spatial resolution of the orthophotos (0.25 m).

The spectral information was extracted from the Sentinel-2A/B images to calculate the seven spectral indices shown in Table 2.4 for each wetland polygon (Figure 2.2). The choice of indices was based on literature review. These indices classify as water/non-water according to a threshold value, but different authors propose different thresholds for the same indices. We aimed to define a unique threshold that can be as global as possible with optimum results. So, for each date and area we tested all the thresholds from −0.50 to 0.50 with a 0.05 step, except for the AWEI(NSH) (Automated Water Extraction Index, No Shadow) and the AWEI(SH) (Automated Water Extraction Index, shadow) indices whose thresholds ranged from −50 to −5000, and the step is detailed in the results section.

Table 2.4. Calculated spectral indices.

INDEX	EQUATION	SOURCE	SENTINEL-2 BANDS
NDWI	[(GREEN − NIR) / (GREEN + NIR)]	[31]	[(B03 − B08) / (B03 + B08)]
MNDWI	[(GREEN – SWIR) / (GREEN + SWIR)]	[32]	[(B03 − B11) / (B03 + B11)]
CEDEX	(NIR / RED) − (NIR / SWIR)	[33]	(B05 / B04) − (B05 / B11)
RE-NDWI	[(GREEN − MIR) / (GREEN + MIR)]	[34]	[(B03 − B05) / (B03 + B05)]
AWEI(SH)	BLUE + 2.5× GREEN − 1.5 × (NIR + SWIR) − 0.25− SWIR	[17]	[B02 + 2.5 × B03 − 1.5 × (B08 + B011) − 0.25 × B12]
AWEI (NSH)	4 × (GREEN−MIR) − (0.25 × NIR + 2.75 × SWIR)	[17]	[4 × (B03 − B11) − (0.25 × B08 + 2.75 × B12)]
B_BLUE	(BLUE − NIR) / (BLUE + NIR)	This study	(B02 − B08) / (B02 + B08)

To validate the results obtained from the Sentinel-2A/B images, we designed a random sampling of 60 points for each date and wetland. The ground control points were distributed randomly within a 20 m buffer around the border of each digitized water polygon. These features were mapped using as a base map orthophotos of high spatial resolution. A large number of both water points nearshore (30 points for each wetland and date, 300 in total) and surrounding non-water land points (30 points for each wetland and date, 300 in total) were selected in these areas with high spectral variability, which makes a total of 600 points for validation. We selected the number of points according to the general guideline provided by Congalton and Green [35], who recommended a minimum of 50 samples for each map class for maps of less than 1 million acres in size and fewer than 12 classes. For all these points, we compared the classification of each index (7 indices in Table 2.4) and each threshold, with the ground-truth images, to assess correct classifications. Overall accuracy and Kappa index were calculated for each random sampling. Overall accuracy was obtained by dividing the number of pixels correctly classified by the total number of pixels sampled [35]. Kappa index was calculated according to Congalton's [36] equation. The best index and threshold were selected according to overall accuracy and Kappa index results.

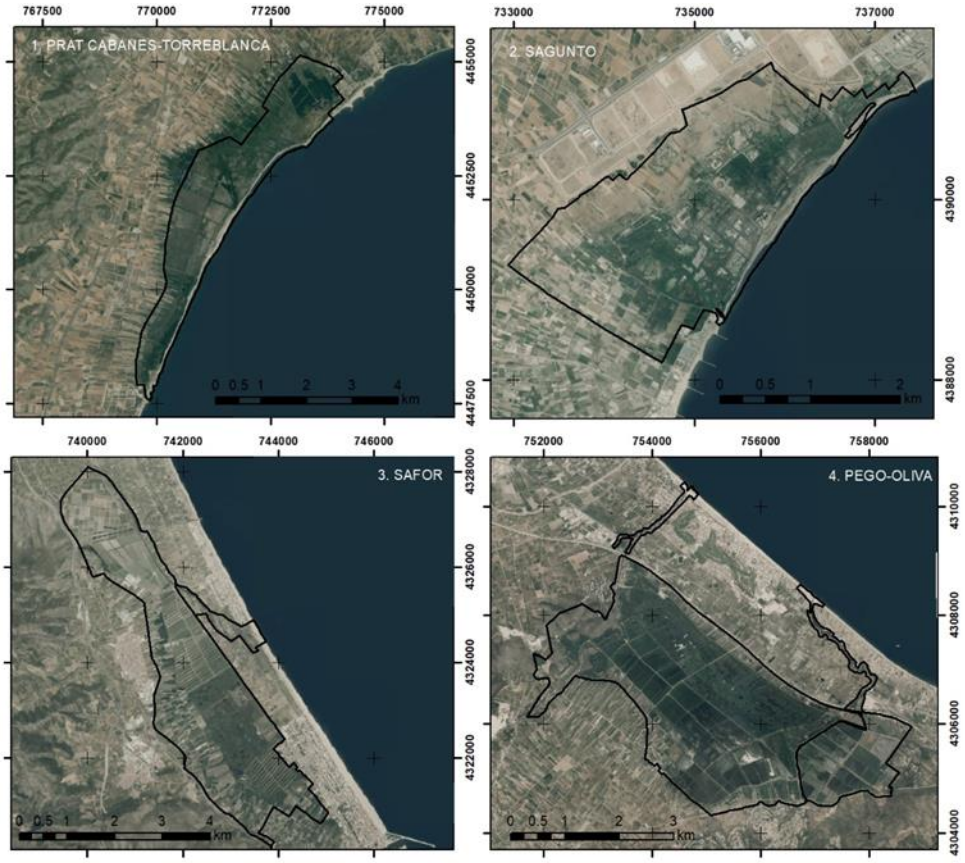

Figure 2.2. Wetlands area according to the official delimitation of the protected area (Valencian Wetland Inventory). Spatial Reference System: European Terrestrial Reference System1989, UTM coordinates Zone 30S.

2.3 RESULTS

Overall accuracy and Kappa index results are represented in Figures 2.3, 2.4, 2.6 and 2.7 with a colour scale. Shaded in yellow appear the indices and thresholds with poorest performance, that is when the classification system from the Sentinel-2A/B images fails to meet the reality defined from the ground-truth images. Shaded in red appear the indices and thresholds with best performance (closer to 1), that is when the classification system from the Sentinel-2A/B images matches the reality defined from the ground-truth images.

In Figure 2.3, the overall accuracy results are presented for all seven tested indices. The tested thresholds ranged are detailed in the methodology section (step detailed in Figure 2.3). The best overall accuracy result (0.89) is for NDWI index with −0.30 threshold. The other indices showed lower overall accuracy results for all the tested thresholds (≤ 0.85).

In Figure 2.4 the Kappa index results are presented for the seven tested indices. The

tested thresholds are the same that for overall accuracy. The best Kappa index result (0.77) is for NDWI index with −0.30 threshold. The other indices showed lower Kappa index results (≤ 0.70) for all the tested thresholds.

The performance of the indices can be graphically observed in detail in Figure 2.5. This figure shows a compilation of images of the indices for their optimal thresholds in a specific area of the outlined water bodies. According to these results, the NDWI index has the best performance for identifying wetland water bodies. One of the factors that could explain the di*ff*erent indices performance can be the lower spatial resolution (20 m) for the bands B5, B11, and B12 used for the indices MNDWI, CEDEX, RE-NDWI, AWEI(SH), and AWEI(NSH). In addition, it was detected that the reflectance values of the bands 11 and 12 on water areas were more variable than B3 and B8 used in the NDWI index.

For further analysis of the NDWI performance, Figures 2.6 and 2.7 show detailed overall accuracy and Kappa index results for each wetland and date.

Overall accuracy results are optimal for −0.30 threshold, with 0.89 average value and maximum values of 0.97 in Safor wetland (2017/2018) and Prat Cabanes-Torreblanca (0.93 in 2018 and 0.95 in 2018) (Figure 2.6). Kappa index results show the highest average value (0.77) for −0.30 threshold. Kappa index results are even better in Cabanes-Torreblanca and Safor wetlands. However, in Sagunto and Pego-Oliva wetland the average Kappa index is lower (0.67 and 0.65 respectively). Considering that the objective is to provide a methodology to characterize water bodies in wetlands as global as possible, this analysis supported the choice of the NDWI index and −0.30 threshold. These results have been obtained for the areas with highest variability, that is the water bodies borders, and could be even more accurate in central areas of land/water covers with less variation in reflectance values.

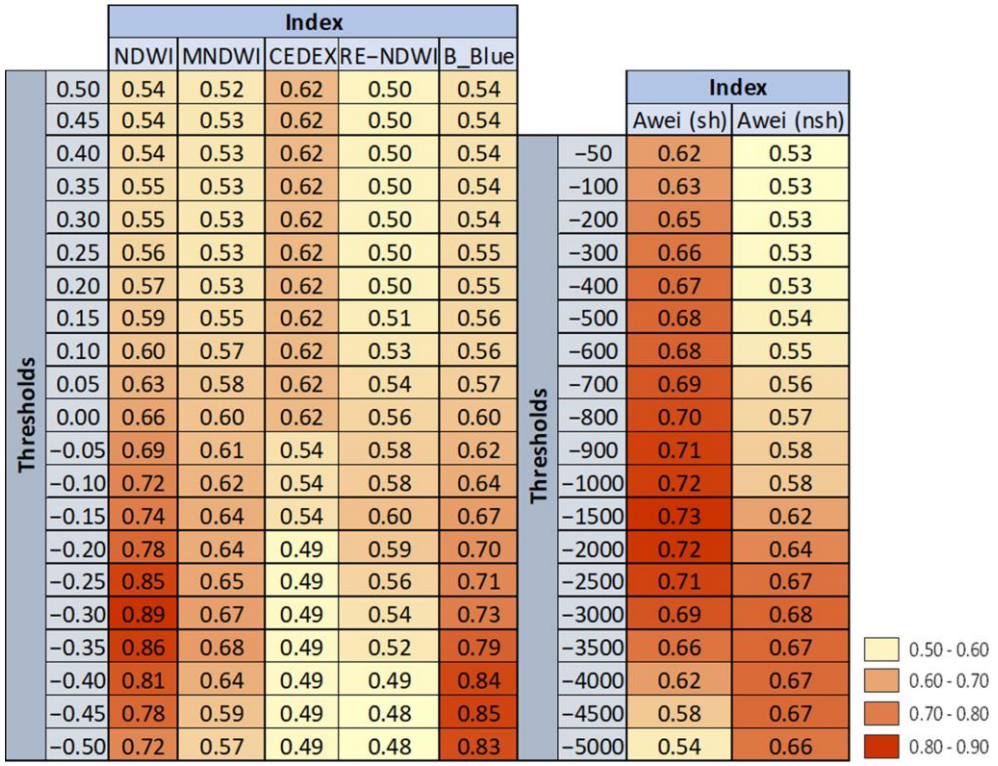

Figure 2.3. Overall accuracy of tested indexes at different thresholds.

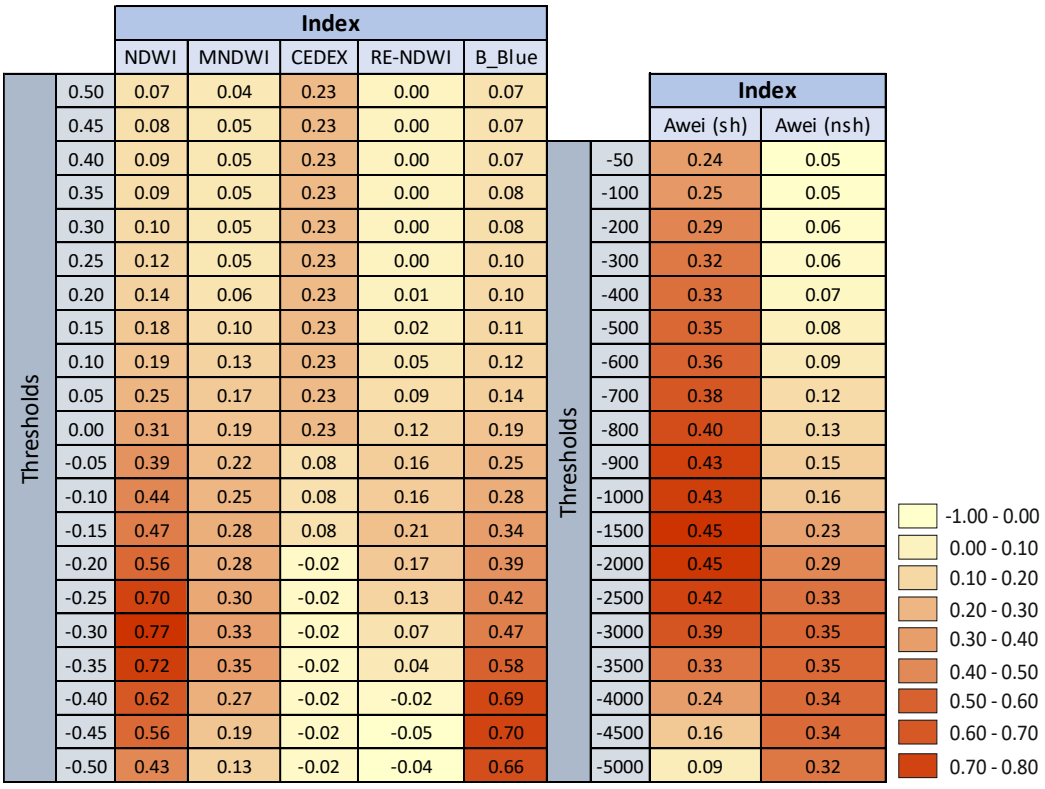

Figure 2.4. Kappa index of tested indexes at different thresholds.

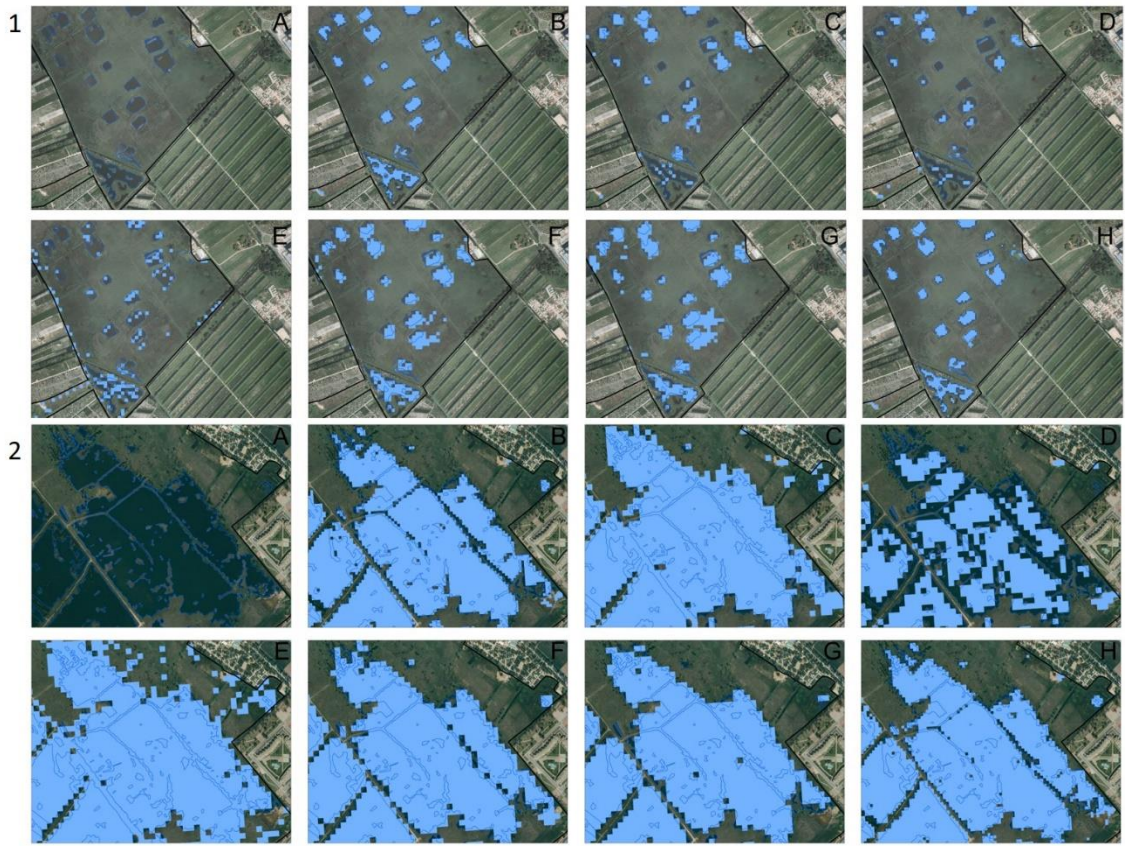

Figure 2.5. Delimited water bodies in two wetlands are represented: (1) Safor wetland 2017 and (2) Prat Cabanes-Torreblanca wetland 2018. A: orthophoto, B: NDWI index (threshold −0.30), C: mNDWI index (threshold −0.35), D: CEDEX index (threshold +0.4), E: Re-NDWI (threshold −0.15), F: Awei sh index (threshold −1500), G: Awei nsh index (threshold −3000) and H: NDWI/BLUE-NIR index (threshold −0.45).

In Figure 2.8 we compare the delimited wetland bodies of water in blue color (A, C, E, G) versus the result of the NDWI index for the threshold -0.30 (B, D, F, H) in the four studied wetlands. Since water sampling points are marked in yellow and non-water in red, we can observe false negatives and false positives results. A good performance of the NDWI and -0.30 threshold can be appreciated in pixels that are further from the border (more homogenous areas). In contrast, false positive and false negative pixels were found in the border areas. In the randomly selection of ground truth points within these areas (20 m to the border to each side), some of them were selected randomly at a distance lower than 10 m of the border, and the pixel size of Sentinel-2A/B bands used in NDWI index was 10 m. The classification result of those pixels depends on the area percentage that corresponds to each class. For example, a water ground truth point can be located in

a non-water (land) class pixel since the percentage of non-water class for that pixel is higher than for water area (see most of the false negative and false positive in Figure 2.8).

	NDWI (Overall accuracy)									
	Cabanes-Torreblanca		Sagunto			La Safor			Pego-Oliva	
	2018	2017	2018	2017	2016	2018	2017	2016	2018	2016
0.50	0.50	0.50	0.50	0.50	0.52	0.50	0.77	0.57	0.50	0.52
0.45	0.50	0.50	0.50	0.50	0.52	0.50	0.78	0.58	0.50	0.52
0.40	0.50	0.50	0.50	0.50	0.52	0.50	0.80	0.60	0.50	0.52
0.35	0.50	0.50	0.50	0.50	0.52	0.50	0.80	0.60	0.50	0.55
0.30	0.50	0.50	0.50	0.50	0.52	0.52	0.80	0.63	0.50	0.55
0.25	0.50	0.50	0.50	0.50	0.52	0.53	0.80	0.70	0.50	0.55
0.20	0.52	0.50	0.50	0.50	0.52	0.55	0.80	0.75	0.50	0.55
0.15	0.60	0.53	0.50	0.50	0.52	0.60	0.80	0.77	0.50	0.57
0.10	0.63	0.55	0.50	0.50	0.52	0.60	0.82	0.77	0.50	0.57
0.05	0.70	0.70	0.50	0.50	0.52	0.60	0.83	0.78	0.52	0.62
0.00	0.72	0.77	0.50	0.50	0.55	0.72	0.85	0.80	0.52	0.63
-0.05	0.80	0.82	0.53	0.55	0.55	0.77	0.93	0.80	0.52	0.67
-0.10	0.85	0.88	0.55	0.55	0.55	0.80	0.93	0.80	0.53	0.73
-0.15	0.83	0.90	0.55	0.63	0.57	0.85	0.93	0.83	0.53	0.73
-0.20	0.85	0.93	0.62	0.68	0.60	0.90	0.95	0.83	0.63	0.78
-0.25	0.88	0.97	0.73	0.75	0.78	0.97	0.97	0.85	0.83	0.78
-0.30	0.93	0.95	0.80	0.83	0.87	0.97	0.97	0.88	0.90	0.75
-0.35	0.88	0.90	0.78	0.88	0.90	0.93	0.93	0.87	0.82	0.72
-0.40	0.73	0.85	0.72	0.90	0.78	0.93	0.92	0.85	0.73	0.70
-0.45	0.62	0.80	0.75	0.87	0.77	0.90	0.88	0.83	0.72	0.65
-0.50	0.52	0.67	0.70	0.75	0.68	0.87	0.83	0.85	0.63	0.67

0.50 - 0.60
0.60 - 0.70
0.70 - 0.80
0.80 - 0.90
0.90 - 1.00

Figure 2.6. Overall accuracy of NDWI index tested at four studies areas and 3 years for the threshold range (−0.50 to 0.50).

		NDWI (Kappa index)									
		Cabanes-Torreblanca		Sagunto			La Safor			Pego-Oliva	
		2018	2017	2018	2017	2016	2018	2017	2016	2018	2016
Thresholds	0.50	0.00	0.00	0.00	0.00	0.03	0.00	0.53	0.13	0.00	0.03
	0.45	0.00	0.00	0.00	0.00	0.03	0.00	0.57	0.17	0.00	0.03
	0.40	0.00	0.00	0.00	0.00	0.03	0.00	0.60	0.20	0.00	0.03
	0.35	0.00	0.00	0.00	0.00	0.03	0.00	0.60	0.20	0.00	0.10
	0.30	0.00	0.00	0.00	0.00	0.03	0.03	0.60	0.27	0.00	0.10
	0.25	0.00	0.00	0.00	0.00	0.03	0.07	0.60	0.40	0.00	0.10
	0.20	0.03	0.00	0.00	0.00	0.03	0.10	0.60	0.50	0.00	0.10
	0.15	0.20	0.07	0.00	0.00	0.03	0.20	0.60	0.53	0.00	0.13
	0.10	0.27	0.10	0.00	0.00	0.03	0.20	0.63	0.53	0.00	0.13
	0.05	0.40	0.40	0.00	0.00	0.03	0.20	0.67	0.57	0.03	0.23
	0.00	0.43	0.53	0.00	0.00	0.10	0.43	0.70	0.60	0.03	0.27
	-0.05	0.60	0.63	0.07	0.10	0.10	0.53	0.87	0.60	0.03	0.33
	-0.10	0.70	0.77	0.10	0.10	0.10	0.60	0.87	0.60	0.07	0.47
	-0.15	0.67	0.80	0.10	0.27	0.13	0.70	0.87	0.67	0.07	0.47
	-0.20	0.70	0.87	0.23	0.37	0.20	0.80	0.90	0.67	0.27	0.57
	-0.25	0.77	0.93	0.47	0.50	0.57	0.93	0.93	0.70	0.67	0.57
	-0.30	0.87	0.90	0.60	0.67	0.73	0.93	0.93	0.77	0.80	0.50
	-0.35	0.77	0.80	0.57	0.77	0.80	0.87	0.87	0.73	0.63	0.43
	-0.40	0.47	0.70	0.43	0.80	0.57	0.87	0.83	0.70	0.47	0.40
	-0.45	0.23	0.60	0.50	0.73	0.53	0.80	0.77	0.67	0.43	0.30
	-0.50	0.03	0.33	0.40	0.50	0.37	0.73	0.67	0.70	0.27	0.33

0.00 - 0.10
0.10 - 0.20
0.20 - 0.30
0.30 - 0.40
0.40 - 0.50
0.50 - 0.60
0.60 - 0.70
0.70 - 0.80
0.80 - 0.90
0.90 - 1.00

Figure 2.7. Kappa index of NDWI index tested at four studies areas and 3 years for the threshold range (−0.50 to 0.50).

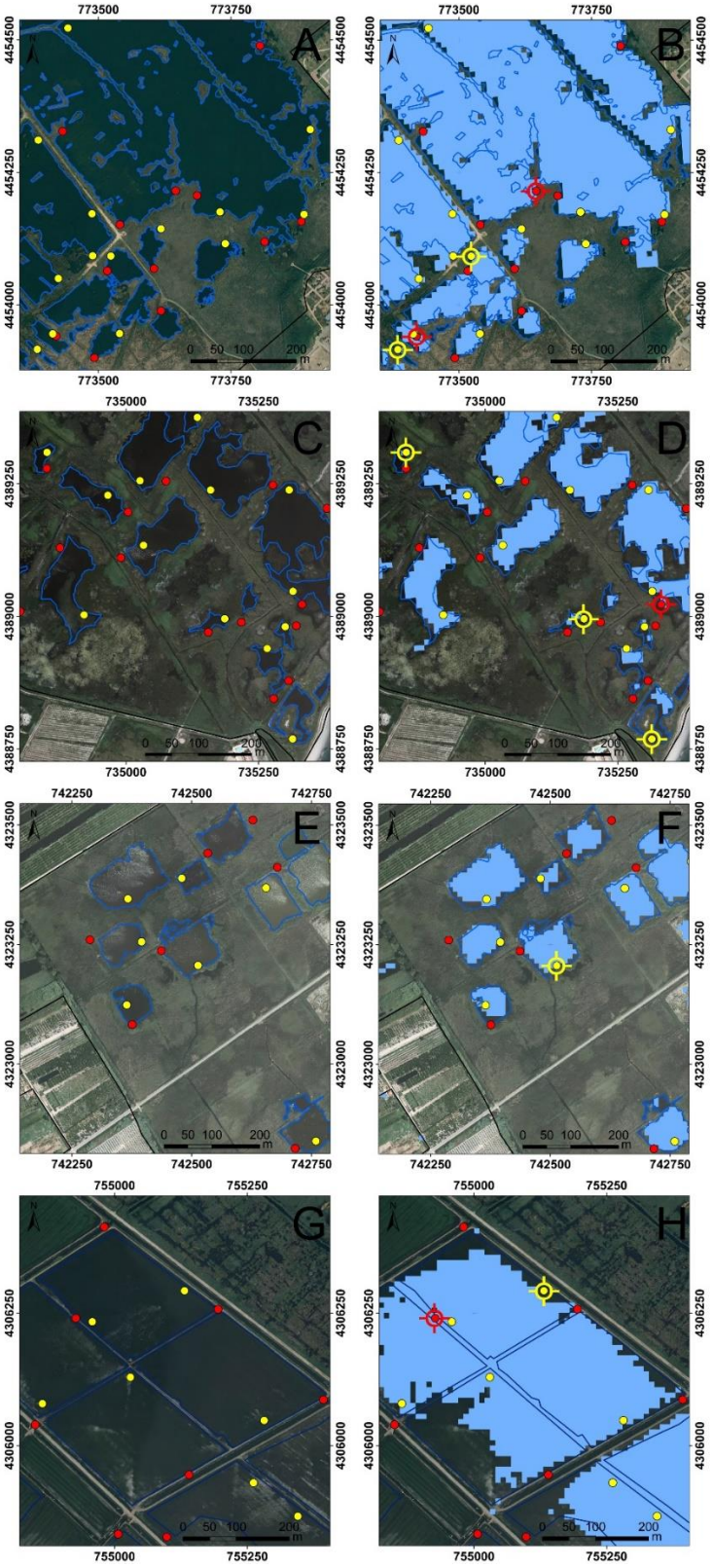

Figure 2.8. Delimited wetland bodies of water in blue color outline (**A**, **C**, **E**, **G**) versus the result of the NDWI index for the threshold −0.30 in light blue (**B**, **D**, **F**, **H**). Water sampling points in yellow and non-water in red. False negatives and false positives are

marked. Figure **A**–**B**: Prat Cabanes-Torreblanca wetland (2018), Figure **C**–**D**: Sagunto wetland (2017), Figure **E**–**F**: La Safor wetland (2017) and figure **G**–**H**: Pego-Oliva wetland (2018).

2.4 DISCUSSION

Sentinel-2A/B images spatial resolution allowed to detect smaller water bodies than previously published works [3,6]. The minimum water body surface detected was 100 m^2. In Figure 2.9, we show the water bodies identified by Sentinel-2A/B in Safor wetland for the three studied dates. The highest flooded surface was 41.93 ha in August 2017 and the lowest 16.57 ha in November 2016. Precipitation is one of the main variables that determine the extent of the flooded area in this type of wetlands, and 2017 was the rainiest period studied (Table 2.1). The flooded surface is not necessarily a continuum but the addition of water bodies that can be connected or not. The average size of flooded areas is around 1500 m^2, so the use of Sentinel-2A/B images is key for detecting these water bodies and avoid underestimating the water surface. It is important to highlight that the NDWI index is not able to detect the water layer underlying marsh vegetation (e.g., *Phragmites australis*) but free water layers. The Ramsar Convention established a Wetland Type Classification System that identifies 42 types grouped into three main categories: marine and coastal, continental, and artificial. Thus, a certain wetland area is identified with a main type of wetland according to its predominance, but it may have more than one type present, this being the most common. The selected study areas are coastal wetlands, and in Table 2.2 we summarize the habitats present. The main free water layers are coastal lagoons, natural eutrophic lakes, and natural dystrophic lakes and ponds. Figure 2.9 shows the habitats present in Safor wetland, water areas are characterized by its size, morphology, vegetation, and period of permanence of the water layer. For instance, natural lakes (locally known as “ullals”) have a permanent water surface along the year, but grasslands are vegetation only periodically inundated. This great variability makes it difficult to monitor the status of these wetlands, mainly due to the small size of some surfaces that makes detection and quantification difficult [37]. Following the described methodology, we have been able to detect all these water surfaces under different inundation conditions.

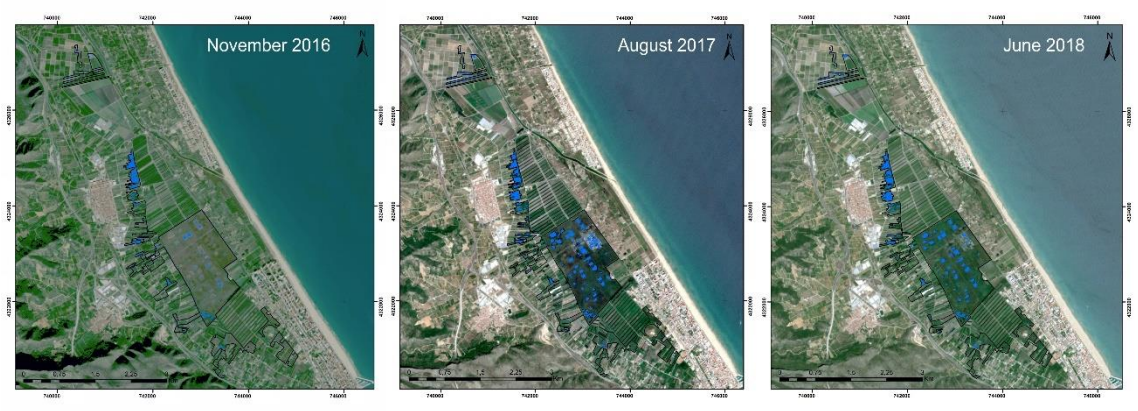

Figure 2.9. Delimited water bodies with the NDWI index in Safor wetland.

In our study the best performing index was the NDWI index [31]. This result is in line with previous studies indicating the high performance of this index for extracting water surfaces [11,38–40]. The results obtained in our study are significant in at least two major aspects. The first one is related to the proposal of a stable and generalizable threshold to delineate water surfaces in the studied coastal wetlands. These results differ from earlier findings indicating that the threshold values for classifying water from non-water are unstable and vary according to date, location, and the subpixel land-cover components [17,41,42]. Other authors applied other indexes such as Awei(sh) and MNDWI to improve NDWI performance. However, this improvement is only observed in areas including dark built surfaces and buildings, because the NDWI often does not distinguish between water areas and built-up land [17,32]. It is important to remark that before applying the NDWI index it is necessary to delimitate the natural wetland area. These ecosystems usually hold protection figures and have an official cartography that can be used as delimitation. Some studies reported that limited spatial resolution of some satellite images (Landsat TM, 30 m, MODIS, 250 m, AVHRR 1 km, SPOT vegetation 1 km) can contain a mixture of land-cover types being this effect more significant in edge pixels [41] and generating difficulties for mapping homogeneous coastal wetlands [43,44]. Ji et al. [41] demonstrated that the threshold for extracting water surfaces depends on the subpixel land-cover components. Some authors suggest the categorization of surface water for image classification [42,44]. In this study, the higher spatial resolution of the Sentinel-2A/B bands (10 m for band 3, Green, and band 8, NIR) allowed to define with more accuracy the boundary of water surfaces avoiding pixels with a mixture of covers (soil, vegetation, water). The minimum surface water areas detected on this study

could not be extracted using moderate spatial resolution images such as Landsat. Other studies have also observed a better performance with Sentinel-2A/B images than Landsat images [46].

The second aspect of this study that should be highlighted is the threshold sign. Early research on this topic proposed a threshold of 0 for the water indexes NDWI and MNDWI [31,32]. Values greater than 0 were classified as water pixels and values lower than 0 as non-water pixels [31,32]. However, what stands out in our analysis was that the best performing thresholds were negative values. This finding is consistent with other studies where values lower than 0 were set for extracting water bodies [38–41]. Ji et al. [41] reported that the mixture of land covers distributed in the same pixel had a strong impact on the NDWI values obtaining negative and variable thresholds according to the relative proportions of soil and vegetation. The negative values for extracting water surfaces may be explained considering the spectral response of the analyzed wetlands. Water quality has a significant effect on reflectance, high values of chlorophyll *a* generate higher reflectance values for the NIR band (B3) than for the GREEN band (B8) (Table 2.2). Consequently, the negative values of the selected threshold are congruous with the spectral response of the water in the analyzed wetlands. In the studied areas, eutrophic and dystrophic lakes water can be classified as complex waters with variable concentration of chlorophyll *a* and other colored substances such as humic acids.

The majority of studies developed in wetlands have focused on calculating global gain or loss of wetland area and have found that agricultural and urban land use conversion are the main causes of wetland loss [47]. This is critical to the success of the no-net-loss wetland conservation international strategy. Additionally, inside of wetlands which hold protection figures, land use change in the surrounding area has a direct effect on water management strategies. In the studied areas, especially in Safor wetland, agricultural and urban use coexist with natural use, and that strongly condition water management. Nowadays, Safor wetland hydrology is anthropogenically manipulated to prevent crop root asphyxia, and to avoid flooding of urban areas. In the wet seasons, water is pumped through irrigation channels into the sea to decrease the phreatic level [24]. This manipulation can produce important impacts in the hydrologic cycle of the wetland that have not been studied. Applying Sentinel-2A/B images to monitor flooded area changes trough the NDWI index will be key to analyze the consequence of these management

actions. This data can be used to assist both wetland managers and practitioners to make decisions about priority management interventions to maintain the ecological character of a wetland. As other studies have already pointed out [5], the use of Earth Observation tools is key for addressing the information gaps faced by wetland managers and practitioners.

2.5 CONCLUSIONS

The results of this study indicated the potential of NDWI index calculated from Sentinel-2A/B images (bands 3 and 8) to extract open water bodies in delimited wetlands. It was observed that a −0.30-threshold generated acceptable results to classify the studied coastal wetlands. This threshold results are proper along the year under different flooding and vegetation conditions, allowing to distinguish water and non-water (soil, vegetation) polygons. The spatial resolution of these images allowed to detect water bodies of reduced size (the average size of flooded areas is around 1500 m^2) compared to previous missions of medium and low resolution. In the studied wetlands, the flooded surface is not necessarily a continuum but the addition of water bodies that can be connected or not depending partly on the pluviometry regime. The information derived from Sentinel-2A/B bands can be very useful to monitor these ecosystems, offering valuable information for managers of these areas, specially to study the effect of hydrologic cycle manipulation.

2.6 REFERENCES

1. Zhao, Q.; Bai, J.; Huang, L.; Gu, B.; Lu, Q.; Gao, Z. A review of methodologies and success indicators for coastal wetland restoration. *Ecol. Indic.* **2016**, *60*, 442–452. [CrossRef]
2. Zhang, L.; Thomas, S.; Mitsch, W.J. Design of real-time and long-term hydrologic and water quality wetland monitoring stations in South Florida, USA. *Ecol. Eng.* **2017**, *108*, 446–455. [CrossRef]
3. Jin, H.; Huang, C.; Lang, M.W.; Yeo, I.Y.; Stehman, S.V. Monitoring of wetland inundation dynamics in the Delmarva Peninsula using Landsat time-series imagery from 1985 to 2011. *Remote Sens. Environ.* **2017**, *190*, 26–41. [CrossRef]
4. Leibowitz, S.G. Isolated wetlands and their functions: An ecological perspective. *Wetlands* **2003**, *23*, 517–531. [CrossRef]
5. Rebelo, L.-M.; Finlayson, C.M.; Strauch, A.; Rosenqvist, A.; Perennou, C.; Tøttrup, C.; Hilarides, L.; Paganini, M.; Wielaard, N.; Siegert, F.; et al. *The Use of Earth Observation for Wetland Inventory, Assessment and Monitoring: An Information Source for the Ramsar Convention on Wetlands*; Ramsar Technical Report, 10; Ramsar Convention Secretaria: Gland, Switzerland, 2018.
6. Li, L.; Vrieling, A.; Skidmore, A.; Wang, T.; Muñoz, A.R.; Turak, E. Evaluation of MODIS Spectral Indices for Monitoring Hydrological Dynamics of a Small, Seasonally-Flooded Wetland in Southern Spain. *Wetlands* **2015**, *35*, 851. [CrossRef]
7. Huang, C.; Peng, Y.; Lang, M.; Yeo, I.-Y.; McCarty, G. Wetland inundation mapping and change monitoring using Landsat and airborne LiDAR data. *Remote Sens. Environ.* **2014**, *141*, 231–242. [CrossRef]
8. Glasgow, H.B.; Burkholder, J.M.; Reed, R.E.; Lewitus, A.J.; Kleinman, J.E. Real-time remote monitoring of water quality: A review of current applications, and advancements in sensor, telemetry, and computing technologies. *J. Exp. Mar. Biol. Ecol.* **2004**, *300*, 409–448. [CrossRef]
9. Guo, M.; Li, J.; Sheng, C.; Xu, J.; Wu, L. A Review of Wetland Remote Sensing. *Sensors* **2017**, *17*, 777. [CrossRef]

10. Fisher, A.; Flood, N.; Danaher, T. Comparing Landsat water index methods for automated water classification in eastern Australia. *Remote Sens. Environ.* **2016**, *175*, 167–182. [CrossRef]

11. Zhou, Y.; Dong, J.; Xiao, X.; Xiao, T.; Yang, Z.; Zhao, G.; Zou, Z.; Qin, Y. Open Surface Water Mapping Algorithms: A Comparison of Water-Related Spectral Indices and Sensors. *Water* **2017**, *9*, 256. [CrossRef]

12. Tian, S.; Zhang, X.; Tian, J.; Sun, Q. Random Forest Classification of Wetland Landcovers from Multi-Sensor Data in the Arid Region of Xinjiang, China. *Remote Sens.* **2016**, *8*, 954. [CrossRef]

13. Liu, T.; Abd-Elrahman, A.; Morton, J.; Wilhelm, V.L. Comparing fully convolutional networks, random forest, support vector machine, and patch-based deep convolutional neural networks for object-based wetland mapping using images from small unmanned aircraft system. *GIsci. Remote Sens.* **2018**, *55*, 243–264. [CrossRef]

14. Rezaee, M.; Mahdianpari, M.; Zhang, Y.; Salehi, B. Deep Convolutional Neural Network for Complex Wetland Classification Using Optical Remote Sensing Imagery. *IEEE J. Sel. Top. Appl. Earth Obs. Remote Sens.* **2018**, *11*, 3030–3039. [CrossRef]

15. Xia, H.; Zhao, W.; Li, A.; Bian, J.; Zhang, Z. Subpixel Inundation Mapping Using Landsat-8 OLI and UAV Data for a Wetland Region on the Zoige Plateau, China. *Remote Sens.* **2017**, *9*, 31. [CrossRef]

16. Díaz-Delgado, R.; Cazacu, C.; Adamescu, M. Rapid Assessment of Ecological Integrity for LTER Wetland Sites by Using UAV Multispectral Mapping. *Drones* **2019**, *3*, 3. [CrossRef]

17. Feyisa, G.L.; Meilby, H.; Fensholt, R.; Proud, S. Automated Water Extraction Index: A New Technique for Surface Water Mapping Using Landsat Imagery. *Remote Sens. Environ.* **2014**, *140*, 23–35. [CrossRef]

18. Tiner, R.W. Remotely-sensed indicators for monitoring the general condition of "natural habitat" in watersheds: An application for Delaware's Nanticoke River watershed. *Ecol. Indic.* **2004**, *4*, 227–243. [CrossRef]

19. Cools, J.; Johnston, R.; Hattermann, F.F.; Douven, W.; Zsuffa, I. Tools for wetland management: Lessons

learnt from a comparative assessment. *Environ. Sci. Policy* **2013**, *34*, 138–145. [CrossRef]

20. Sebastiá-Frasquet, M.-T.; Altur, V.; Sanchis, J.-A. Wetland Planning: Current Problems and Environmental Management Proposals at Supra-Municipal Scale (Spanish Mediterranean Coast). *Water* **2014**, *6*, 620–641. [CrossRef]

21. Mediterranean Wetlands Observatory (MWO). *Mediterranean Wetlands Outlook 2012*; Technical report; Mediterranean Wetlands Observatory c/o Tour du Valat: Arles, France, 2012.

22. Mediterranean Wetlands Observatory (MWO). *Mediterranean Wetlands Outlook 2018*; Technical report; Mediterranean Wetlands Observatory c/o Tour du Valat: Arles, France, 2018.

23. Sanjaume, E.; Pardo-Pascual, J.E.; Segura-Beltran, F. Mediterranean Coastal Lagoons. In *The Spanish Coastal Systems*; Morales, J., Ed.; Springer: Cham, Switzerland, 2019.

24. Sebastiá, M.T.; Rodilla, M.; Sanchis Blay, J.A.; Altur Grau, V.J.; Gadea Perez, M.I.; Falco Giaccaglia, S.L. Influence of nutrient inputs from a wetland dominated by agriculture on the phytoplankton community in a shallow harbour at the Spanish Mediterranean coast. *Agric. Ecosyst. Environ.* **2012**, *152*, 10–20. [CrossRef]

25. Pena-Regueiro, J.; Sebastiá-Frasquet, M.-T.; Estornell Cremades, J. Analysis of highly variable water surfaces in humid areas using Remote Sensing. In Proceedings of the XVIII Congreso de la Asociación Española de Teledetección (AET 2019), Hacia una visión global del cambio climático, Valladolid, Spain, 24–27 September 2019. (In Spanish)

26. Ramsar Sites Information Service. Available online: https://rsis.ramsar.org/ (accessed on 16 April 2020).

27. IVIA. Available online: http://riegos.ivia.es/datos-meteorologicos (accessed on 16 April 2020).

28. Soria García, J.M.; Romo, S.; Pastor Palacios, A.; García Picazo, A.; Aledón

Catalá, T.; Calvo García, S.; Flor Izquierdo, J.; Arribas Fernández, I. Evaluación de la conservación de los humedales costeros de la Comunidad Valenciana mediante imágenes de Landsat. In Proceedings of the XVI Congreso de la Asociación Española de Teledetección. Teledetección: Humedales y Espacios Protegidos, Sevilla, Spain, 21–23 October 2015.

29. EUNIS. Available online: https://eunis.eea.europa.eu/index.jsp (accessed on 16 April 2020).

30. Acharya, T.D.; Subedi, A.; Lee, D.H. Evaluation of Water Indices for Surface Water Extraction in a Landsat 8 Scene of Nepal. *Sensors* **2018**, *18*, 2580. [CrossRef]

31. Mcfeeters, S.K. The use of the Normalized Difference Water Index (NDWI) in the delineation of open water

features. *Int. J. Remote Sens.* **1996**, *17*, 1425–1432. [CrossRef]

32. Xu, H. *Modification of normalised difference water index (NDWI) to enhance open water features in remotely sensed imagery, Int. J. Remote Sens.* **2006**, *27*, 3025–3033.

33. Ángel-Martínez, M.C. *Aplicación de la Teledetección en la Localización de Superficies de Agua*; CEDEX: Madrid, Spain, 1994.

34. Klemenjak, S.; Waske, B.; Valero, S.; Chanussot, J. Unsupervised river detection in RapidEye data. In Proceedings of the IEEE International Geoscience and Remote Sensing Symposium, Munich, Germany, 22–27 July 2012; pp. 6860–6863.

35. Congalton, R.G.; Green, K. *Assessing the Accuracy of Remotely Sensed Data: Principles and Practices*; Lewis Publisher: Boca Raton, FL, USA, 1999.

36. Congalton, R.G. A Review of Assessing the Accuracy of Classifications of Remotely Sensed Data. *Remote Sens. Environ.* **1991**, *37*, 35–46. [CrossRef]

37. Gallant, A. The challenges of remote monitoring of wetlands. *Remote Sens.* **2015**, *7*, 10938–10950. [CrossRef]

38. Kaplan, G.; Avdan, U. Mapping and Monitoring Wetlands Using SENTINEL 2 Satellite Imagery. *ISPRS Ann. Photogramm. Remote Sens. Spat. Inf. Sci.* **2017**, *IV*, 271–277. [CrossRef]

39. Soria-García, J.M.; Romo, S.; Aledón-Catalá, T.; Flor-Izquierdo, J.; Calvo-García, S.; Pastor-Palacios, A.; García-Picazo, A.; Arribas-Fernández, I. Monitoring autumnal flooding in the Albufera Natural Park (Valencia, Spain) by Lansat imagery. In Proceedings of the XVI Congreso de la Asociación Española de Teledetección, Teledetección: Humedales y Espacios Protegidos, Sevilla, Spain, 21–23 October 2015.

40. Wilson, N.R.; Norman, L.M.; Villarreal, M.; Gass, L.; Tiller, R.; Salywon, A. Comparison of remote sensing indices for monitoring of desert cienegas. *Arid Land Res. Manag.* **2016**, *30*, 460–478. [CrossRef]

41. Ji, L.; Zhang, L.; Wylie, B. Analysis of Dynamic Thresholds for the Normalized Di*ff*erence Water Index.

Photogramm. Eng. Remote Sens. **2009**, *75*, 1307–1317. [CrossRef]

42. Verpoorter, C.; Kutser, T.; Tranvik, L. Automated mapping of water bodies using Landsat multispectral data.

Limnol. Oceanogr.-Meth. **2012**, *10*, 1037–1050. [CrossRef]

43. Ramsey, E.W.; Laine, S.C. Comparison of Landsat Thematic Mapper and High Resolution Photography to Identify Change in Complex Coastal Wetlands. *J. Coast. Res.* **1997**, *13*, 281–292.

44. Zomer, R.J.; Trabucco, A.; Ustin, S.L. Building spectral libraries for wetlands land cover classification and hyperspectral remote Sensing. *J. Environ. Manag.* **2009**, *90*, 2170–2177. [CrossRef]

45. Sun, F.; Sun, W.; Chen, J.; Gong, P. Comparison and improvement of methods for identifying waterbodies in remotely sensed imagery. *Int. J. Remote Sens.* **2012**, *33*, 6854–6875. [CrossRef]

46. Jara, C.; Delegido, J.; Ayala, J.; Lozano, P.; Armas, A.; Flores, V. Study of wetlands in the Ecuadorian Andes through the comparison of Landsat-8 and Sentinel-2 images. *Rev. Teledetección* **2019**, *53*, 45–57. [CrossRef]

47. Fickas, K.C.; Cohen, W.B.; Yang, Z. Landsat-based monitoring of annual wetland change in the Willamette Valley of Oregon, USA from 1972 to 2012. *Wetl. Ecol. Manag.* **2016**, *24*, 73. [CrossRef]

3 CAPÍTULO 3:
SENTINEL-2 ANALYSIS OF FLOODED AREAS: APPLIED CASE STUDY – LA SAFOR WETLAND, SPAIN

Pena-Regueiro, J., Sebastiá-Frasquet, M. T., Aguilar-Maldonado, J. A., Estornell, J., Sanchis-Blay, J. A., Morell-Monzó, S., & Altur-Grau, V. 2020. Sentinel-2 analysis of flooded areas: applied case study-La safor wetland, Spain. WIT Transactions on Ecology and the Environment, 242, 63-70. https://doi.org/10.2495/WP200061

3.1 INTRODUCTION

Coastal wetlands are important ecosystems that are endangered because of intensive human pressure in these areas [1]. Wetlands provide a wide range of ecosystem services, particularly they are important providers of all water-related ecosystem services, among them their capacity to maintain and improve water quality, flood control, groundwater replenishment, shoreline stabilisation and storm protection and climate change mitigation and adaptation [2]–[4]. Wetlands play an important role in maintaining local water quality. They can act as filtering systems, removing sediment, nutrients (mainly nitrogen and phosphorus) and pollutants (such as pesticides from agricultural runoff) from water. Their holding capacity helps control floods and prevents water logging of crops and adjacent urban areas [3], [5]. Preserving and restoring them can often provide the level of flood control more affordable than dredge operations and levees [5]. In fact, there are studies that calculate the benefits of economical activities in wetlands such as intensive agriculture and shrimp farms, and they are between 60% and 75% lower – in the long term – than the benefits from wetland conservation and sustainable use [2], [6]. Nowadays, projects to restore their functions are being designed and implemented.

Remotely sensed data can provide spatial maps of water bodies, with different accuracy depending on the sensor, that can be used to increase the knowledge of these areas [7]–[10]. The analysis of remote data can be based on supervised classification and the definition of water indices and their subsequent classification using thresholds [9], [10]. From 2015 onward, Sentinel-2A/B images are available (ESA), with high temporal resolution and bands of 10 m that allow to extract small-sized water bodies [7]. LIDAR (Light Detection and Ranging or Laser Imaging Detection and Ranging) data can be used to obtain synoptic digital elevation models (DEMs). The information on wetland elevation obtained from LIDAR data is very accurate and can be used for different purposes such as habitat mapping and flood inundation mapping [11]. The accuracy of the LIDAR-derived DEM can range from 0.03 to 0.25 m depending on the vegetation cover classes [11].

The objective of this study is to analyse the effects of the flooded surface on land uses by remote sensing and Airborne LiDAR data on a Mediterranean coastal wetland "La Safor wetland". Currently, the municipalities of this wetland are competing for

European funds for projects to recover hydraulic infrastructures in protected areas. So, a complete diagnosis of the areas most vulnerable to flooding is necessary.

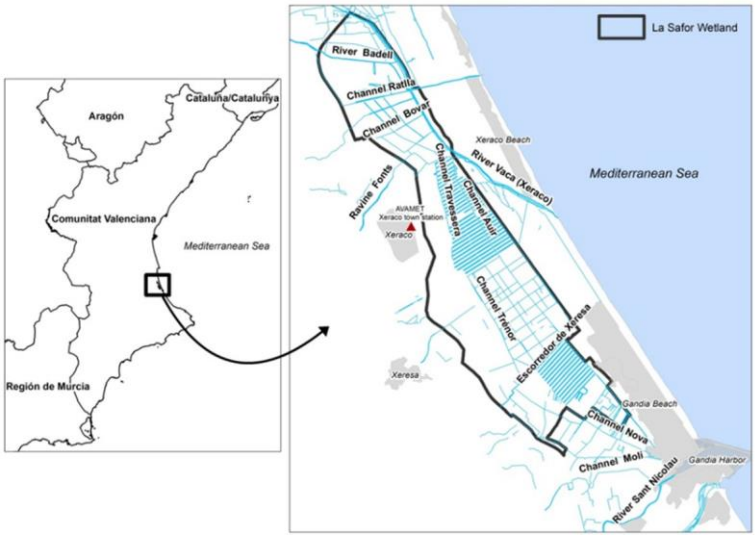

Figure 3.1. Study area location. The red triangle is the Xeraco town meteorological station.

3.2 MATERIALS AND METHODS

3.2.1 STUDY AREA

La Safor wetland is in south Valencia, Spain and extends to four municipalities (Gandia, Xeresa, Xeraco and Tavernes de la Valldigna) (Figs 1 and 2). It is included in both the Valencian Wetlands Inventory, and in the Spanish Wetlands, and at international level, is a Special Protection Areas (SPAs) for birds and Site of Community Importance (SCI). This coastal wetland is above a detrital aquifer, and its main freshwater input comes from groundwater discharge of the adjacent karstic aquifers and is separated from the sea by a sand bar [1]. The flooded surface is variable and depends on pluviometry among other factors [7]. La Safor wetland has suffered intense agricultural transformations mainly from the seventies onward [1]. Nowadays, the main land uses are citrus and horticultural crops according to the Corine Land Cover obtained from the Valencian Cartography Institute (Fig. 3.2).

Two watercourses are the main drainage of the wetland, San Nicolás and Vaca Rivers, to the north and south respectively (Fig. 3.1). Both rivers drain the wetland and flows into the Mediterranean Sea. San Nicolás flows into the Gandia Harbour and Vaca

River flows directly into the sea in Xeraco. There is a built grid of channels that served for irrigation purposes before it has been substituted by drip irrigation. These channels also contributed to wetland drainage as they were connected either to the above described rivers or directly to the sea. However, two main factors caused the deterioration and even partial disappearance of these channels. The change in the irrigation system caused an important reduction in maintenance tasks by farmers. The urban pressure, especially in Gandia municipality, caused for example the disappearance of Escorredor de Xeresa in its final course to the sea (Fig. 3.3). In 1956, this channel outflow in behind the dunes to a channel parallel to the sea. Partially due to this abandonment of hydraulic infrastructures there exists flooding problems in the agricultural and urban areas.

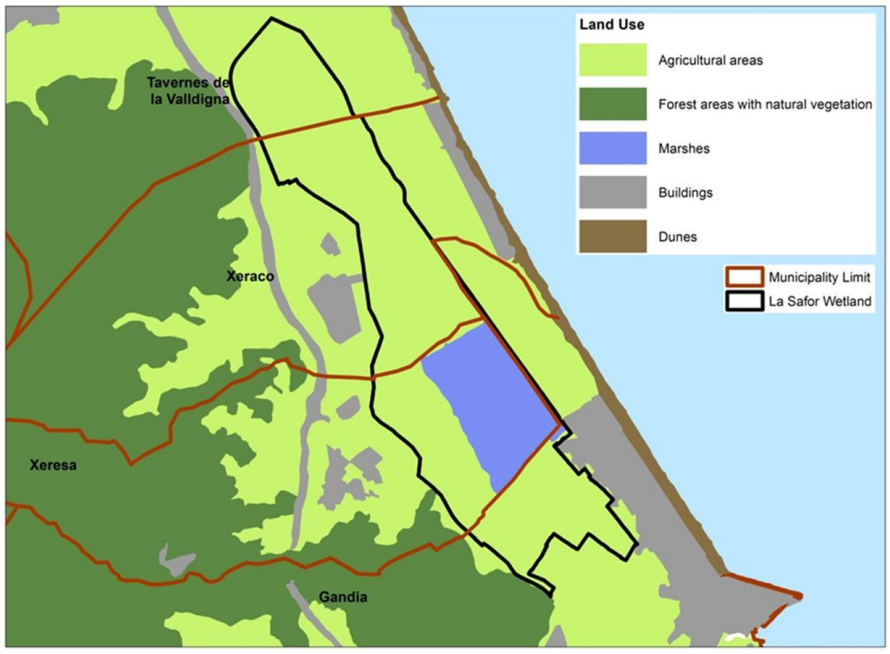

Figure 3.2. Land uses and municipality limits in the La Safor wetland.

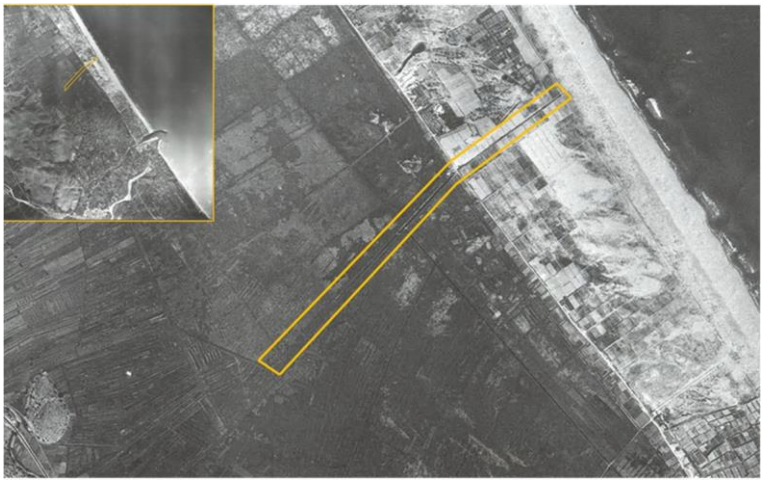

Figure 3.3. Aerial image, 1956. Marked in yellow is the channel "Escorredor de Xeresa".

3.2.2 IMAGE PROCESSING

The official cartography of protected areas (Valencian Wetland Inventory) was used to delimitate wetland (Figs 1 and 2). The LIDAR-derived DEM was calculated for 2 m pixel, the orthometric heights information was obtained from LiDAR sensor with a density of 0.5 points/m2 (PNOA 2007 CC BY 4.0 www.scne.es). Sentinel-2A images from the Multispectral Instrument (MSI) processed at level 1C were obtained from Copernicus (https://scihub.copernicus.eu/dhus/#/home). The atmospheric correction was done with Sen2Cor tool (version 02.05.05) using SNAP software (ESA, version 6.0.0). The NDWI index was calculated according to Pena-Regueiro et al. [7] see eqn (1):

$$NDWI = \frac{B03-B08}{B03+B08} \qquad (1)$$

B03 and B08 are Sentinel-2 bands with 10 m spatial resolution. For each date, we delimited the water polygons using the -0.30, threshold defined by Pena-Regueiro et al. [7]. The acquisition date of the Sentinel 2A image was chosen to show the higher extent of the flooded area. This depends on the precipitation regime, so pluviometry data was obtained from the closest meteorological station, Xeraco town station (Fig. 3.1) [12].

3.3 RESULTS AND DISCUSSION

The LIDAR-derived DEM can be observed in Fig. 3.4. La Safor wetland is in a depressed area between karstic relieves and the Mediterranean Sea. Most of the protected area is below 2.5 m.a.s.l. In the north part, there is an agricultural area

dedicated to horticultural crops that is below sea level (between -1.5–0 m.a.s.l.), represented by the white area in Fig. 3.4(b).

From the 1970s onward, a new production system called “bancs” was developed in La Safor wetland [1] that raised the height of agricultural plots with the materials dredged from adjoining plots which became ponds. Also, mining licenses for peat were granted when excavating up to one and a half meters below ground level. In the 1980s and 1990s, the agricultural transformation projects continued to create large citrus farms [1]. This transformation can be appreciated in Fig. 3.4, plots between 1.5–2.5 m adjoining plots between 0.5–1 m (dark blue-pink areas), and plots between 3–5 m adjoining plots between 1.5–2.5 m (green-dark blue areas). The most depressed plots correspond to the excavated ponds, and the highest to the “bancs”.

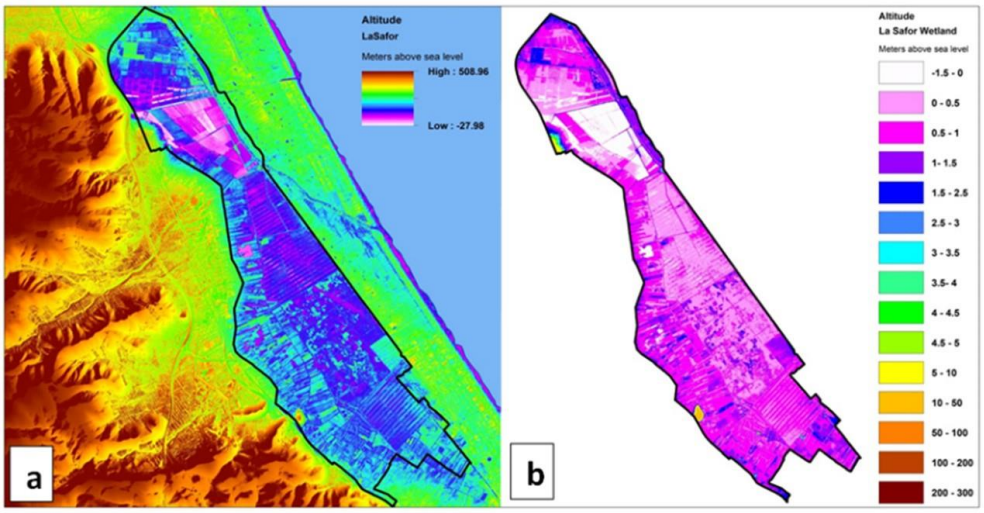

Figure 3.4. LIDAR-derived digital elevation model.

In Fig. 3.5, we can observe the results of mapping water bodies by the NDWI methodology [7]. The Sentinel-2A image was captured on January 16, 2017. The results show a total flooded surface of 1.46 km^2. The image data was selected for two reasons. The average annual precipitation for the Xeraco town meteorological station is 709.2 mm, and the two months before the image data there was an accumulated precipitation of 326.7 mm. Then, the image was captured after a wet period with maximum precipitation in 24 hours of 50.6 mm on November 28, 2016, 71.8 mm on December 5, 2016 and two consecutive days with 46.1 mm on December 18 and 19, 2016. Usually, dense vegetation prevents remote sensing indices to detect water, and we can only observe free vegetation water bodies. But, on November 9, 2016, there

was a fire in the wetland that burned 90 Ha (Fig. 3.6). The disappearance of dense marsh vegetation made possible to appreciate the water layer after the rainy period. The main water polygon (1 km^2 flooded area) is in an area called "Les Galerasses" which is where marsh is better conserved (Fig. 3.2). We can also appreciate, north and south of this bigger water polygon, longitudinal polygons that correspond to the above-described ponds. In the most depressed area, white polygon in Fig. 3.4, we do not appreciate relevant flooding. This can be explained because in these plots there is a big farm of horticultural crops, and they have four water pumps to discharge water to the Vaca River.

Local authorities (Gandia, Xeresa, Xeraco and Tavernes councils) usually need to deal with conflicting interests among different users, i.e., owners, farmers, irrigators, hunters, fishermen, residents, conservationists, and companies. Farmers are grouped in irrigation communities, such as Gandia's Irrigation Community. For these users, it is very important to avoid crops flooding, because this can cause root asphyxia and loss of productivity [13]. Then, they control several water pumps in the wetland (inside and outside of the protected area), and they turn them on after important rain event to discharge water through the irrigation channels to the sea. This evacuating capacity is not homogenous in all the wetland, Gandia has more facilities, while Xeraco and especially Xeresa have more difficulties due to the abandonment or disappearance of hydraulic infrastructures (i.e., Escorredor de Xeresa).

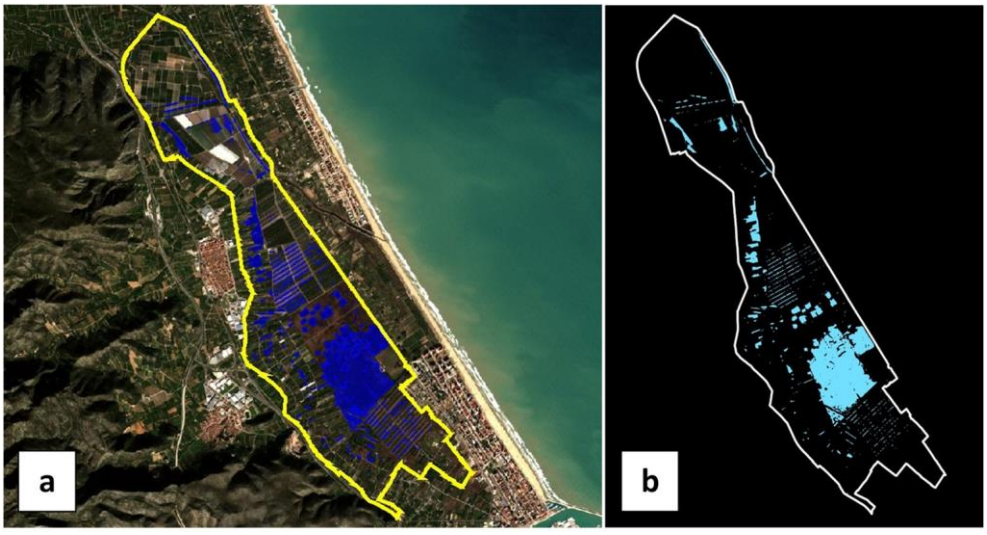

Figure 3.5. La Safor wetland: (a) Natural colour image and NDWI mask, January 16, 2017; and (b) NDWI mask with higher contrast, January 16, 2017.

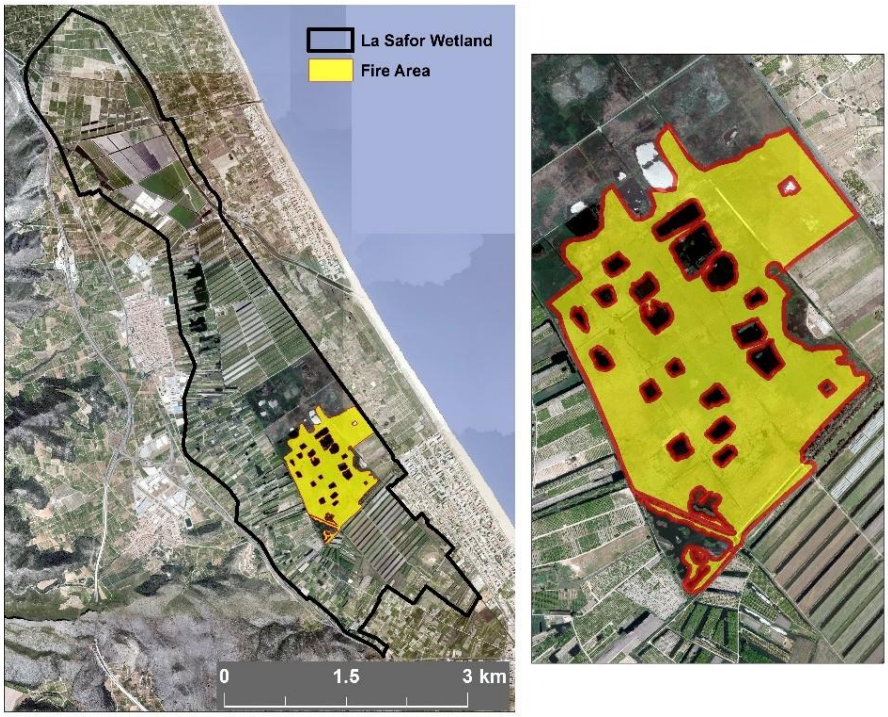

Figure 3.6. In yellow: fire area burned on November 9, 2016 the in La Safor wetland.

In 2014, 91.9% of La Safor Wetland was private land, divided in small properties and big farms. There is consensus that private land ownership complicates management of protected areas and limits the scope of action of the various administrations [1]. One solution to this increasing problem is the purchase of land by the administration [14]. In 2018, the Territorial Action Plan for the Green Infrastructure of the Coast of the Valencian Community was passed by Decree 58/2018, dated May 4. Thanks to the approval of this plan, the public administration has been able to buy several plots on the north limit of the Gandia beach urban area. This action makes possible the recovery of the "Escorredor de Xeresa" old watercourse through this current public land.

The corrective measures that are included in small projects competing for different fund sources, such as European funds, are based on this analysis of land uses, the LIDAR-derived DEM and the map of flooded areas by NDWI index. Corrective measure must also have into account the need of considering all conflicting uses and ecosystem services provided by the wetland for integral management. The first measure is the restoration of the Channel Travessera (Fig. 3.1). Currently, this is the main discharge of the wetland area in the municipalities of Xeresa and Xeraco. The restoration will be executed in different phases. The main objective is elevating the

separation between the marsh and the crop area and building discharge connections between them. So, in case of important rain event the agricultural area can drain to the marsh area, and to the ponds. This measure will fulfil different purposes, it will reduce the flooding problems of the agricultural area, it will increase the flooded area in the marsh, and it will allow a higher recharge of the aquifer avoiding direct discharge to the sea.

3.4 CONCLUSION

The remote sensing and Airborne LiDAR data analysis allowed to identify and map the flooded surface. For successful wetland management, it is key having into account all conflicting uses and ecosystem services provided by the wetland. In wetlands coexist uses with different needs such as agricultural and environmental use, and managers need to reach an equilibrium. Agriculture is consolidated in the La Safor wetland after long time, and it has implemented some measure to avoid productivity loss that are not the best environmentally (i.e. water pumps draining the fields to the sea). After our analysis, the corrective measures proposed a search to increase the flooded marsh area and protect the fields, allowing a higher recharge of the aquifer.

3.5 REFERENCES

[1] Sebastiá-Frasquet, M.-T., Altur, V. & Sanchis, J.-A., Wetland planning: Current problems and environmental management proposals at supra-municipal scale (Spanish Mediterranean coast). *Water*, **6**, pp. 620–641, 2014.

[2] Convention on Wetlands of International Importance (Ramsar Convention). www.ramsar.org. Accessed on: 13 Jun. 2020.

[3] Millennium Ecosystem Assessment, *Ecosystems and Human Well-Being: Synthesis*, Island Press: Washington, DC, 2005.

[4] Mitsch, W.J., Bernal, B. & Hernandez, M.E., Ecosystem services of wetlands. *International Journal of Biodiversity Science, Ecosystem Services & Management*, **11**(1), pp. 1–4, 2015.

[5] Why are Wetlands Important? U.S. Environmental Protection Agency, Wetlands Protection and Restoration. https://www.epa.gov/wetlands/why-are-wetlands-important. Accessed on: 13 Jun. 2020.

[6] Balmford, A. et al., Economic reasons for conserving wild nature. *Science*, **297**(5583), pp. 950–953, 2002.

[7] Pena-Regueiro, J., Sebastiá-Frasquet, M.-T., Estornell, J. & Aguilar-Maldonado, J.A., Sentinel-2 application to the surface characterization of small water bodies in wetlands. *Water*, **12**, pp. 1487, 2020.

[8] Huang, C., Peng, Y., Lang, M., Yeo, I.-Y. & McCarty, G., Wetland inundation mapping and change monitoring using Landsat and airborne LiDAR data. *Remote Sensing of Environment*, **141**, pp. 231–242, 2014.

[9] Zhou, Y. et al., Open surface water mapping algorithms: A comparison of water-related spectral indices and sensors. *Water*, **9**, pp. 256, 2017.

[10] Tian, S., Zhang, X., Tian, J. & Sun, Q., Random forest classification of wetland landcovers from multi-sensor data in the arid region of Xinjiang, China. *Remote Sensing*, **8**, pp. 954, 2016.

[11] Hladik, C. & Alber, M., Accuracy assessment and correction of a LIDAR-derived salt marsh digital elevation model. *Remote Sensing of Environment*, **121**, pp. 224–235, 2012.

[12] AVAMET. Valencian Association of Meteorology. https://www.avamet.org/. Accessed on: 13 Jun. 2020.

[13] Sebastiá, M.-T., Rodilla, M., Sanchis, J.-A., Altur, V., Gadea, I. & Falco, S., Influence of nutrient inputs from a wetland dominated by agriculture on the phytoplankton community in a shallow harbour at the Spanish Mediterranean coast. *Agriculture, Ecosystems & Environment*, **152**, pp. 10–20, 2012.

[14] Maltby, E., Acreman, M., Blackwell, M.S.A., Everard, M. & Morris, J., The challenges and implications of linking wetland science to policy in agricultural landscapes— Experience from the UK National Ecosystem Assessment. *Ecological Engineering*, **56**, pp. 121–133, 2013.

4 CAPÍTULO 4:
REMOTE SENSING TEMPORAL RECONSTRUCTION OF THE FLOODED AREA IN “TABLAS DE DAIMIEL” INLAND WETLAND 2000–2021

Pena-Regueiro J., Estornell J., Aguilar-Maldonado J.A., Sebastiá-Frasquet M.T. 2023. Remote Sensing Temporal Reconstruction of the Flooded Area in "Tablas de Daimiel" Inland Wetland 2000-2021. Sensors, 23(8):4096. https://doi.org/10.3390/s23084096

4.1 INTRODUCTION

It is a fact that wetlands play a key role in the hydrological cycle, and the hydrological conditions have a vital role on the ecological status of wetlands [1]. However, human activity causes changes in this cycle, and is one of the main causes of wetland degradation. Activities such as land reclamation for agriculture, dams, drainage, or surface water diversions cause the lowering of groundwater tables, the disappearance of springs and the decrease of flooded areas in wetlands, that can even end in the full desiccation triggering spontaneous combustion of peatlands [2 - 5].

The role of flooding extent and duration is crucial for biodiversity (wildlife habitat) and other wetland ecosystem services (e.g., carbon storage, water quality, storing floodwater, and maintaining the water levels in the dry season) [6]. In ecology, historical trends and observation of long-term change is central to understanding [7]. So, to select the most adequate conservation and restoration measures of wetlands, and to monitor their effectiveness we require information about their hydrological conditions. Typically, hydrological monitoring of wetlands is done by in situ measures (piezometers and gauging stations) that may provide good temporal resolution but over a limited number of observation points [1, 8]. However, gauge measurements offer little information to detect spatial patterns, like flooding status, because usually distance between gauges is several kilometers or even more [1, 8-10]. So, only with in situ measures we cannot analyze the surface changes in these highly dynamic ecosystems.

A common approach to assess the spatial and temporal variability of water bodies is to use long-term (>25–30 years) remote sensing datasets. Satellite imagery has notoriously improved water bodies monitoring in terms of detecting changes over time and space [11]. The advances in remote sensing technology have allowed diverse hydrological applications such as monitoring fluctuations of lake or dam surface or mapping small water bodies [12 - 16]. Remote sensing data from Landsat satellites (Landsat 5 (TM), Landsat 7 (ETM +), and Landsat 8 (OLI)) has been widely used since the launch of Landsat thematic mapper (TM) on March 1, 1984 (Roy et al. 2014). But Landsat has significant drawbacks to monitor wetlands. The Landsat spatial resolution of 30 m is unsuitable to monitor water bodies with surface area 0.1–5 ha (surface area monitoring error > 20% or higher) [15, 17]. Water surface classification accuracy varies according to the water body size and shape complexity [15]. This is especially relevant

in arid and semiarid regions [11]. These regions are frequently affected by droughts, and this cause a more intensive use of groundwater that worsens the problems caused by the absence of precipitation. This turns into smaller unconnected water bodies than in other climates, then spatial resolution is a key parameter [15]. Also, the 16-days temporal resolution of these sensors can be a limiting factor to interpret wetlands dynamics [13, 15].

The Sentinel-2 satellite launched by the European Space Agency (ESA) in 2015 includes a constellation of two polar-orbiting satellites with 5-days temporal resolution and a maximum of 10 m spatial resolution [13, 15, 18] The higher resolution of Sentinel-2, both spatial and temporal, can significantly improve the monitoring range, especially for small sites that cannot be covered by the Landsat satellite [8, 11, 13, 15, 18]. Some studies have assessed a multi-sensor approach that takes advantage of Landsat and Sentinel-2 [12, 15, 16]. The combined Sentinel-2 and Landsat dataset theoretically allows to reduce the temporal resolution to about three days [16]. The use of both satellites allows to reconstruct a longer study period to detect trends and analyze the effect of restoration measures or climatic variability. To correctly interpret long data, it is necessary first to compare both sensors for the same period and area.

From these remote sensing images, we can extract water pixels through different methodologies, among these, water indices are one of the more widely used because they are more reproducible and then more generalizable [13]. Commonly applied indices include the normalized difference water index (NDWI), modified normalized difference water index (MNDWI), normalized difference moisture index (NDMI), Normalized Difference Vegetation Index (NDVI), Automated Water Extraction Index (AWEI) [8, 14, 18]. By selecting the appropriate threshold for these indices, the image pixels can be categorized into water or non-water, and wetland inundation conditions can be mapped.

The main objectives of this research are to reconstruct the flooded area in Tablas de Daimiel National Park (TDNP) wetland for the 2000-2021 period using Landsat and Sentinel-2 sensors, and to assess the TDNP state through an anomaly analysis of the total water body surface. The anomaly of the total water body surface will be related to precipitation, river flow and piezometric level anomalies to discern the variable that explains most of this semi-arid region wetland. The flooded area will be calculated by first choosing the optimal water index and threshold for each sensor.

4.2 MATERIALS AND METHODS

4.2.1 STUDY AREA

Tablas de Daimiel is a floodplain wetland in central Spain, in the confluence of the Cigüela and Guadiana Rivers, in the municipalities of Daimiel and Villarrubia de los Ojos, within the province of Ciudad Real (439400 m, 4333500 m, zone 30, UTM, European Terrestrial Reference System 1989, Figure 4.1). It is located at an altitude of 617 m. Climate in the region is typically continental and semiarid, characterized by a low average annual rainfall and recurrent droughts. Data from the meteorological station of Las Tablas de Daimiel show that the average annual rainfall is 376 mm for the historic register from 2001/02 to 2021/22, with a wide range of variation: a minimum of 182 mm, in the hydrologic year 2004/05, and a maximum of 589.8 mm, in 2009/10.

Tablas de Daimiel was declared Natural Park (TDNP) by Decree 1874/1973 of 28 June; also, it is a Biosphere Reserve since 1981, and it is included in the Ramsar Convention on Wetlands since 1982. It was declared Special Protection Area (SPA) by Decree 82/2005 of 12 July and Special Area of Conservation (SAC) by Decree 187/2015 of 7 August. (SiteCode: ES0000013 of the Natura 2000 Network).

The surface of the TDNP is 3,030 ha of which approximately 1,800 ha are subjected to flooding, with an average water depth of 0.90 m [7]. Under natural conditions, the wetland received inflows from the overflow from the rivers Guadiana and Cigüela and by contributions from groundwater [2, 19]. Cigüela River provided brackish water on a seasonal basis. Since 1988, water from the Tagus River basin is diverted into the National Park through Cigüela River [2, 19]. Guadiana River and the Mancha Occidental aquifer discharged freshwater. The thickness of this groundwater system exceeds 400 m in some sectors [4].

Groundwater extraction for irrigation in the upper Guadiana River basin affects this system since the early seventies of the last century [7, 19]. By the end of that decade, extractions exceeded TDNP inflows for the first time [2, 20]. Between 1974 and 1987 the irrigated area increased from 30,000 to 125,000 ha, so in 1987 groundwater extraction nearly doubled the aquifer's replenishment rate on a consistent basis (580 Mm3/year vs. 320 Mm3/year) [21, 22]. The intensive groundwater use together with drought periods caused that groundwater levels dropped drastically, and the decrease in the flooded

surface of TDNP. In 1986, the TDNP was completely dry and burned a third of the surface [21, 22]. The degradation process of this ecosystem caused again the drying up of the wetland from 2004 to 2009, and a smoldering peat fire started inside the TDNP in August

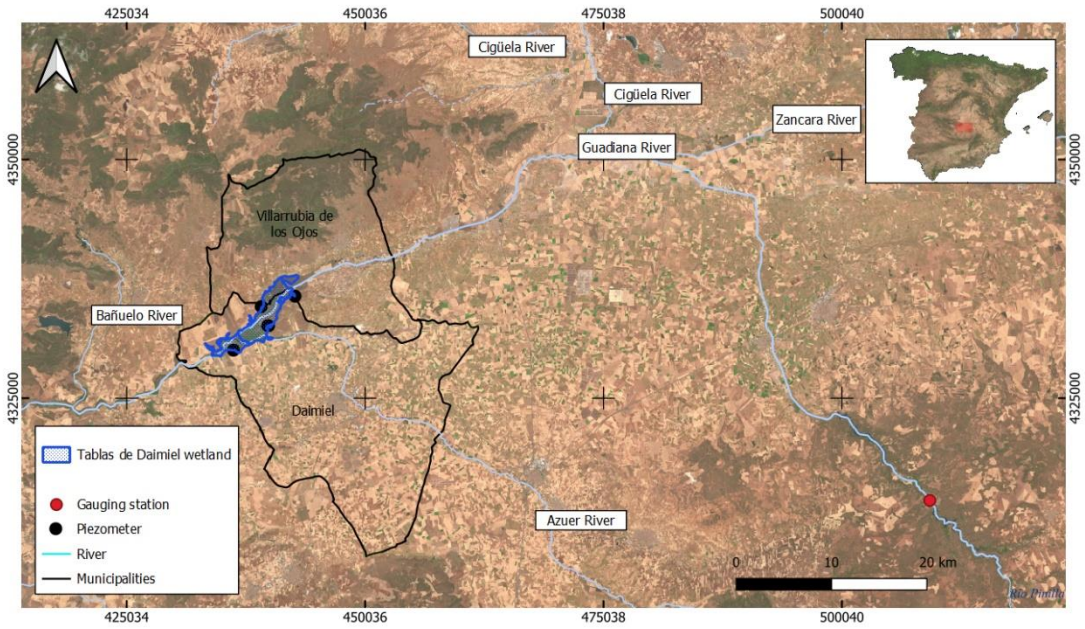

Figure 4.1. Study area including the perimeter of the Tablas de Daimiel National Park (blue polygon), gauging stations (red points), piezometers (black points), rivers (cyan lines) and municipalities in which the studied wetland is located (black polygons).

4.2.2 IMAGE PROCESSING

Sentinel-2A/B images processed at level 1C were obtained from Copernicus (https://scihub.copernicus.eu/dhus/#/home). The atmospheric correction was done with Sen2Cor tool (version 02.05.05) using SNAP software (ESA, version 6.0.0). The following reference parameters were defined: aerosol and MID LAT (Auto); ozone (value 0, determined automatically by the processor); Bidirectional Reflectance Distribution Function (BRDF) correction (value 21, standard recommended value); BRDF lower (value 0.22, standard value of the lower limit of the correction factor BRDF); visibility (40 km, appropriate value for the Iberian Peninsula); altitude (615 m above sea level). Landsat images TM Collection 2 Level-2 were obtained from USGS servers: Landsat-8 OLI (https://espa.cr.usgs.gov/index/) and Landsat-7 ETM+ and Landsat-5 (https://earthexplorer.usgs.gov/).

Images of high spatial resolution were used for validation. These images were obtained from the Spanish National Cartography Institute (IGN) Orthophoto 2017 and 2018 CC BY 4.0 © (spatial resolution 0.25 m, https://www.ign.es/web/ign/portal) and Google Earth ©. The dates of these images were the closest to Sentinel-2A/B, Landsat-8 OLI and Landsat-5 TM image acquisitions. The full list of images used in this study by date is provided in Appendix A, Table A1.

The official cartography of this protected area (Natural Parks Net, Ministry for the Ecological Transition and the Demographic Challenge) was used to delimitate the wetland (Figure 4.1). We delimited the water and non-water polygons for each validation image. These polygons were delineated through visual examination using as a base map high-resolution images (orthophotos) and was done with the software ArcGis 10.5 (ESRI 2016. ArcGIS Desktop: Release 10.5 Redlands, CA: Environmental Systems Research Institute). The visual delimitation was possible considering the high spatial resolution of the orthophotos (0.25 m). Water polygons smaller than 100 m2 were excluded, for Sentinel-2A/B analysis considering the maximum spatial resolution of Sentinel-2A/B bands used in this study. For Landsat-8 OLI and Landsat-5 TM analysis water polygons smaller than 900 m2 were excluded considering these sensors spatial resolution.

The spectral information was extracted from the Sentinel-2A/B, Landsat-8 OLI and Landsat-5 TM images to calculate the six spectral indices shown in Table 4.1 for the wetland polygon (Figure 4.1). The choice of indices was based on literature review [8]. These indices classify as water/non-water according to a threshold value, but different authors propose different thresholds for the same indices. We aimed to define a unique threshold that can be as global as possible with optimum results. So, for each date and sensor we tested all the thresholds from −0.50 to 0.50 with a 0.05 step, except for the AWEI(NSH) (Automated Water Extraction Index, No Shadow) and the AWEI(SH) (Automated Water Extraction Index, shadow) indices whose thresholds ranged from −50 to −5000, and the step is detailed in the results section.

Table 4.1: Calculated spectral indices

INDEX	EQUATION	SOURCE	SENTINEL-2 BANDS
NDWI	[(GREEN - NIR) / (GREEN + NIR)]	[26]	[(B03 - B08) / (B03 + B08)]
MNDWI	[(GREEN - SWIR2) / (GREEN + SWIR2)]	[27]	[(B03 - B11) / (B03 + B11)]
CEDEX	(NIR/RED) - (NIR/SWIR)	[28]	(B05/B04) - (B05/B11)
RE-NDWI	[(GREEN - MIR) / (GREEN + MIR)]	[29]	[(B03 - B05) / (B03 + B05)]
AWEI(SH)	BLUE + 2.5* GREEN − 1.5* (NIR + SWIR) − 0.25* SWIR	[12]	[B02 + 2.5 x B03 − 1.5 x (B08+ B011) − 0.25 x B12]
AWEI (NSH)	4 *(GREEN-MIR) − (0.25*NIR + 2.75*SWIR)	[12]	[4 x (B03-B11) - (0.25 x B08+2.75 x B12)]
INDEX	**EQUATION**	**SOURCE**	**LANDSAT-8 OLI**
NDWI	[(GREEN - NIR) / (GREEN + NIR)]	[26]	[(B03 - B05) / (B03 + B05)]
MNDWI	[(GREEN – SWIR1) / (GREEN + SWIR1)]	[27]	[(B03 – B06) / (B03 + B06)]
CEDEX	(NIR/RED) - (NIR/SWIR)	[28]	(B05/B04) - (B05/B06)
RE-NDWI	[(GREEN - RED) / (GREEN + RED)]	[29]	[(B03 - B04) / (B03 + B04)]
AWEI(SH)	BLUE + 2.5 x GREEN − 1.5 x (NIR + SWIR1) − 0.25 x SWIR2	[12]	[B02 + 2.5 x B03 − 1.5 x (B05+ B06) − 0.25 x B07]
AWEI (NSH)	4 x (GREEN-SWIR1) − (0.25 x NIR + 2.75 x SWIR2)	[12]	[4 x (B03-B06) - (0.25 x B05+2.75 x B07)]
INDEX	**EQUATION**	**SOURCE**	**LANDSAT-5 TM**
NDWI	[(GREEN - NIR) / (GREEN + NIR)]	[26]	[(B02 – B04) / (B02 + B04]
MNDWI	[(GREEN – SWIR1) / (GREEN + SWIR1)]	[27]	[(B02 – B05) / (B02 + B05]
CEDEX	(NIR/RED) - (NIR/SWIR)	[28]	[(B04 / B03) - (B04 / B05]
RE-NDWI	[(GREEN - RED) / (GREEN + RED)]	[29]	[(B02 – B03) / (B02 + B03]
AWEI(SH)	BLUE + 2.5 x GREEN − 1.5 x (NIR + SWIR1) − 0.25 x SWIR2	[12]	[B01 + 2,5 x B02 – 1,5 x (B04+B05) - 0,25 x B07]
AWEI (NSH)	4 x (GREEN-SWIR1) − (0.25 x NIR + 2.75 x SWIR2)	[12]	[4 x (B02 – B05) – (0,25 x B04 + 2,75 x B07)]

To validate the results obtained from the Sentinel-2A/B, Landsat-8 OLI and Landsat-5 TM images, we designed a random sampling of 60 points (30 water/ 30 non-water) for each sensor and date of the high spatial resolution images used in this study (see Appendix A, Table A1). Landsat-5 results were validated using three orthophotos (03/01/2005, 24 & 28/07/2006, 13 & 14/07/2009 - 31/08/2009). For Landat-8 and Sentinel-2A/B were used other three orthophotos (27 & 28/06/2015, 13/11/2015, 28/09/2018). A total of 540 points were considered for validation (180 points for each sensor imagery).

The ground control points were distributed randomly in the entire wetland surface. We selected the number of points according to the general guideline provided by Congalton and Green [24], who recommended a minimum of 50 samples for each map class for maps of less than 1 million acres in size and fewer than 12 classes. For the points sampled for each sensor (180), we compared the classification of each index (6 indices in Table 4.1) and each threshold, with the ground-truth images, to assess correct classifications. Overall accuracy index was calculated for each random sampling. [24]. The best index and threshold were selected according to overall accuracy results [8, 25].

We made a temporal reconstruction of water bodies surface in TDNP since January 2000 to October 2021, with the best index using Landsat-8 OLI, Landsat-7 ETM+ and Landsat-5 TM (Table A1). Sentinel-2 A/B was also used for the period June 2015 to October 2021. We compared the results of water surfaces derived from Landsat-8 and Sentinel-2 for the period June 2015 to October 2021. This analysis is important to evaluate the performance of both sensors, and to see if we can effectively increase temporal resolution by completing time series with images from both sensors.

To better assess the TDNP state we made an anomaly analysis of the total water body surface along the study period using the data obtained from Landsat-8 OLI, Landsat-7 ETM+ and Landsat-5 TM series.

Surface data was averaged by quarter calculating the Water Surface Anomaly Index IAWi (Equation 1).

$$\boldsymbol{IAW_i} = \frac{\boldsymbol{A_{WAi} - A_{WAaverage}}}{\boldsymbol{A_{WAsd}}} \qquad \text{Equation 1}$$

IAWi being the index of the Water Surface Anomaly for a quarter i,

AWAi is the average water surface in the quarter i, ALAaverage is the average water surface in the quarter of the period analyzed (January 2000 to October 2021) and AWAsd is the standard deviation of the water surface in the quarter of the period analyzed. Based on these values, the quarters with positive and negative anomalies were analyzed.

Precipitation data from the meteorological station of Las Tablas de Daimiel was obtained (https://eportal.mapa.gob.es/websiar/SeleccionParametrosMap.aspx?dst=1). With these values, the Precipitation Anomaly Index was calculated, IAPi (Equation 2) [8, 26].

$$IAP_i = \frac{P_i - P_{average}}{P_{sd}}$$ Equation 2

IAPi being the index of the Precipitation Anomaly for a quarter i, Pi is the average precipitation in the quarter i, Paverage is the quarter average precipitation in the period analyzed (hydrologic year 2001 to 2021) and Psd is the standard deviation of precipitation in the quarter of the period analyzed.

Flow data were obtained from the Guadiana River gauge in Ruidera municipality, 15 km upstream of TDNP (https://sig.mapama.gob.es/redes-seguimiento/?herramienta=aforos) (Figure 4.1). The Flow Anomaly Index was calculated, IAFi (Equation 3).

$$IAF_i = \frac{F_i - F_{average}}{F_{sd}}$$ Equation 3

IAFi being the index of the Flow Anomaly for a quarter i, Fi is the average flow in the quarter i, Faverage is the quarter average flow in the period analyzed (hydrologic year 2000 to 2021) and Fsd is the standard deviation of flow in the quarter of the period analyzed.

Finally, the Piezometric data were obtained from 4 piezometers surrounding TDNP (Figure 4.1). The data used for the analysis was water depth. Piezometers European codes were: ES040ESBT000404042, ES040ESBT000404046, ES040ESBT000404145 and ES040ESBT000404294, and were all located in the Mancha Occidental I aquifer (https://sig.mapama.gob.es/redes-seguimiento/?herramienta=Piezometros). With these values, the Piezometric Anomaly Index was calculated, IAPZi (Equation 4)

$$IAPZ_i = \frac{PZ_i - PZ_{average}}{PZ_{sd}}$$ Equation 4

IAPZi being the index of the Piezometric Anomaly for a quarter i, PZi is the average piezometric level in the quarter i, PZaverage is the quarter average piezometric level in the period analyzed (hydrologic year 2009 to 2021) and PZsd is the standard deviation of piezometric level in the quarter of the period analyzed.

Spearman correlation coefficient was calculated between the variables water surface, precipitation, flow and piezometric level by quarters (Table 4.2).

4.3 RESULTS

Extraction of water bodies was obtained from Sentinel-2 A/B, Landsat-5, Landsat-7 ETM+ and Landsat-8 images (Table A1). To do this, six water indices (Table 4.1) and a set of thresholds were analyzed. For Landsat-5 images, the most accurate results were obtained when the MNDWI (0.88) and AWEI (nsh) (0.88) water indices were selected applying the thresholds values of -0.15 and -900, respectively (Figure 4.2a). For Landsat-8 images, the maximum overall accuracy was obtained for MNDWI (0.99) using a threshold value of -0.25 and -0.30 (Figure 4.2b). For these images, accurate results were also obtained for AWEI(nsh) (0.98), AWEI(sh) (0.97) and NDWI (0.96) water indices (Figure 4.2b). For AWEI (nsh) the highest values of overall accuracy were obtained for the thresholds -4000, -4500 and -5000 (Figure 4.2b). For AWEI(sh) water index the selected threshold was -2000 and for NDWI -0.25 and -0.30 (Figure 4.2b). For Sentinel-2 images, high performances in terms of overall accuracy were found for NDWI (0.99, threshold -0.20), MNDWI (0.98, thresholds -0.05 and -0.1), AWEI (sh) (0.98, thresholds -800, -900, -1000, - 1500) and AWEI(nsh) (0.98, thresholds -1000 to -4500) (Figure 4.2c). From these results, MNDWI index with a threshold of -0.15 was selected for Landsat-5 images to extract water bodies. Although, the same global accuracy was obtained for AWEI(nsh) index and threshold -900, the former index was selected since a lower performance was observed in areas close to the border of the water polygons. For Lansat-8 images it was selected the MNDWI index and a threshold of -0.25. The threshold value of -0.30, which generated the same accuracy, was disregarded since it was observed the same lower performance in areas close to the border of water surfaces. For Sentinel-2 images the NDWI index and a threshold of -0.20 was selected for extracting water bodies. Water areas were computed for each analyzed image in the period 2000-2021 using these indices and thresholds. Then, the Water Surface Anomaly Index was calculated for the analysis period (Equation 1).

Thresholds	NDWI	MNDWI	CEDEX	RE-NDWI
0.50	0.50	0.50	0.73	0.50
0.45	0.50	0.50	0.73	0.50
0.40	0.50	0.50	0.73	0.50
0.35	0.50	0.50	0.73	0.50
0.30	0.50	0.50	0.73	0.50
0.25	0.50	0.50	0.73	0.50
0.20	0.50	0.50	0.73	0.50
0.15	0.50	0.51	0.73	0.50
0.10	0.50	0.52	0.73	0.50
0.05	0.52	0.54	0.73	0.50
0.00	0.59	0.63	0.73	0.69
-0.05	0.64	0.71	0.55	0.54
-0.10	0.68	0.77	0.55	0.50
-0.15	0.58	0.88	0.55	0.50
-0.20	0.52	0.82	0.55	0.50
-0.25	0.47	0.61	0.55	0.50
-0.30	0.50	0.50	0.55	0.50
-0.35	0.51	0.50	0.55	0.50
-0.40	0.50	0.50	0.55	0.50
-0.45	0.50	0.50	0.55	0.50
-0.50	0.50	0.50	0.55	0.50

Thresholds	Awei (sh)	Thresholds	Awei (nsh)
-50	0.63	-5000	0.50
-100	0.63	-10000	0.50
-200	0.63	-15000	0.51
-300	0.63	-20000	0.54
-400	0.63	-25000	0.61
-500	0.64	-30000	0.66
-600	0.64	-35000	0.72
-700	0.64	-40000	0.77
-800	0.64	-45000	0.82
-900	0.64	-50000	0.88
-1000	0.64	-55000	0.82
-1500	0.64	-60000	0.76
-2000	0.65	-65000	0.69
-2500	0.68	-70000	0.64
-3000	0.69	-75000	0.58
-3500	0.69	-80000	0.54
-4000	0.70	-85000	0.53
-4500	0.70	-90000	0.52
-5000	0.70	-95000	0.51

0.50 - 0.60
0.60 - 0.70
0.70 - 0.80
0.80 - 0.90

a)

Thresholds	NDWI	MNDWI	CEDEX	RE-NDWI
0.50	0.65	0.89	0.83	0.50
0.45	0.68	0.89	0.83	0.50
0.40	0.72	0.91	0.83	0.50
0.35	0.74	0.92	0.83	0.50
0.30	0.78	0.92	0.83	0.50
0.25	0.80	0.93	0.83	0.51
0.20	0.82	0.94	0.83	0.50
0.15	0.87	0.94	0.83	0.62
0.10	0.88	0.94	0.83	0.69
0.05	0.89	0.94	0.83	0.73
0.00	0.90	0.94	0.83	0.81
-0.05	0.91	0.95	0.86	0.75
-0.10	0.91	0.96	0.86	0.70
-0.15	0.93	0.98	0.86	0.60
-0.20	0.94	0.98	0.86	0.51
-0.25	0.96	0.99	0.86	0.50
-0.30	0.96	0.99	0.86	0.50
-0.35	0.94	0.97	0.86	0.50
-0.40	0.93	0.94	0.86	0.50
-0.45	0.91	0.91	0.86	0.50
-0.50	0.83	0.79	0.86	0.50

Thresholds	Awei (sh)	Thresholds	Awei (nsh)
-50	0.67	-5000	0.69
-100	0.71	-10000	0.72
-200	0.78	-15000	0.76
-300	0.81	-20000	0.77
-400	0.82	-25000	0.79
-500	0.84	-30000	0.80
-600	0.84	-35000	0.81
-700	0.85	-40000	0.81
-800	0.87	-45000	0.81
-900	0.87	-50000	0.82
-1000	0.89	-55000	0.82
-1500	0.93	-60000	0.85
-2000	0.97	-65000	0.87
-2500	0.94	-70000	0.93
-3000	0.86	-75000	0.97
-3500	0.79	-80000	0.97
-4000	0.73	-85000	0.98
-4500	0.64	-90000	0.98
-5000	0.60	-95000	0.98

0.50 - 0.60
0.60 - 0.70
0.70 - 0.80
0.80 - 0.90

b)

Thresholds	NDWI	MNDWI	CEDEX	RE-NDWI
0.50	0.55	0.73	0.92	0.50
0.45	0.57	0.78	0.92	0.50
0.40	0.61	0.81	0.92	0.50
0.35	0.68	0.83	0.92	0.51
0.30	0.76	0.86	0.92	0.52
0.25	0.82	0.88	0.92	0.59
0.20	0.84	0.92	0.92	0.66
0.15	0.84	0.94	0.92	0.72
0.10	0.91	0.95	0.92	0.74
0.05	0.91	0.96	0.92	0.71
0.00	0.93	0.97	0.92	0.73
-0.05	0.93	0.98	0.87	0.75
-0.10	0.96	0.98	0.87	0.71
-0.15	0.98	0.97	0.87	0.69
-0.20	0.99	0.97	0.87	0.57
-0.25	0.98	0.97	0.87	0.50
-0.30	0.93	0.95	0.87	0.50
-0.35	0.85	0.93	0.87	0.50
-0.40	0.78	0.86	0.87	0.50
-0.45	0.77	0.70	0.87	0.50
-0.50	0.73	0.58	0.87	0.50

Thresholds	Awei (sh)	Thresholds	Awei (nsh)
-50	0.96	-5000	0.92
-100	0.97	-10000	0.92
-200	0.97	-15000	0.94
-300	0.97	-20000	0.95
-400	0.97	-25000	0.96
-500	0.97	-30000	0.97
-600	0.97	-35000	0.96
-700	0.97	-40000	0.97
-800	0.98	-45000	0.97
-900	0.98	-50000	0.97
-1000	0.98	-55000	0.98
-1500	0.98	-60000	0.98
-2000	0.97	-65000	0.98
-2500	0.96	-70000	0.98
-3000	0.91	-75000	0.98
-3500	0.82	-80000	0.98
-4000	0.74	-85000	0.98
-4500	0.71	-90000	0.98
-5000	0.61	-95000	0.97

0.50 - 0.60
0.60 - 0.70
0.70 - 0.80
0.80 - 0.90

Figure 4.2. Overall accuracies for a set of thresholds applied to the Landsat-5 **(a)**, Landsat-8 **(b)** and Sentinel-2 images **(c)**. Light shaded colors show the indices and thresholds with poorest performance. Shaded in red color are used for indices and thresholds with the most accurate (closer to 1).

The Water Surface Anomaly Index showed several patterns in the analyzed peri-od (Figure 4.3a and b). From 2001 to 2003 positive and negative anomalies were detected without a clear trend. Between the second quarter of 2004 and the first quarter of 2005 positive anomalies were obtained. From this quarter to the first quarter of 2006 anomalies close to 0 were observed. Then, a longer period (3t-2006 to 1t-2010) with relevant negative anomalies is shown. After this phase, significant positive anomalies were observed until the third quarter of 2013 when a period with anomalies close to 0 were observed. This trend continued until the second quarter of 2019 when a set of significant negative anomalies were detected until 2021. In Figure 4.3 the Precipitation Anomaly Index (Equation 2) is also represented. Although some quarters showed positive and negative anomalies concurrent with water surface anomaly, other quarters showed opposite behavior for the anomaly indices (47% of the quarters) and absolute values of anomaly were significantly different in almost all quarters. In this sense, Spearman correlation analysis between these two parameters was calculated obtaining a value of -0.049 and P-value 0.677 indicating a lack of significant statistical relation-ship between them.

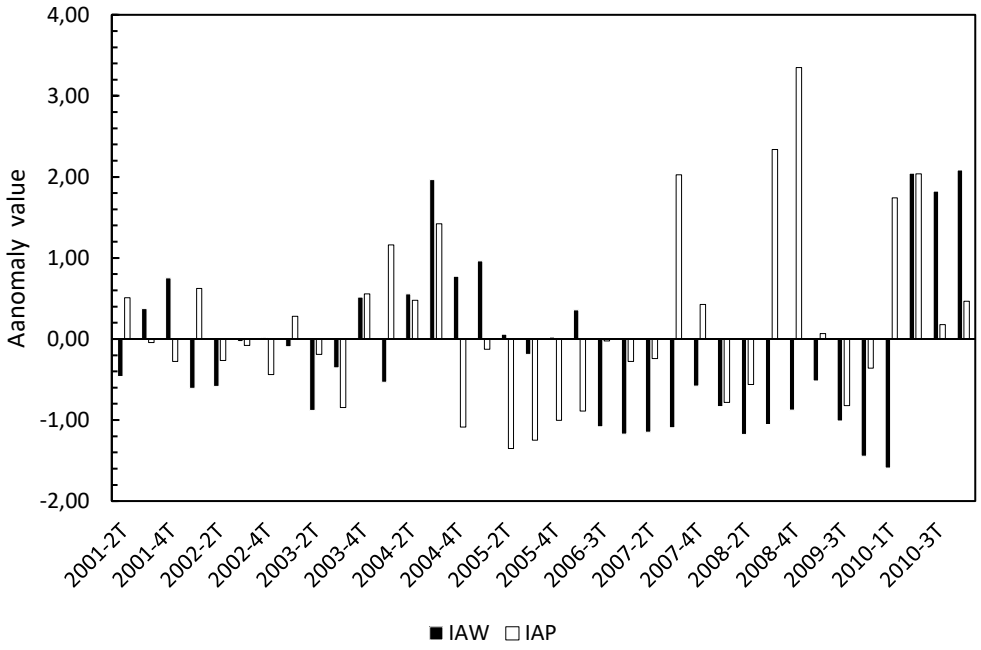

a)

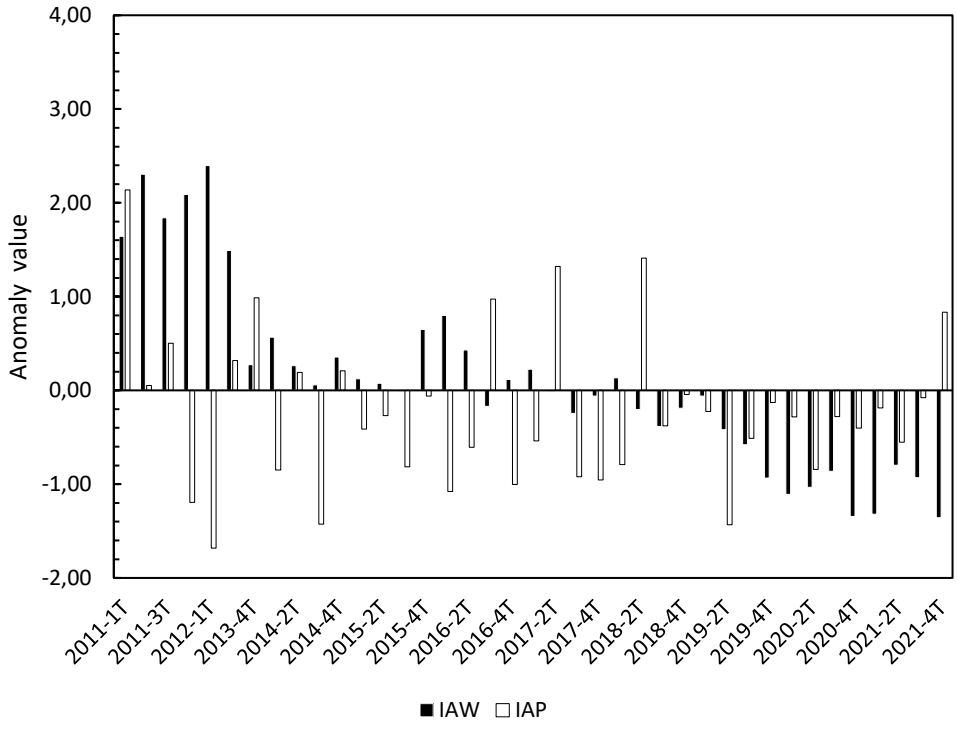

b)

Figure 4.3. Water Surface Anomaly Index (IAW) and Precipitation Anomaly Index (IAP) in the period 2001-2010 **(a)** and 2011 – 2021 **(b).**

Table 4.2: Spearman coefficient values among anomaly indices.

	IAW		IAF		IAF	
	Spearman Coefficient	P-value	Spearman Coefficient	P-value	Spearman Coefficient	P-value
IAP	-0.049	0.677				
IAF	0.369	0.003				
IAPZ	-0.406	0.009			0.109	0.544
IAP			0.087	0.488		

In Figure 4.4 a comparison among Water Surface Anomaly Index (Equation 1) and Flow Anomaly Index (Equation 3) is shown. In this case, concurrent positive and negative anomalies of these two indices were observed for more than 50% of the analyzed quarters. In this context, negative values of IAWi and IAFi were observed for the period 3t-2006 to 1t-2009 and positive values from 2t-2010 to 1t-2012. In this case the Spearman correlation analysis generated a value of 0.369 and a significative P-value (Table 4.2) indicating, although in a moderate way, the existence in some periods of statistical relationship between the water surface and river flow anomalies.

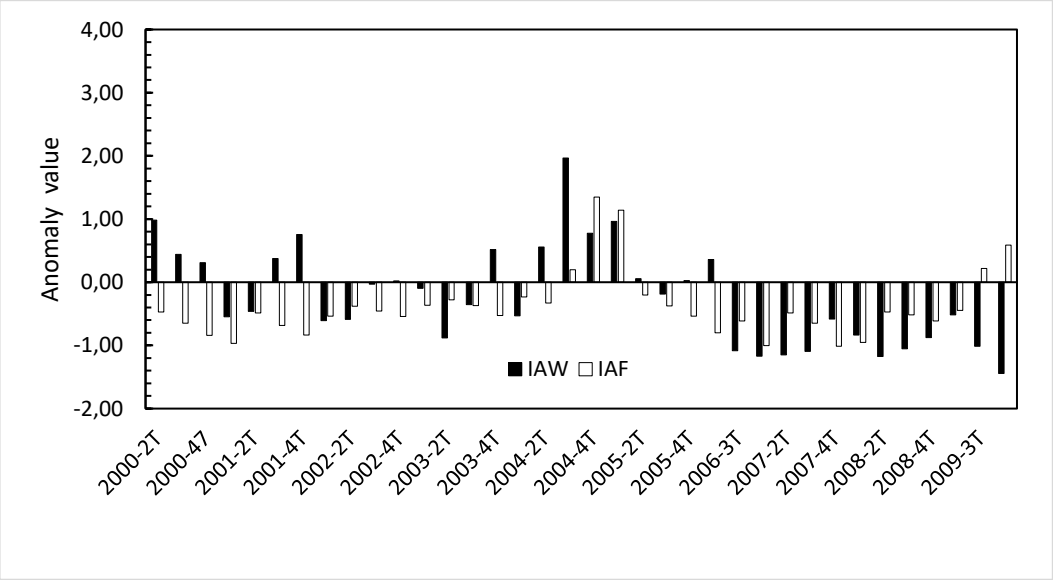

a)

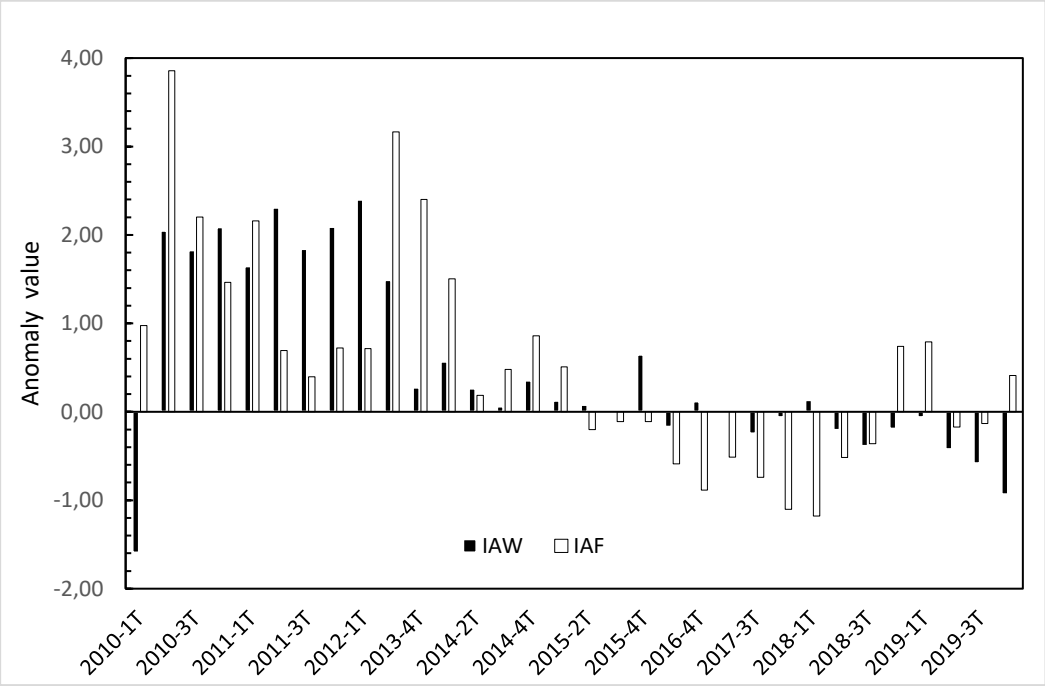

b)

Figure 4.4. Water Surface Anomaly Index (IAW) and Flow Anomaly Index (IAF) in the period 2001-2010 (a) and 2011 – 2021 (b).

In Figure 4.5 a comparison among Water Surface Anomaly Index (Equation 1) and Piezometric Anomaly Index (Equation 4) is shown. In this case, equal distribution patterns were detected in some quarters for the analyzed period (2009-2020). The highest positive anomalies derived from Piezometric Anomaly Index indicate low availability of groundwater (highest water depth). This occurred from the 3rd quarter of 2009 to the 1st quarter of 2010. For this period, significant negative anomalies for water surfaces were observed. This same pattern was detected for the period 2nd quarter to 4th quarter of 2020. In contrast, the highest positive anomalies for water surfaces (3rd quarter of 2010 – 3rd quarter 2013) occurred during the lowest negative anomalies of Piezometric Index. The low Piezometric Anomaly Index means that groundwater level is close to ground level. Similar patterns were observed from 2nd quarter of 2015 to 2nd quarter of 2016. For the rest of quarters in the analyzed period, water surface anomalies close to 0 matched with negative anomalies for piezometric anomalies values, indicating that groundwater outcrops into surface. The Spearman coefficient for these two anomalies was -0.406 and

the obtained P-value indicates a moderate inverse statistical relationship between piezometric level and water surface anomalies.

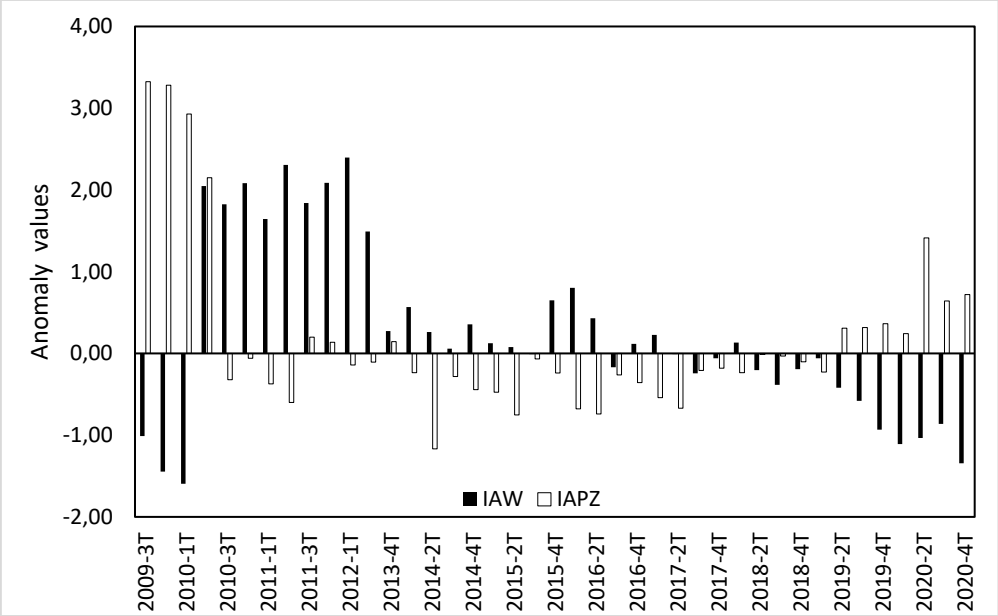

Figure 4.5. Water Surface Anomaly Index (IAW) and Piezometric Anomaly Index (IAPZ) in the period 2009 – 2021.

To compare the results of water surfaces derived from Landsat-8 and Sentinel-2 a linear regression model was calculated (Figure 4.6). An R2 value of 0.91 was obtained for this analysis indicating a high correspondence between the water surfaces derived from both sensors.

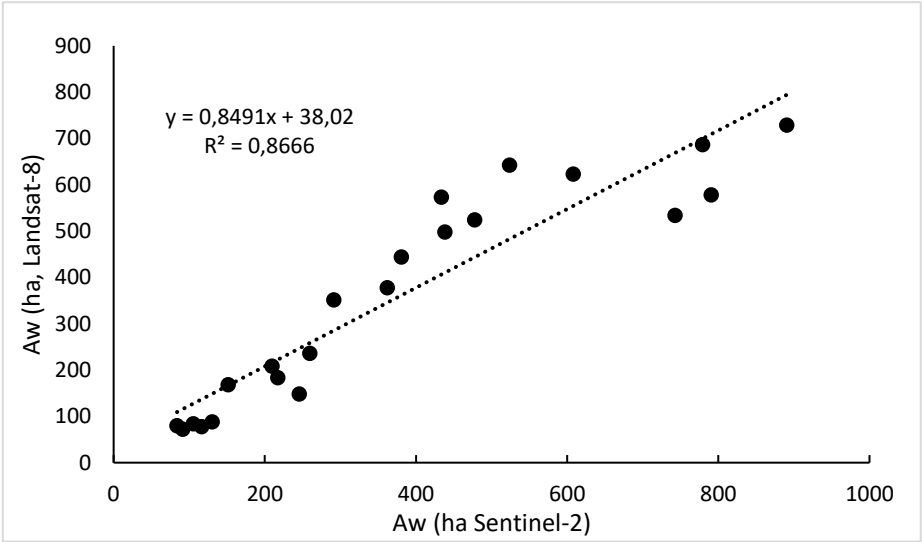

Figure 4.6. Comparison between water areas derived from Landsat-8 and Sentinel-2A/B images in the period 2015 - 2021.

4.4 DISCUSSIONS

The selected indices were the MNDWI index with a threshold of −0.15 for Landsat-5 images, the MNDWI index and a threshold of −0.25 for Lansat-8 images, and the NDWI index and a threshold of −0.20 for Sentinel-2 images. These indices are among the most used for detecting water surfaces with both sensors, as they have a high ability to separate water zones from other coverages [6, 14, 18]. The NDWI index often identifies built-up areas as water. For solving this problem, the modified NDWI (MNDWI) is obtained using MIR band instead of the NIR band [14, 27]. Pena et al. (2020) [8] also found that the best performing index was the NDWI for Sentinel-2 images in Mediterranean wetlands characterized by the presence of small water bodies, although their results were optimal for −0.30 threshold. Delimited natural area obtained from official cartography were used in both this research and Pena et al. (2020) [8], which allows to overcome this NDWI limitation. Adequate thresholds are required for accurate water extraction, but there is no specific rule for setting the threshold as it depends more on the region [14].

Climatic variability has a direct effect on surface water distribution, and the impacts of drought on surface water have been well documented [6]. Droughts are becoming more common around the world [6], and to monitor its impact on wetland flooded surface it is necessary to compile information on water surface, and on meteorological, hydrological, and hydrogeological variables. In this research we studied the evolution of water surface on a quarter basis thanks to remote sensing data, and we selected precipitation, river flow and piezometric levels as representative variables of the hydrological cycle. The water surfaces estimated in this study provide evidence to understand the surface water changes of the TDNP wetland. Assessing the state of groundwater dependent wetlands is complicated and more in arid and semiarid regions where recharge through precipitation may be concentrated in time [2]. The anomaly indices studied enable to identify the hydrological variables that have a major impact on water surface. Our results showed a lack of statistically significant relationship between Water Surface Anomaly Index and Precipitation Anomaly Index. In contrast, a significant positive relation (0.369) between Water Surface Anomaly Index and Flow Anomaly Index, and a significant negative relation (-0.406) between Water Surface Anomaly Index and Piezometric Anomaly Index were found.

The absence of significant correlation between surface water cover and precipitation in wetlands has been pointed by other authors [18]. Tough it may seem there is no correlation between water surface and precipitation we can observe some key moments in the historical evolution of TDNP in Figure 4.3. The most notorious in the 2nd quarter of 2010, when after the high positive precipitation anomaly registered in the 1st and 2nd quarter of 2010 the water surface anomaly changed from negative to positive values. This positive water surface anomaly remained until the 4th quarter of 2016 when it showed an oscillating behaviour between negative and positives values for about a year and a half. This matches one of the periods when the TDNP was almost completely flooded from 2010 to 2013 [2, 7], and the positive water surface anomalies were the highest. In this period groundwater naturally began to discharge into the wetland and springs reappeared [2]. Prior to this wet period, we can observe in Figure 4.3 negative Precipitation Index Anomalies since 4th quarter of 2004 to 4th quarter of 2009. This period corresponds to a severe drought that affected this region and caused important deterioration to the TDNP that ended in spontaneous peatland fires [2, 23]. These fires were extinguished only after 2010 flooding [2, 23]. Since 2014, another drought period started with almost all quarters showing negative Precipitation Index Anomalies. But Water Surface Index Anomalies started the negative trend on 2nd quarter of 2018. This lag between negative precipitation and water surface anomalies could be attributed to the resilience of the groundwater system, and the temporal sequence of droughts where the first drought that manifests itself is meteorological, then in surface water and then in groundwater.

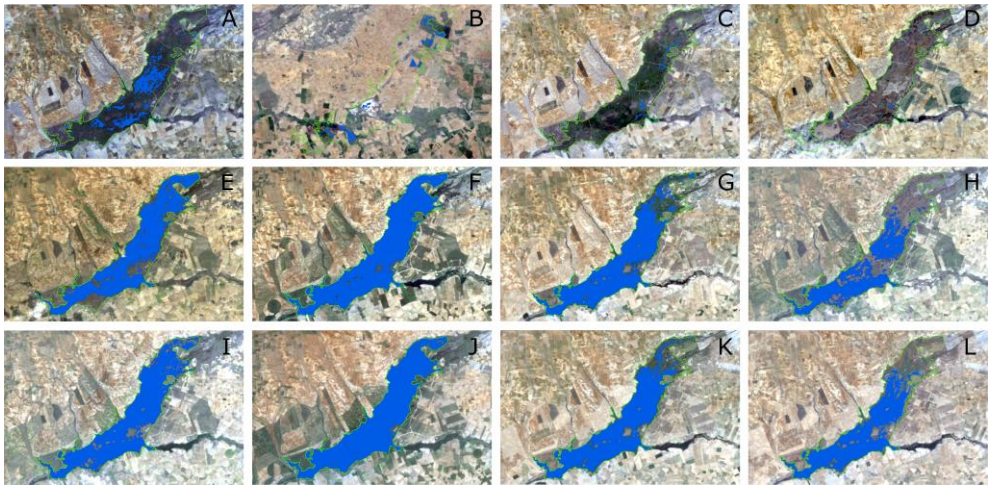

Figure 4.7. Water bodies in the Tablas de Daimiel National Park delimited according to the mNDWI spectral index. Landsat-5 TM images (threshold −0.15): (**A**) September 2008, (**B**) April 2009, (**C**) July 2009, (**D**) November 2009, (**E**) January 2010, (**F**) May

2010, (**G**) July 2010, (**H**) December 2010, (**I**) February 2011, (**J**) April 2011, (**K**) July 2011, and (**L**) October 2011.

The correlation of Water Surface Anomaly Index with Flow Anomaly Index and Piezometric Anomaly Index is similar but of opposite sign. Flow data was obtained from the Guadiana River gauging station which is the main contributor to TDNP and the historical data series is more complete than Cigüela River. No significant correlation was observed between Precipitation Anomaly Index and Flow Anomaly Index (Table 4.2). Guadiana River flow highly relies also on groundwater discharges from the Mancha Occidental aquifer. Several factors can influence this absence of significant correlations. First, in TDNP oscillations in water depth have been attributed to preferential infiltration in some sectors due to the heterogeneity of geological formation in this region which includes rapid circulation in karstified sectors and slow flow in areas with low-permeability sediments [2, 3, 28]. Also, the intensive groundwater pumping for irrigation has been reported as the cause of a notorious dissociation between the surface and groundwater networks for much of the 1970–2014 period [2, 4]. It is during unusually wet periods that significant reduction in groundwater extractions and increased groundwater recharge are observed [2]. In these periods, such as the 2010 to 2014 (Figure 4.5) water depth is very shallow and the springs outcrops maintaining a positive water surface anomaly.

With regards to spatial resolution of both sensors, we found an acceptable agreement between the estimated water surface between Landsat-8 and Sentinel-2 (R^2 = 0.87) (Figure 4.6). The differences could be attributed to several factors. One important factor is changes in water surface due to different image acquisition data. These ecosystems are highly variable and water surface can change in a short time period. But other factor could be associated to the different spatial resolution. After a dry period, when groundwater starts to outcrop, forms unconnected puddles, that will connect to form bigger water bodies if favorable conditions remain [7]. Then, the higher spatial resolution of Sentinel-2 (10 m) can detect smaller water bodies than Landsat-8 (30 m) [18] period analyzed variability patterns in the study area.

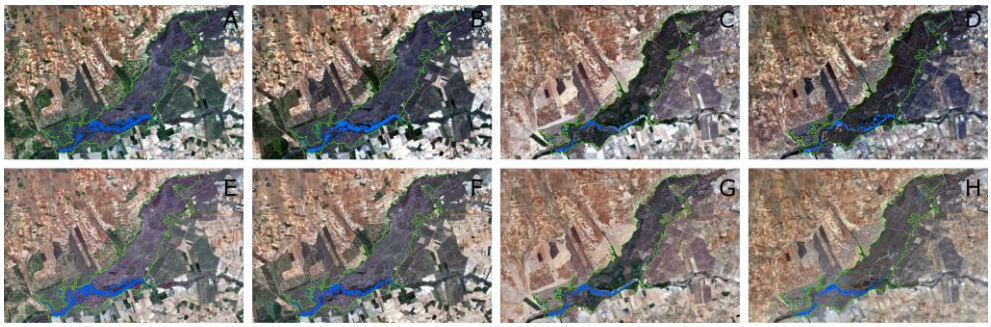

Figure 4.8. Water bodies in the Tablas de Daimiel National Park delimited according to the mNDWI Landsat-8 OLI images; (**A**) March 2021, (**B**) April 2021, (**C**) August 2021, and (**D**) October 2021. spectral index for Landsat-8 OLI (threshold −0.25) and NDWI for Sentinel-2 A/B (threshold −0.20). Sentinel-2 A/B images: (**E**) March 2021, (**F**) April 2021, (**G**) August 2021, and (**H**) October 2021.

4.5 CONCLUSIONS

The results of this study indicate the applicability of Landsat and Sentinel-2 images to evaluate the temporal variation of water bodies in the Tablas de Daimiel wetland. This study enabled detecting periods of average or above-average water surfaces, and dry periods with flooded surfaces under average conditions. To this end, a preliminary study of water indices was applied to extract water bodies reporting different indices and thresholds for each sensor satellite. Precipitation, flow, and piezometric anomaly indices were compared to the water surface anomaly index, revealing a poor relationship between precipitation and water surface anomalies. In contrast, remarkable results were found for flow and piezometric anomalies observing significant relationships among them. The extraction of water surfaces using Sentinel-2 and Landsat-8 images was also compared. The results indicate a good correlation between these two sensors. Although the higher resolutions of Sentinel-2 images recommend their suitability compared to Landsat images, these results reveal the potential of Landsat images for analyzing historical periods of water surface. The information withdraw of this research contributes to monitoring the state of endangered wetlands, helping to adapt management plans that leads to a well-preserved state of conservation.

4.6 APPENDIX A

Table A.1 List of images used in the study by date.

Ortophotos	Sentinel-2 A/B	Landsat-8 OLI	LANDST 7 ETM+	Landsat-5 TM
				19/01/2000
				11/06/2000
				29/07/2000
				04/12/2000
			29/01/2001	
			30/05/2001	
			08/07/2001	
			13/11/2001	
			01/02/2002	
			02/06/2002	
			11/07/2002	
			29/09/2002	
			08/03/2003	
			11/05/2003	
				06/07/2003
				10/10/2003
				11/03/2004
				06/06/2004
				25/08/2004
				13/11/2004
03/01/2005				**31/12/2004***
				06/04/2005
				27/07/2005
				29/09/2005
				24/04/2006
				14/07/2006
24 & 28/07/2006				**30/07 2006 ***
				16/02/2007
				07/05/2007

Ortophotos	Sentinel-2 A/B	Landsat-8 OLI	LANDST 7 ETM+	Landsat-5 TM
				02/08/2007
				05/10/2007
				13/03/2008
				23/04/2008
				20/08/2008
				30/09/2008
				01/04/2009
				06/07/2009
13 & 14/07/2009 31/08/2009				**23/08/2009 ***
				11/11/2009
				30/01/2010
				06/05/2010
				25/07/2010
				16/12/2010
				02/02/2011
				07/04/2011
				28/07/2011
				16/10/2011
		12/04/2013		
		01/07/2013		
		08/12/2013		
		19/02/2014		
		01/05/2014		
		05/08/2014		
		11/12/2014		
		12/01/2015		
		20/05/2015		
27 & 28/06/2015	**29/07/ 2015***	**23/07/2015***		
13/11/2015	**26/11/2015***	**28/11/2015***		
	04/02/2016	16/02/2016		
	13/06/2016	07/06/2016		
	02/08/2016	10/08/2016		

Ortophotos	Sentinel-2 A/B	Landsat-8 OLI	LANDST 7 ETM+	Landsat-5 TM
	11/10/2016	29/10/2016		
	08/02/2017	17/01/2017		
	09/04/2017	07/04/2017		
	07/08/2017	13/08/2017		
	06/10/2017	16/10/2017		
	08/02/2018	21/02/2018		
	04/05/2018	05/05/2018		
	17/08/2018	16/08/2018		
28/09/2018	**01/10/ 2018***	**03/10/2018***		
	04/01/2019	07/01/2019		
	29/05/2019	15/05/2019		
	02/08/2019	03/08/2019		
	06/10/2019	06/10/2019		
	14/01/2020	10/01/2020		
	17/06/2020	18/06/2020		
	21/08/2020	21/08/2020		
	10/10/2020	08/10/2020		
	14/03/2021	17/03/2021		
	18/04/2021	18/04/2021		
	06/08/2021	08/08/2021		
	20/10/2021	27/10/2021		
	18/01/2022			

4.7 REFERENCES

1. Chen, Y.; Qiao, S.; Zhang, G.; Xu, Y.J.; Chen, L.; Wu, L. Investigating the potential use of Sentinel-1 data for monitoring wetland water level changes in China's Momoge National Nature Reserve. *PeerJ* **2020**, *8*, 8616. https://doi.org/10.7717/peerj.8616

2. Castaño, S.; de la Losa, A.; Martínez-Santos, P.; Mediavilla, R.; Santisteban, J.I. Long-term effects of aquifer overdraft and recovery on groundwater quality in a Ramsar wetland: Las Tablas de Daimiel National Park, Spain. *Hydrological Processes* **2018**, *32*, 2863– 2873. https://doi.org/10.1002/hyp.13225

3. Castaño, S., Martínez-Santos, P., & Martínez-Alfaro, P. E. Evaluating infiltration losses in a Mediterranean wetland: Las Tablas de Daimiel National Park, Spain. *Hydrological Processes* **2008**, *22*, 5048–5053

4. Martínez-Santos, P.; De Stefano, L.; Martínez-Alfaro, P. E.; Llamas, M. R. Wetland restoration in the Mancha Occidental aquifer, Spain: A critical perspective on water, agricultural and environmental policies. *Restoration Ecology* **2008**, *16*(3), 511–521.

5. Custodio, E. Aquifer overexploitation: What does it mean? *Hydrogeology Journal* **2002**, *10*(2), 254–277

6. Varghese, D.; Radulović, M.; Stojković, S.; Crnojević, V. Reviewing the Potential of Sentinel-2 in Assessing the Drought. *Remote Sens.* **2021**, *13*, 3355. https://doi.org/10.3390/rs13173355

7. Aguilera, H.; Moreno L. Lessons learnt from semi-arid wetland degradation. Las Tablas de Daimiel National Park. *Boletín Geológico y Minero* **2019**, *130* (4): 711-728 ISSN: 0366-0176 DOI: 10.21701/bolgeomin.130.4.007

8. Pena-Regueiro, J.; Sebastiá-Frasquet, M.-T.; Estornell, J.; Aguilar-Maldonado, J.A. Sentinel-2 Application to the Surface Characterization of Small Water Bodies in Wetlands. *Water* **2020**, *12*, 1487. https://doi.org/10.3390/w12051487

9. Li, L.; Vrieling, A.; Skidmore, A.; Wang, T.; Muñoz, A.R.; Turak, E. Evaluation of MODIS Spectral Indices for Monitoring Hydrological Dynamics of a Small, Seasonally-Flooded Wetland in Southern Spain. *Wetlands* **2015**, *35*, 851.

10. Huang, C.; Peng, Y.; Lang, M.; Yeo, I.-Y.; McCarty, G. Wetland inundation mapping and change monitoring using Landsat and airborne LiDAR data. *Remote Sens. Environ*. **2014**, *141*, 231–242. https://doi.org/10.1016/j.rse.2013.10.020

11. Kolarik, E.; Roopsind, A.; Pickens, A.; Brandt, J.S. A satellite-based monitoring system for quantifying surface water and mesic vegetation dynamics in a semi-arid region, *Ecological Indicators* **2023**, *147*, 109965, https://doi.org/10.1016/j.ecolind.2023.109965

12. Choudhary, S.S., Ghosh, S.K. Surface Water Area Extraction by Using Water Indices and DFPS Method Applied to Satellites Data. *Sens Imaging* **2022**, *23*, 33. https://doi.org/10.1007/s11220-022-00403-4

13. Doña, C.; Morant, D.; Picazo, A.; Rochera, C.; Sánchez, J.M.; Camacho, A. Estimation of Water Coverage in Permanent and Temporary Shallow Lakes and Wetlands by Combining Remote Sensing Techniques and Genetic Programming: Application to the Mediterranean Basin of the Iberian Peninsula. *Remote Sens.* **2021**, *13*, 652. https://doi.org/10.3390/rs13040652

14. Soltani, K., Amiri, A., Zeynoddin, M. Isa Ebtehaj, Bahram Gharabaghi & Hossein Bo-nakdari Forecasting monthly fluctuations of lake surface areas using remote sensing techniques and novel machine learning methods. *Theor Appl Climatol* **2021**, 143, 713–735. https://doi.org/10.1007/s00704-020-03419-6

15. Perin, V., Tulbure, M. G., Gaines, M. D., Reba, M. L., & Yaeger, M. A. A multi-sensor satellite imagery approach to monitor on-farm reservoirs. *Remote Sens. Environ.* **2022**, *270*, 112796. https://doi.org/10.1016/j.rse.2021.112796

16. Yilmaz, O.S., Gulgen, F., Balik Sanli, F. et al. The Performance Analysis of Different Water Indices and Algorithms Using Sentinel-2 and Landsat-8 Images in Determining Water Surface: Demirkopru Dam Case Study. Arab J Sci Eng **2023**, https://doi.org/10.1007/s13369-022-07583-x

17. V. Perin, M.G. Tulbure, M.D. Gaines, M.L. Reba, M.A. Yaeger On-farm reservoir monitoring using Landsat inundation datasets Agric. *Water Manag*. **2021**, *246*, 106694, 10.1016/j.agwat.2020.106694

18. Zhang, L.; Hu, Q.; Tang, Z. Using Sentinel-2 Imagery and Machine Learning Al-gorithms to Assess the Inundation Status of Nebraska Conservation Easements during 2018–2021. *Remote Sens*. **2022**, *14*, 4382. https://doi.org/10.3390/rs14174382

19. Álvarez-Cobelas, M., Cirujano, S., & Sánchez-Carrillo, S. Hydrological and botanical man-made changes in the Spanish wetland of Las Tablas de Daimiel. *Biological Conservation* **2001**, *97*, 89–98. https://doi.org/10.1016/S0006-3207(00)00102-6

20. Sánchez-Soler, M. J., & Carrasco, M. **1996**. La Sociedad: El Plan de Regeneración Hídrica. In M. Y. Álvarez Cobelas, & S. Cirujano (Eds.), Las Tablas de Daimiel. Ecología acuática y sociedad (pp. 253–265). Madrid: Publicaciones del Organismo Autónomo de Parques Nacionales.

21. López-Camacho, B.; De Bustamante, I.; Dorado, M.; Arauzo, M. **1996**. Hidrología. En, Álvarez, M.; Cirujano, S. (Eds.) Las Tablas de Daimiel: Ecología acuática y sociedad. Dirección General de Conservación de la Naturaleza. Consejo Superior de Investigaciones Científicas. Madrid. p. 57-63

22. Ruiz de la Hermosa Las Tablas de Daimiel National Park. Implications of its manage-ment and administration on the Water Agreement| *Cuad. Soc. Esp. Cienc. For*. **2019**, *45*(1): 79-92. https://doi.org/10.31167/csecfv2i45.19498

23. Moreno Merino, L.; Jiménez Hernández, M.E.; Aguilera Alonso, H.; Jiménez, P.; de la Losa Román, A. The 2009 Smouldering Peat Fire in Las Tablas de Daimiel National Park (Spain). *Fire Technology* **2011**, *47*, 519-538 https://doi.org/10.1007/s10694-010-0172-y

24. Congalton, R.G.; Green, K. Assessing the Accuracy of Remotely Sensed Data: Principles and Practices; Lewis Publisher: Boca Raton, FL, USA, 1999.

25. Mollick, T., Md Golam A., and Sabrina K. Geospatial-based machine learning techniques for land use and land cover mapping using a high-resolution unmanned aerial vehicle image. *Remote Sensing Applications: Society and Environment* **2023**, *29* 100859. https://doi.org/10.1016/j.rsase.2022.100859

26. Valencia, J.M.; García, C.E.; Montero, D. Anomalías de vegetación asociadas con el fenómeno del ENOS en el valle geográfico del río Cauca, Colombia. *Rev. de Teledetección* **2017**, *50*, 89-99. 10.4995/raet.2017.7715

27. Xu, H. Modification of normalised difference water index (NDWI) to enhance open water features in remotely sensed imagery. *Int J Remote Sens* **2006**, 27, 3025–3033. https://doi.org/10.1080/01431160600589179

28. Castaño, S., Mediavilla, R., Santisteban, J. I., De la Losa, A., & Martínez-Santos, P. Aportación al conocimiento del comportamiento hidrogeológico del límite Terciario-Cuaternario en el entorno del Parque Nacional de las Tablas de Daimiel. *Geogaceta* **2013**, 54(111), 114.

5 CAPÍTULO 5: DISCUSIÓN

El objetivo principal de esta tesis fue la extracción de masas de agua libre en humedales a partir de imágenes de satélite Landsat y Sentinel-2. Para ello, se aplicaron diferentes índices de agua. Los resultados de esta investigación indican que los índices de agua seleccionados para cartografiar las masas de agua libre dependen de los satélites utilizados. En este sentido, se evaluaron imágenes Sentinel-2, Landsat 5 y Landsat 8. Estos satélites disponen de bandas espectrales con características diferentes, ya sea el ancho de banda, la resolución espacial o el número de bandas que disponen para registrar la energía procedente de la superficie terrestre. Estas diferencias en las características de las bandas espectrales de los satélites pueden explicar los diferentes índices de agua utilizados para extraer las masas de agua de los humedales estudiados. De esta manera el índice MNDWI fue seleccionado en el caso de las imágenes Landsat 5 y Landsat 8 y el índice NDWI para el caso de las imágenes Sentinel-2. En relación con este último tipo de imágenes, hay que destacar que el mismo índice de agua (NDWI) fue seleccionado en todos los humedales analizados. La selección de este índice coincide con estudios preliminares (Wilson et al., 2016; Kaplan et al., 2017; Zhou et al., 2017). No obstante, la aplicación de este índice puede presentar alguna limitación en zonas oscuras que no corresponden a superficies de agua y construidas (Xu, 2006; Feyisa et al., 2014). En este sentido se partió de una cartografía con la delimitación de los humedales analizados lo que permitió extraer información espectral de estos espacios limitando el alcance de los problemas asociados a este índice debido a una menor variabilidad de la zona de estudio. El índice MNDWI se calcula con la banda del infrarrojo de onda corta (banda 11 de Sentinel-2). Esta banda presenta una resolución espacial de 20 m. En contraste, la mayor resolución espacial de las bandas utilizadas para calcular el índice NDWI a partir de imágenes Sentinel-2 (B3 y B8 con resolución espacial de 10 m) puede favorecer una mejor delimitación de las zonas inundadas especialmente en las zonas de borde. Resulta evidente que el uso de imágenes Landsat en estos humedales tiene un alcance limitado debido a la resolución espacial de estos tipos de imágenes. Por otro lado, el índice MNDWI mostró un rendimiento adecuado para extraer masas de agua en el humedal de las Tablas de Daimiel. Este índice fue utilizado de manera satisfactoria en otros estudios para extraer superficies de agua. En este caso el contraste entre la reflectancia espectral

de la banda del verde y del infrarrojo de onda corta puede permitir una mejor delimitación de las zonas inundadas (Vivek et al., 2015; Moghaddam et al., 2015; Ali et al., 2019).

Además del estudio de los índices de agua, también se realizó un análisis de los umbrales que se aplicaron a los índices para extraer las masas de agua libre. En este contexto algunos autores propusieron la selección del umbral 0 en los índices de agua NDWI y MNDWI (McFeeters, 1996; Xu, 2006). Valores superiores a este umbral en el índice de agua indican la presencia de superficie con agua. Sin embargo, cabe destacar que en todos los humedales estudiados en esta tesis los resultados más precisos se obtuvieron al utilizar umbrales negativos. Estos resultados también fueron hallados en otros estudios (Ji et al., 2009; Wilson et al., 2016; Kaplan et al., 2017). En esta tesis, los umbrales que proporcionaron los resultados más precisos al aplicarlos sobre los índices de agua seleccionados utilizando imágenes Sentinel-2 fueron similares, -0,20 en el caso de las Tablas de Daimiel y un valor homogéneo de -0.30 para los cuatro humedales costeros analizados. En el caso de las imágenes Landsat-5 se seleccionó un umbral de -0,15 y en el caso de Landsat-8 un umbral de -0,25. Estos valores negativos de umbrales pueden estar asociados con la respuesta espectral de estas masas de agua a la presencia de material disuelto o particulado (por ejemplo, fitoplancton) o al efecto del fondo en las masas más someras. En cuanto a los resultados obtenidos en la superficie de agua utilizando imágenes Landsat, los resultados fueron más precisos al utilizar las imágenes del sensor OLI de Landsat-8. Otros autores también comprobaron un mayor rendimiento de las imágenes de este sensor en comparación a otros satélites Landsat (Mishra et al., 2016; Poursanidis et al., 2015). Mejoras en la calibración radiométrica, rangos de longitud de ondas más estrechos en las bandas espectrales y una mayor relación señal/ruido pueden explicar estas diferencias (Mishra et al., 2016; Poursanidis et al., 2015). Por otro lado, las diferencias en los umbrales entre los humedales costeros analizados y el de las Tablas de Daimiel para las imágenes Sentinel-2 pueden tener también una relación con la metodología seguida para seleccionar las muestras de validación en ambas zonas. En el caso de los primeros, las muestras de validación se seleccionaron en una zona de 20 m alrededor del borde de cada masa de agua. De esta manera se tuvo en cuenta la alta variabilidad de estas zonas de borde. Esta selección de umbrales se consideró adecuada para poder obtener unos resultados más precisos en estas zonas, significativas en términos de superficie teniendo en cuenta el pequeño tamaño de las masas de agua de estos humedales costeros. En cambio, en el humedal de las Tablas de Daimiel se optó por el

criterio de distribución de las muestras de validación por todo el perímetro del humedal. En este humedal, se comprobó que al realizar los análisis a partir de muestras localizadas en los bordes se obtuvieron falsos positivos de superficie de agua lo que puede estar asociado a una mayor variabilidad de suelos en este tipo de humedales.

A partir de los índices y umbrales seleccionados se obtuvo una cartografía de masas de agua libre. Estos resultados son utilizados para obtener la misma información en otras fechas de manera que se pueda llevar a cabo un análisis histórico de la evolución de estos espacios y determinar un índice que nos permita conocer el estado hidrológico del humedal. En esta tesis se calculó el índice de anomalías de superficie de agua por trimestres del año hidrológico.Esta periodicidad se escogió teniendo en cuenta la menor disponibilidad de imágenes Landsat. A partir de este índice se obtuvo información de los periodos del humedal con anomalías negativas y positivas de la superficie de agua en el periodo analizado. Los resultados obtenidos a partir de estos análisis coindicen con la información que se dispone del parque. Así, cabe destacar los periodos comprendidos entre el 2006 - 2010 y entre 2019 – 2021 donde se registraron niveles muy bajos de superficie inundada. En cambio, durante el periodo comprendido entre 2010 y 2012 (Castaño et al., 2018; Aguilera et al., 2019) se observaron anomalías positivas significativas de superficie de agua.

Para obtener un mejor conocimiento de las posibles causas de variación de los valores de anomalías se tuvieron en cuenta variables meteorológicas, hidrológicas e hidrogeológicas. En esta investigación se consideraron la precipitación, el caudal fluvial y el nivel piezométrico del acuífero como variables representativas del ciclo hidrológico. Se calculó el índice de anomalía de cada una de estas variables y se realizó un análisis de correlación con el índice de anomalía de superficie de agua. Los índices de anomalía estudiados permiten identificar entre estas las variables que tienen mayor impacto sobre las aguas superficiales. Los resultados mostraron que la relación entre el Índice de Anomalía de la Precipitación y el de Superficie de Agua fue estadísticamente no significativa. Otros autores también señalaron la ausencia de correlación significativa entre la cobertura de agua superficial y la precipitación en los humedales (Zhang et al., 2022). Por el contrario, se encontró una relación positiva significativa (0,369) entre el Índice de Anomalía de la Superficie del Agua y el Índice de Anomalía del caudal, y una

relación negativa significativa (-0,406) entre el Índice de Anomalía de la Superficie del Agua y el Índice de Anomalía Piezométrica.

Los valores de superficie inundada de la serie temporal obtenidos por los satélites Landsat-8 y Sentinel-2 se compararon en el humedal de las Tablas de Daimiel con resultados satisfactorios. Este análisis corrobora que ambas fuentes de información se pueden utilizar de forma complementaria para obtener una serie de datos más larga, contando con la información de las imágenes Landsat desde su primera fecha de lanzamiento. Por otra parte, combinar ambas fuentes a partir de la fecha de lanzamiento de Sentinel-2 puede permitir incrementar la frecuencia de imágenes, lo cual podría ser necesario en períodos de alta nubosidad. No obstante, la mayor resolución temporal, espacial y espectral de las imágenes del satélite Sentinel-2 recomiendan su uso permitiendo realizar un seguimiento más completo de la evolución de los humedales.

5.1 REFERENCIAS

1. Aguilera, H. y Moreno L. 2019. Lessons learnt from semi-arid wetland degradation. Las Tablas de Daimiel National Park. Boletín Geológico y Minero, 130 (4): 711–728. https://doi.org/10.21701/bolgeomin.130.4.007
2. Castaño, S., de la Losa, A., Martínez-Santos, P., Mediavilla, R., Santisteban, J.I. 2018. Long-term effects of aquifer overdraft and recovery on groundwater quality in a Ramsar wetland: Las Tablas de Daimiel National Park, Spain. Hydrological Processes, 32, 2863–2873. https://doi.org/10.1002/hyp.13225
3. Feyisa, G.L., Meilby, H., Fensholt, R., Proud, S. 2014. Automated Water Extraction Index: A New Technique for Surface Water Mapping Using Landsat Imagery. Remote Sensing of Environment. 2014, 140, 23–35. https://doi.org/10.1016/j.rse.2013.08.029
4. Ichsan Ali, M., Darma Dirawan, G., Hafid Hasim, A., Rais Abidin, M. 2019. Detection of Changes in Surface Water Bodies Urban Area with NDWI and MNDWI Methods. International Journal of Advanced Science and Technology, 9 (3), 946–951.
5. Ji, L., Zhang, L., Wylie, B. 2009. Analysis of Dynamic Thresholds for the Normalized Difference Water Index. Photogrammetric Engineering & Remote Sensing, 75 (11), 1307–1317.
6. Kaplan, G., Avdan, U. 2017. Mapping and Monitoring Wetlands Using SENTINEL 2 Satellite Imagery. ISPRS Annals of the Photogrammetry, Remote Sensing and Spatial Information Sciences, Volume IV-4/W4, 2017. 4th International GeoAdvances Workshop, 14–15 October 2017, Safranbolu, Karabuk, Turkey.
7. Mcfeeters, S.K. 1996. The use of the Normalized Difference Water Index (NDWI) in the delineation of open water features. International Journal of Remote Sensing, 17, 1425–1432.
8. Mishra, N., Helder, D., Barsi, J., Markham, B. 2016. Continuous calibration improvement in solar reflective bands: Landsat 5 through Landsat 8. Remote Sensing of Environment, 185, 7–15, https://doi.org/10.1016/j.rse.2016.07.032.
9. Moghaddam, M.H.R., Sedighi, A., Fayyazi, M.A. 2015. Applying MNDWI index and linear directional mean analysis for morphological changes in the Zarriné-

Rūd River. Arabian Journal of Geosciences 8, 8419–8428. https://doi.org/10.1007/s12517-015-1795-6

10. Poursanidis, D., Chrysoulakis, N., Mitraka, Z. 2015. Landsat 8 vs. Landsat 5: A comparison based on urban and peri-urban land cover mapping. International Journal of Applied Earth Observation and Geoinformation, 35, 259–269, https://doi.org/10.1016/j.jag.2014.09.010.
11. Vivek Singh, K., Setia, R., Sahoo, S., Prasad A., Pateriya B. 2015. Evaluation of NDWI and MNDWI for assessment of waterlogging by integrating digital elevation model and groundwater level. Geocarto International, 30(6), 650–661, https://doi.org/10.1080/10106049.2014.965757
12. Wilson, N.R., Norman, L.M., Villarreal, M., Gass, L., Tiller, R., Salywon, A. 2016. Comparison of remote sensing indices for monitoring of desert cienegas. Arid Land Research and Management, 30, 460–478.
13. Xu, H. 2006. Modification of normalised difference water index (NDWI) to enhance open water features in remotely sensed imagery. International Journal of Remote Sensing, 27, 3025–3033.
14. Zhang, L., Hu, Q., Tang, Z. 2022. Using Sentinel-2 Imagery and Machine Learning Algorithms to Assess the Inundation Status of Nebraska Conservation Easements during 2018–2021. Remote Sensing, 14, 4382. https://doi.org/10.3390/rs14174382
15. Zhou, Y., Dong, J., Xiao, X., Xiao, T., Yang, Z., Zhao, G., Zou, Z., Qin, Y. 2017. Open Surface Water Mapping Algorithms: A Comparison of Water-Related Spectral Indices and Sensors. Water, 9, 256. https://doi.org/10.3390/w9040256

6 CAPÍTULO 6: CONCLUSIONES Y FUTURA INVESTIGACIÓN

6.1 CONCLUSIONES

Las principales conclusiones que se atribuyen a esta tesis son las siguientes:

- Los resultados de este estudio indicaron la aplicabilidad del índice NDWI calculado a partir de imágenes Sentinel-2A/B (bandas 3 y 8) para extraer masas de agua libre en humedales delimitados, observando que para el umbral -0.30 se generaron resultados satisfactorios en los humedales mediterráneos costeros analizados, y el umbral -0.20 para clasificar un humedal de interior con alta discontinuidad y variabilidad en sus masas de agua libre y alto valor medioambiental, como el caso estudiado de Tablas de Daimiel. Estos resultados indican la idoneidad de este índice de agua en ambas zonas de estudio. Sin embargo, los valores de los umbrales seleccionados, aunque similares, no coincidieron lo que sugiere la necesidad de realizar un análisis previo de los umbrales adaptado a las diferentes zonas de estudio. No obstante, los valores de estos umbrales para determinar las masas de agua a partir del índice de agua (NDWI) fueron homogéneos en cada zona de estudio y en periodos diferentes.
- Este estudio demostró la aplicabilidad de las imágenes Landsat para evaluar la variación temporal de las masas de agua. En este sentido se identificaron periodos con anomalías positivas y negativas de la superficie de lámina de agua libre a través del cálculo del índice de anomalía. Además, se estudió la correlación del índice de anomalía de la superficie de agua con los índices de anomalía de la precipitación, del caudal y del nivel piezométrico del acuífero. Este análisis reveló una relación no significativa entre las anomalías de precipitación y las anomalías de la superficie del agua. En contraste, se halló una relación estadísticamente significativa entre las anomalías de caudal y piezométricas, y la anomalía de la superficie de agua.
- El análisis de correlación entre las superficies de agua obtenidas utilizando imágenes Sentinel-2 y Landsat-8 revelaron una alta correlación entre los resultados de ambos sensores. Sin embargo, se recomienda el uso de las imágenes Sentinel-2 por su mayor resolución temporal y espacial permitiendo detectar zonas de agua aisladas que pueden aflorar especialmente en periodos de sequía.

Estas imágenes también permiten realizar un seguimiento más continuo de su evolución favoreciendo caracterizar patrones de cambio.

- La combinación analítica de datos de teledetección y datos LiDAR permitió identificar y cartografiar la superficie inundada y las zonas con menor elevación. Esta información resulta de especial interés para realizar una gestión adecuada de los humedales teniendo en cuenta todos los usos conflictivos y los servicios ecosistémicos proporcionados por los humedales.

6.2 FUTURA INVESTIGACIÓN

La disponibilidad de una mayor colección de imágenes históricas del satélite Sentinel-2 es un aspecto a tener en cuenta a medida que se vayan registrando nuevas imágenes, lo que permitirá realizar estudios sobre la variación de las masas de agua en humedales en periodos temporales más largos. En este sentido se podrán calcular índices de anomalías de agua siguiendo la metodología aplicada en esta tesis para las imágenes Landsat y permitiendo identificar periodos en los que el humedal presente estados deficitarios de agua. Las imágenes Sentinel-2 presentan dos ventajas en relación con las imágenes Landsat aplicadas en esta tesis. Por un lado, su mayor resolución espacial permite detectar masas de agua de menor tamaño, aspecto de especial interés en los humedales costeros analizados y en periodos con una menor presencia de agua ya que favorece la localización de las masas de agua libre aisladas. Así mismo, la mayor resolución temporal de este tipo de imágenes permitirá realizar un seguimiento más continuo de la evolución de estos espacios. Esta información puede contribuir a un mejor conocimiento del funcionamiento de estos ecosistemas y de los factores que influyen en sus cambios. Estos análisis no se han podido llevar a cabo con las imágenes Sentinel-2 debido a que la serie histórica de estas imágenes aún no cubre un intervalo de tiempo suficiente.

Por otro lado, en esta tesis se han seleccionado diferentes índices de agua y umbrales en función del tipo de humedales y de sensores. Poder analizar no solo la extensión de la superficie del agua sino la calidad del agua, a través de la estimación de parámetros como la clorofila *a*, puede constituir una información valiosa para la conservación y gestión de

estos espacios. La relación entre los valores de los umbrales aplicados en esta tesis y los valores de los parámetros de calidad de agua es un análisis que merece ser explorado.

Imágenes de satélite en el dominio óptico Sentinel-2 y Landsat se han aplicado en esta investigación. La utilización de otros conjuntos de datos como datos batimétricos o imágenes radar (imágenes satélite Sentinel -1) permitirían plantear otros análisis para la detección de superficies inundadas en humedales. La posibilidad de disponer información batimétrica de estos espacios, aunque la profundidad no sea muy elevada, permitiría conocer la variación del volumen de agua de los humedales, aspecto de especial interés para conocer la evolución de estos y sus cambios. Por otro lado, la inclusión de imágenes radar en estos estudios puede tener cierta aplicabilidad para detectar masas aguas cubiertas por vegetación. En este sentido sería necesario analizar el rendimiento de este tipo de imágenes en estas condiciones combinando este conjunto de datos con la información espectral en el dominio espectral.